A Hyperbolic model for Degradation in Tension mode-I Fracture of Masonry

Implementation and Validation in Engineering masonry model

Srinidhi B. R.

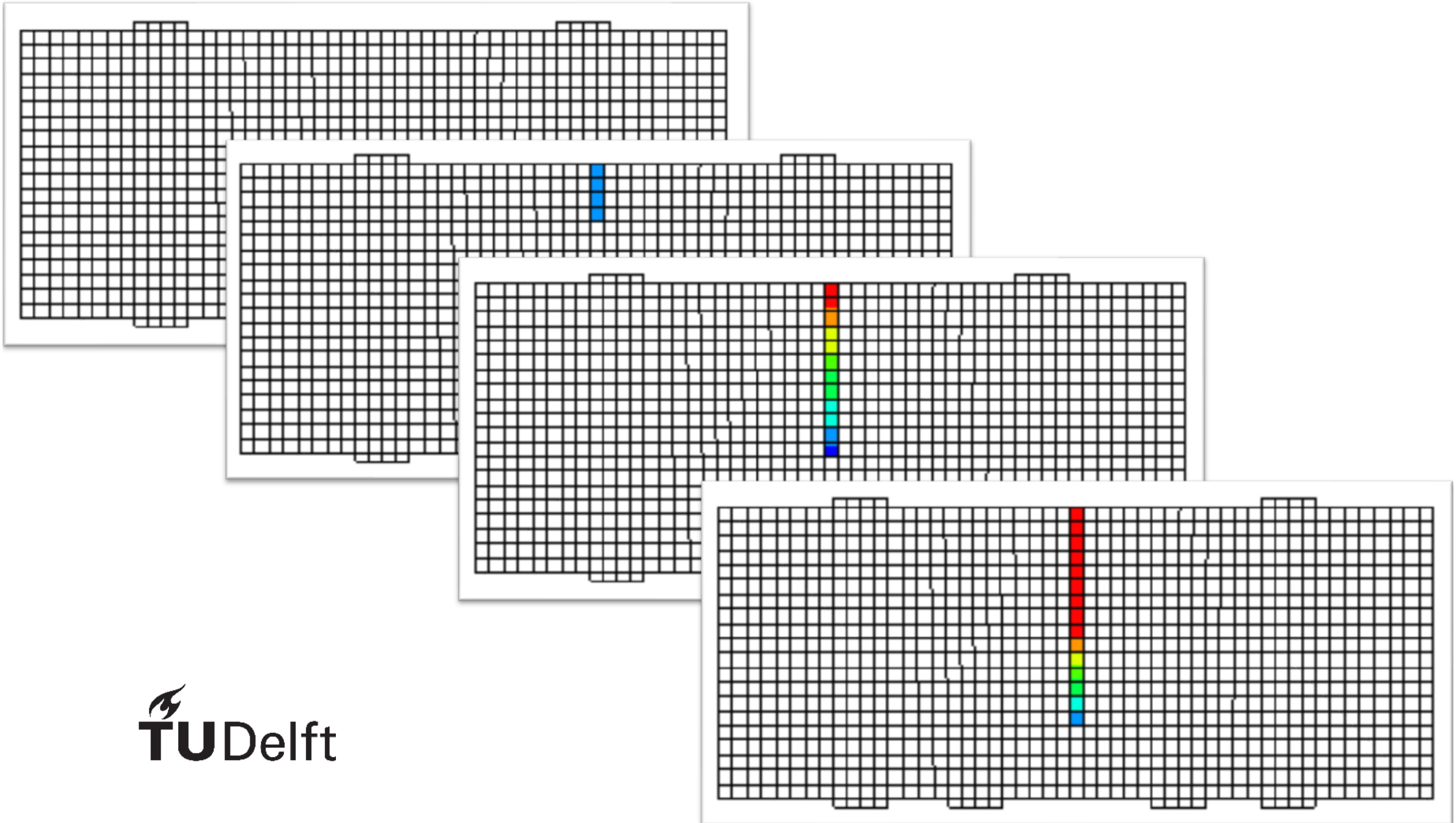

TU Delft

“A Hyperbolic model for Degradation in Tension mode-I Fracture of Masonry”

Implementation and Validation in Engineering Masonry Model

Master Thesis

by

Srinidhi Bindiganavile Ramadas

in partial fulfilment of the requirements for the degree of

Master of Science

in Civil Engineering

at the Delft University of Technology

Student number:	4614216	
Project duration:	April 2018-November 2018	
Thesis committee:	Prof.dr.ir. Jan Rots	TU Delft, chair
	Dr. Francesco Messali	TU Delft, supervisor
	Ir. Paul Korswagen	TU Delft, mentor and supervisor
	Ir. Cor Kasbergen	TU Delft, supervisor

Abstract

The growing need to understand the behaviour of un-reinforced masonry (URM), subjected to repeated light man-made earthquakes caused by the extraction of gas in the north-eastern part of The Netherlands has resulted in intense research to determine the exact process of crack initiation and propagation. The historical masonry buildings and Dutch terraced houses in Groningen are prone to light damages which become severe upon repeated lateral earthquake loading. Although there are material models that describe the behavior of modern brick masonry, they do not accurately represent the mechanical properties of 19th century clay brick masonry. This led to a large-scale research into the mechanical behavior of un-reinforced masonry and an orthotropic continuum macro-model called the Engineering Masonry Model (EMM) was proposed. The existing tension constitutive model in EMM assumes a secant unloading-reloading branch which does not consider the strength degradation of URM under repeated loading. Since tension mode-I fracture results in cracking of URM, it is important to study the effects of repeated loading on the propagation of the crack and its effects on the capacity of the structure.

This thesis presents a degradation model to represent the strength deterioration of URM observed during repeated loading. The constitutive model formulated in this thesis is based on hyperbolic functions along with a secant slope for the unloading- reloading branch. To justify the model assumptions, a single linear 4-node element is analysed with the new model and the effect of varying different components of the constitutive equations is established. The window bank spandrel sample modeled as a 4-point bending test is analysed using the new model for 10, 30 and 100 repetitions. It is shown that the hyperbolic model can predict accurately the stress reduction within each repetition displacement set and also represent the crack width widening and crack propagation accurately when compared to the experimental results. The new model is tested on a wall with a window opening sample and the results closely matched that of the experiment. Finally, recommendations are provided for further development of the hyperbolic model and calibration of the material properties.

Acknowledgments

Here, I would like to acknowledge the people who have given me their time and support over the duration of my thesis.

First, to the members of my assessment committee: My mentor and supervisor, Paul Korswagen, without whose support this thesis would have been incomplete. Right from introducing me to the topic, reviewing my work regularly, to inspiring me with his impeccable work ethic, he was very supportive and that is why I am able to write this thesis today. Thank you for always being available to discuss my project and for providing such positive and constructive feedback on my drafts.

Francesco Messali, for his support throughout the entire duration of my thesis. Your simplistic explanation to my weird code related questions showed me the importance of strong fundamentals. Your willingness to promptly answer any question I had with great consideration was invaluable.

Cor Kasbergen, for giving feedback with easier solutions to my modeling questions. I will always be grateful to our coffee break conversations and frequent update meetings which gave me good insights into my thesis.

Prof. Jan Rots, for providing interesting suggestions and invaluable feedback during my committee meetings, and for inspiring a rigorous academic approach.

Manimaran Pari and Michele Longo, for their help and feedback on the topic and troubleshooting with DIANA.

All the friends I have made at TU Delft, from providing lively scientific discussions, to sharing the burden of thesis life, I consider myself to be fortunate to be associated with such individuals.

And last but not the least, my family back in India, for giving me the courage and support to study abroad. The love and blessings from my parents cannot be understated and I hope I have made them proud.

Thank you.
Srinidhi B. R.
Delft, November 2018

Contents

Chapter 1

Introduction

1.1 General overview

Many historical buildings and residential houses from the 19th century are made of un-reinforced masonry (URM) and built using clay bricks and lime mortar across Europe, especially in the Netherlands. Huge openings at irregular intervals and no standard guidelines or knowledge about the strength of the masonry are some of the characteristics of these structures [Rots et al., 2016]. These buildings were not designed to withstand earthquakes, as such a load was unimaginable at that time in the Netherlands. In recent years, the extraction of natural gas has resulted in the loss of strength of the underlying soil and has led to an induced earthquake type of situation in the northern part of the Netherlands [Rots et al., 2016]. The houses and historical cites in the city of Groningen have been slowly deteriorating due to repeated low intensity earthquakes. Understanding the behavior of masonry subjected to low intensity earthquakes requires the knowledge of basic mechanical properties of such a composite material.

The majority of the time it is difficult to predict the behavior of such masonry structures as they were built from bricks made of clay and simple lime mortar to hold them together. There were no codes or standard guidelines for the various construction practices and quality control methods back then [ARUP, 2013]. Most of these buildings have poor response to earthquakes. This renders the extension of modern masonry testing methods and properties to describe old masonry, difficult and vague [ARUP, 2013]. Hence, simple and robust finite element simulations for large scale applications, making use of macro modeling techniques are the most preferred approach for overcoming these obstacles and understanding the behavior of structures in an economical manner.

Over the years, many researchers have developed finite element packages starting from simple 2D models capable of reproducing in-plane failure mechanisms to complex and complete 3D model techniques capable of showing both in-plane and out-plane failures [Schreppers et al., 2016]. Most of these methods define a set of conditions or rules that have to be satisfied in order to be able to achieve good results with experiments. Few models like the total strain based crack model, which were extensively used for numerical analysis, do not accurately include the energy dissipation and the progressive damage criteria that occur in a masonry structure subjected to cyclic loading [Schreppers et al., 2016]. These methods are time consuming and have limitations when it comes to specific applications such as representing the effects of earthquake loads, especially for the buildings in the Groningen province in the Netherlands [Schreppers et al., 2016].

Hence, DIANA FEA BV along with TU Delft provided a simple continuum material model capable of validating such structures and also applicable to modern masonry buildings. This model was first implemented in DIANA 10.1 in 2016 under the name Engineering Masonry Model (EMM) and has been put through rigorous tests to keep it updated with new developments [Schreppers et al., 2016]. Although a good agreement was obtained by using this model for both in-plane and out-of-plane masonry walls under cyclic loading, it was found that the degradation aspect and the stress loss accompanying it was not properly represented in the case of numerous cyclic quasi-static or dynamic analysis done to validate the model [Schreppers et al., 2016]. Researchers found that masonry under cyclic loading showed promising results comparable to practical applications rather than a monotonic type [Oliveira, 2003]. This led to extensive research to study the effects of fatigue and repetitive loading on masonry in both compression and tension [Abrams et al., 1985]. Figure 1.1 shows a comparison between the existing EMM model and the experimental result for a window bank sample tested under 10, 30 and 100 repetitions. It can be clearly noticed that the existing constitutive model in EMM does not show cyclic degradation which is a clear deviation from the experimental results. Consequently, a need to improve the degradation aspect of the EMM to better predict the response of masonry walls has emerged.

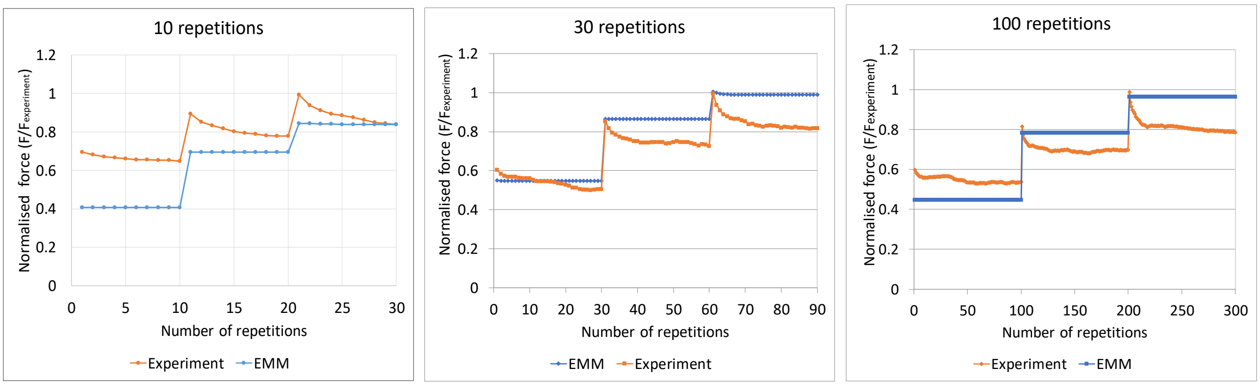

Figure 1.1: Force reduction vs number of repetitions for 10, 30 and 100 repetition samples.

Abrams et al. found that under cyclic compressive tests of brick masonry prisms subjected to varying amounts of sustained and alternating stress levels indicated reductions in compressive strengths as large as 30% of static compressive strength [Abrams et al., 1985]. Hence, importance is given to the behavior of masonry structures under fatigue loading and reproducing the exact behavior using finite elements.

Lourenco (1998) studied the effect of repeated loading and behaviour of a masonry unit and proposed the characteristic cracking pattern of clay brick masonry for uniaxial and biaxial strength as shown in Figure 1.2 [Lourenco, 1998].

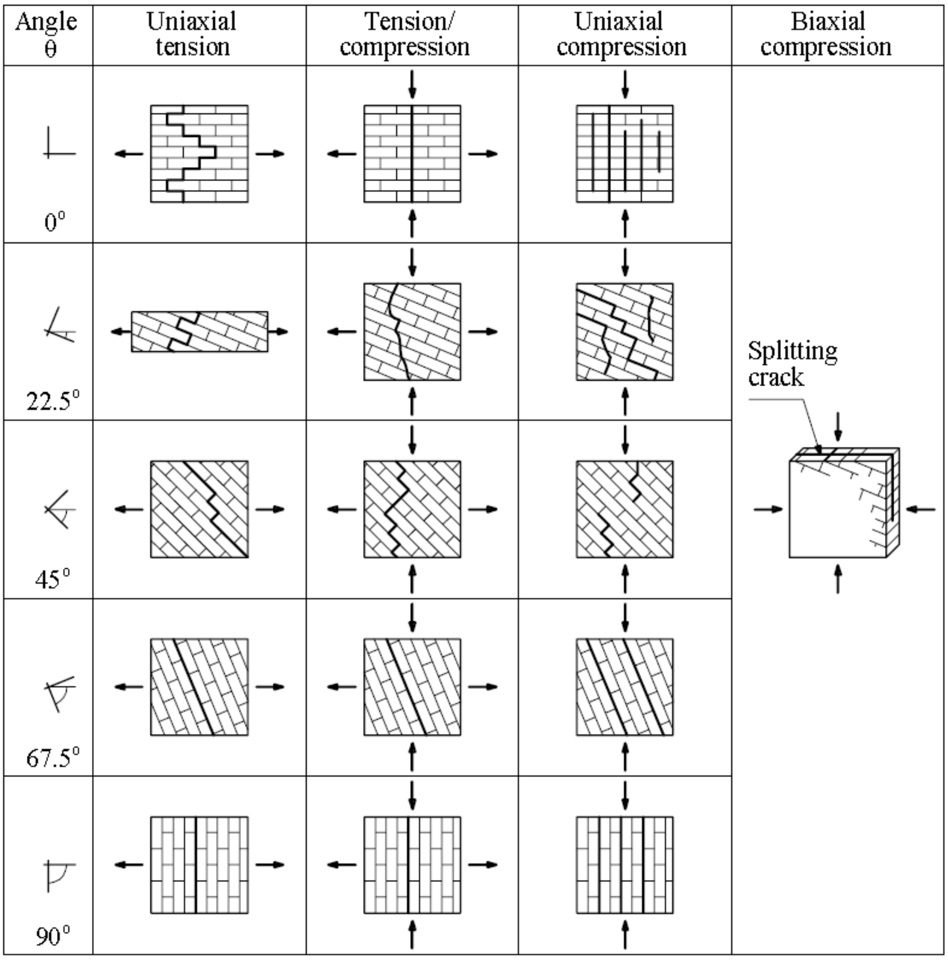

Figure 1.2: Modes of failure of solid clay brick masonry units. [Lourenco, 1998]

Park et al. (1987) studied the different aspects of hysteresis and proposed rules to model such a loading for finite element packages which included stiffness and strength degradation as important characteristics of material [Park et al., 1987] [Figure 1.3].

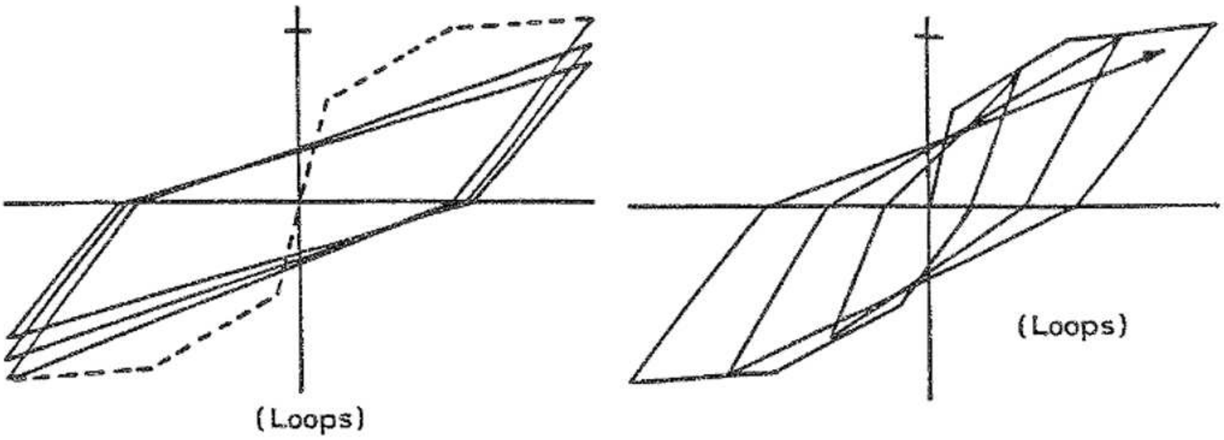

Figure 1.3: Strength degradation (left). Stiffness degradation (right). [Park et al., 1987]

1.2 Aim of this research

The intent of this research is to develop a constitutive model that accurately represents the strength degradation behavior due to tension mode-I fracture of masonry under repetitive loading. This thesis seeks to build upon the constitutive models proposed by Hordijk et al (1991), Yankelevsky et al (1989), Naraine et al (1989) and Otter et al (1989) by improving and expanding the existing features of the EMM model that do not accurately represent the degradation aspect of masonry.

A preliminary study of the existing constitutive models has led to the following key research questions.

1. Why is it important to consider the degradation of masonry structures?
2. How has degradation been implemented in other composite materials like concrete?
3. How can degradation be implemented effectively and efficiently in EMM for DIANA?
    - Is there a damage index already considered in the EMM?
    - What input parameters will the degradation depend on?
    - Why implement degradation only in tension mode I model of EMM and not in shear or compression?

1.3 Thesis outline

Each chapter of this report describes the step by step procedure for the implementation of degradation in EMM followed by validation and comparison with the experimental results. Chapter 2 provides a detailed and essential literature review starting from the different types of failure in masonry, relation between concrete and masonry, the numerical models used to predict the failure of concrete and progressive cracking of concrete under cyclic loading and the methods in which degradation has been considered for different materials. Chapter 3 deals with the formulation of a mathematical model and is followed by the constitutive equations and the changes that need to made to the existing model. Chapter 3 further includes the FORTRAN coding changes in the user supplied subroutine. Chapter 4 deals with the detailed experimental results from the report “Damage sensitivity of Groningen Masonry structures - Experimental and computational studies” [Korswagen et al., 2017] and justifies the need for a material model with strength degradation. Finally, Chapter 5 provides the comparison of experimental and numerical results of the new model against a window bank sample for 10, 30 and 100 repetitions.

Chapter 2

Review of Literature

This literature can be divided into two parts, first, the material behavior under different types of loading and second, the constitutive material models that have been proposed to represent them. The tension mode-I fracture of concrete will be explored under repetitive loading, since both concrete and masonry are heterogeneous materials and the smeared crack approach is of main focus.

2.1 Mechanical behavior of Brick Masonry

Masonry is a heterogeneous assemblage of units and joints. Units are such as bricks, blocks, ashlars, adobes, irregular stones and others. Joints can be mortar made out of clay, bitumen, chalk, lime/cement, glue or other. The behaviour of masonry is much dependent not only on the composition of units and joints, but also on how they are arranged and treated [Angelillo et al., 2014].

2.1.1 Local Failure modes

Basically there are three failure modes that are visible locally in masonry structures [Angelillo et al., 2014].

1. The first one is seen as a detachment fracture due to the brittleness of the materials as shown in Figure 2.1.
2. The second mode is a mixed type fracture or detachment alternating to lines of sliding such as those of in-plane shear shown in Figure 2.2.
3. The third mode is the crushing of the material under compression as shown Figure 2.3.

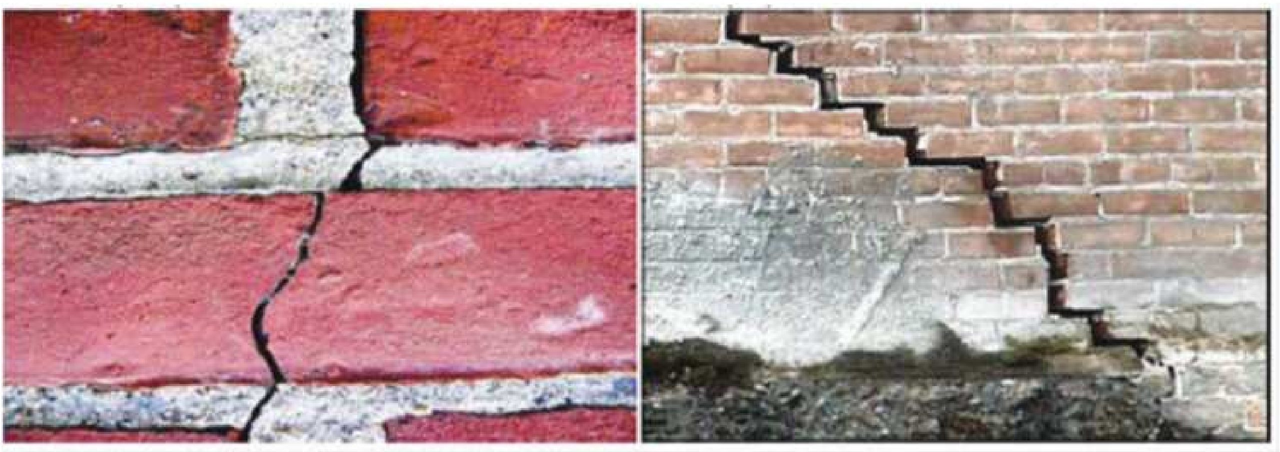

Figure 2.1: Detachment fracture in brick-masonry walls [Angelillo et al., 2014]

Figure 2.2: Detachment and sliding due to combined compression and shear [Angelillo et al., 2014]

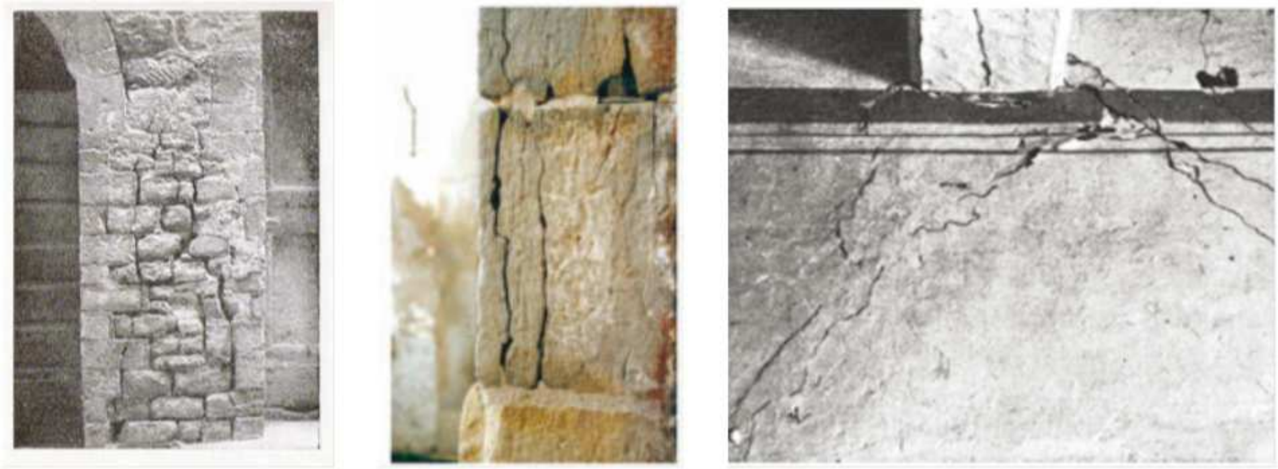

Figure 2.3: Crushing due to compression [Angelillo et al., 2014]

Masonry is a composite material and accurate tests need to be performed on the component materials, masonry assemblies and small masonry structures including the study of three main mechanical behavior which are compression, tension and shear failures. A basic modern notion in the mechanical behavior of masonry is softening, which is a gradual decrease of mechanical resistance under a continuous increase of deformation forced upon a material specimen or structure. Softening is a salient feature of masonry, concrete, stone as they fail due to progressive internal cracking [Angelillo et al., 2014].

2.1.2 Compression

Compression strength tests on a unit can be easily performed and give a good indication of the general quality of the material used. For compressive failure, experimental data seems to indicate that both local and continuum fracturing processes govern the behaviour [Angelillo et al., 2014]. The area underneath the stress vs deformation curve is the compressive fracture energy Gc [Angelillo et al., 2014]. Refer Figure 2.4.

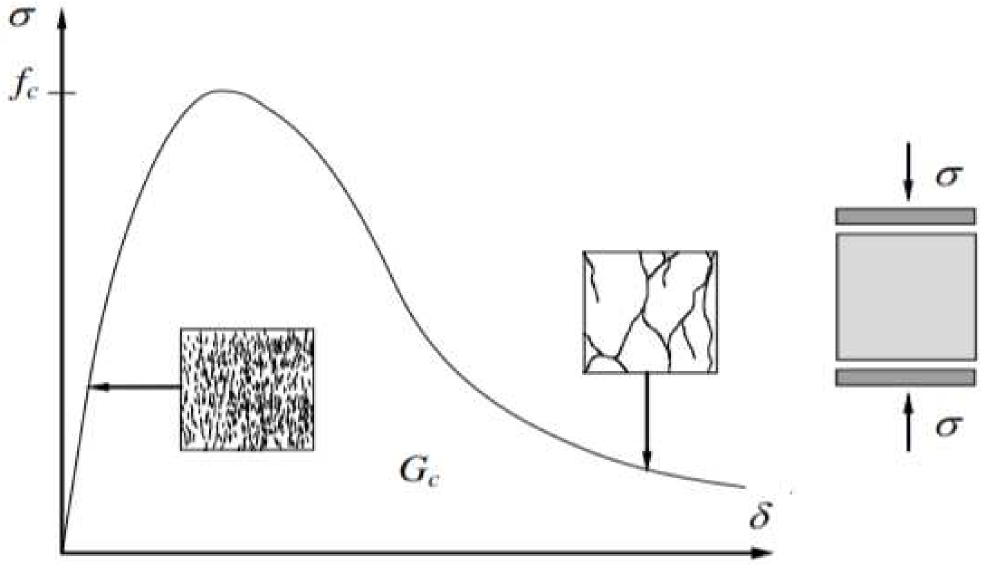

Figure 2.4: Softening under compression [Angelillo et al., 2014]

Recently research has been carried out to determine the compressive behaviour of masonry in existing buildings using in-situ core drilling methods to reproduce a low-strength historical masonry [Pelà et al., 2016] [Figure 2.5]. Cyclic compressive tests on specimens as per standard codes and non-standard tests such as core samples have been performed and the compressive failure pattern has been studied [Pelà et al., 2016]. Refer Figure 2.6.

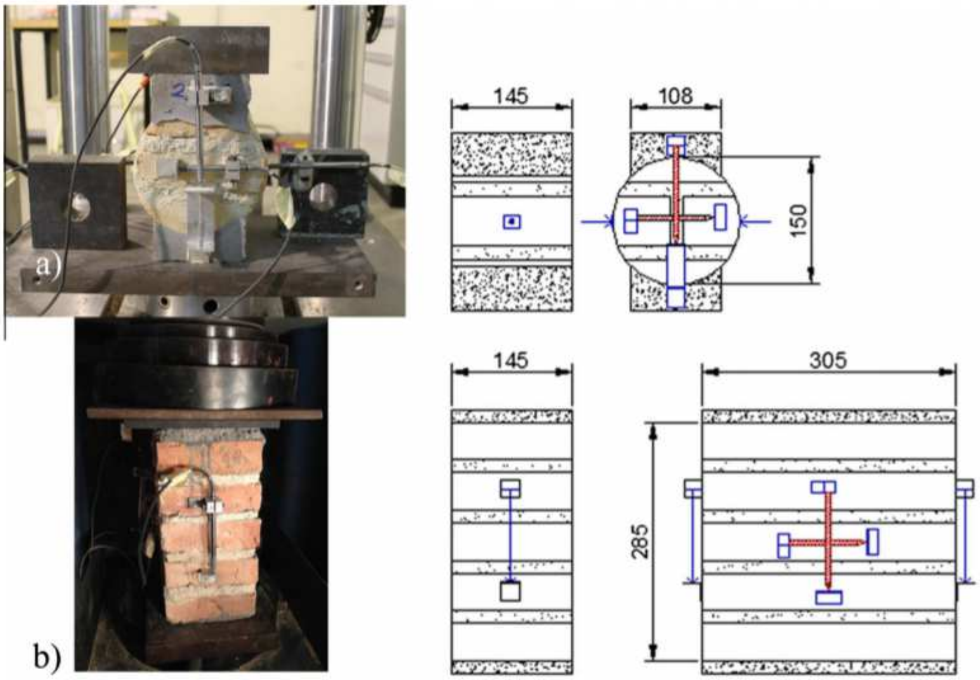

Figure 2.5: Experimental setups of compression tests a)cylindrical specimen b) stacked-bone specimen (dimensions in mm) [Pelà et al., 2016]

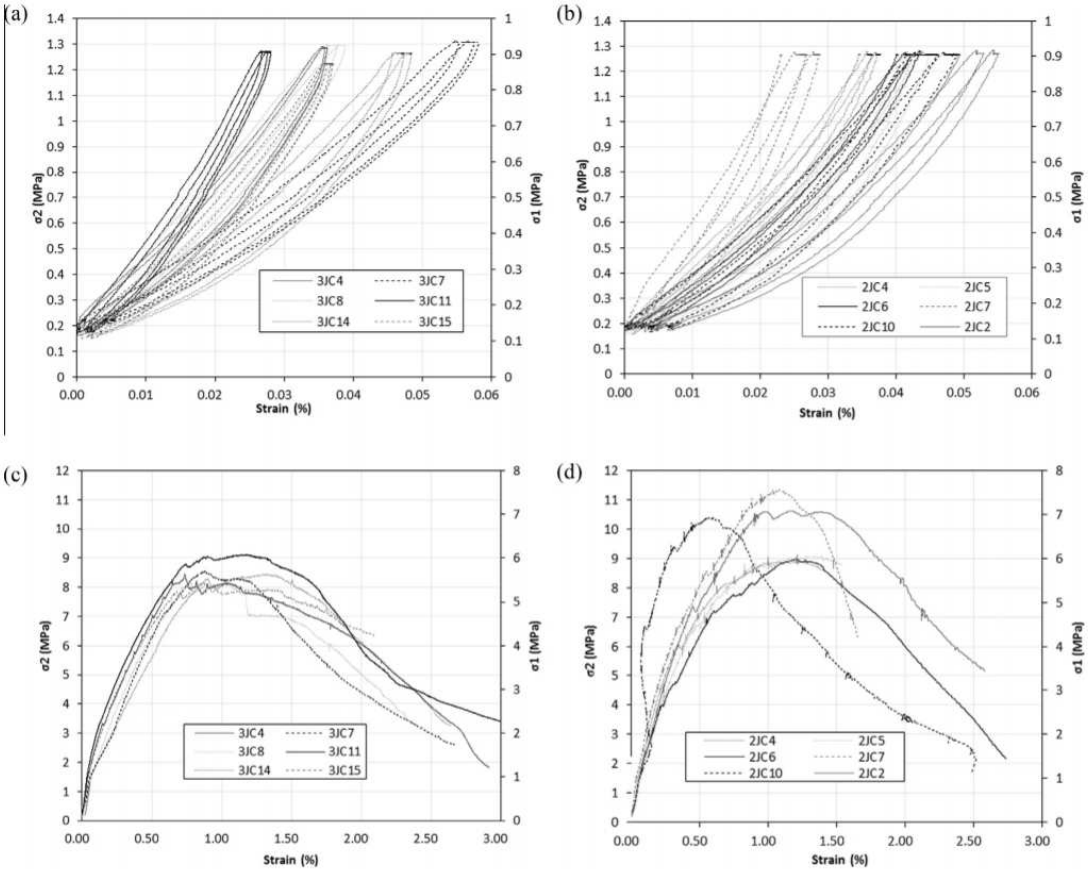

Figure 2.6: Experimental results of compression tests a-b)cyclically loaded specimen c-d) Monotonically loaded specimen [Pelà et al., 2016]

2.1.3 Tension

Softening is commonly attributed to the heterogeneity of the material, due to the presence of different phases and material defects, like flaws and voids [Lourenco et al., 2002]. The initial stresses and cracks as well as variations of internal stiffness and strength cause progressive crack growth when the material is subjected to increasing deformation [Lourenco et al., 2002]. Initially, the micro cracks are stable which means that they grow only when the load is increased. Around the peak load an acceleration of crack formation takes place and the formation of macro cracks starts [Lourenco et al., 2002]. The macro cracks are unstable, which means that the load has to decrease to avoid an uncontrolled growth. In a deformation controlled test the macro crack growth results in softening and localization of cracking in a small zone, while the rest of the specimen unloads [Lourenco et al., 2002]. This phenomenon is very salient in tension fracture of bricks, brick mortar interface. In a tensile test of a quasi-brittle material, such as brick, it is possible to obtain a stress-elongation diagram (σ-u) in the form indicated in Figure 2.7, provided that the test is carried out under displacement control [Lourenco et al., 2002].

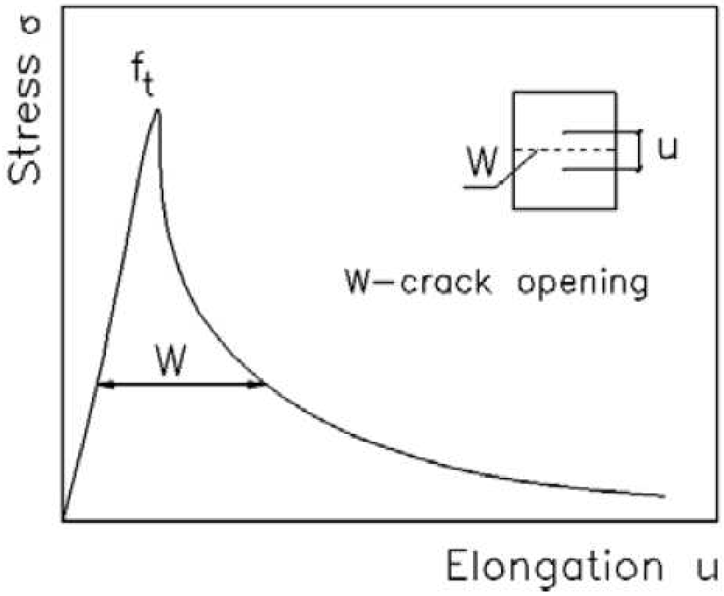

Figure 2.7: stress elongation diagram [Lourenco et al., 2002]

The illustrated behavior indicates that, after reaching the peak load, the strength does not drop immediately to zero. Instead the strength is gradually reduced in a process denoted as “softening” [Lourenco et al., 2002]. The behavior up to the peak can be considered linear, but after the peak significant non-linearity is found in the response. The postpeak behavior can assume two different shapes, as illustrated in Figure 2.8, depending on the end restraints of the tested specimen. In Figure 2.8(a) the behavior is justified by the rotation of the specimen during

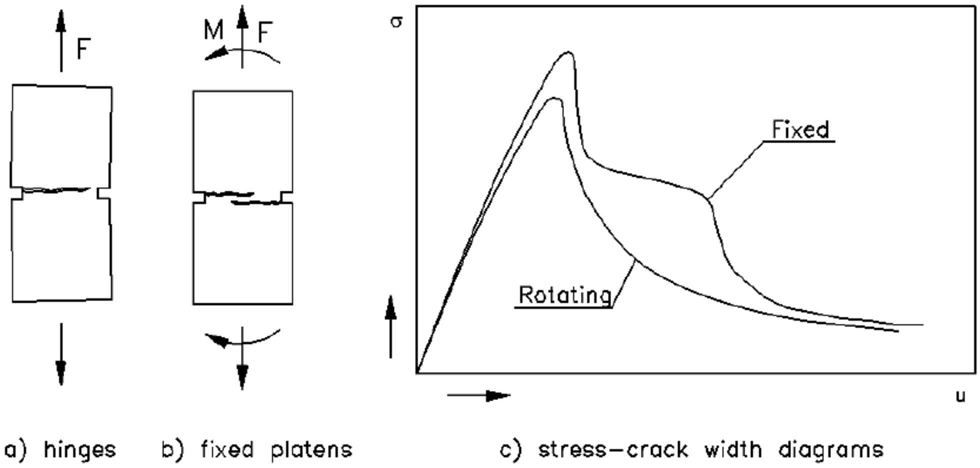

Figure 2.8: Rotating vs fixed restraints [Lourenco et al., 2002]

the loading operation, where the crack proceeds from one side of the specimen to the other side. In case of Figure 2.8(b), fixed (non-rotating) platens, a bending moment is introduced and multiple cracks will appear. This results in a slightly larger tensile strength and a higher value of energy dissipated (fracture energy)Lourenco et al. [2002].

Tension bond behaviour of brick and mortar interface is often the weakest link in masonry assemblages [Angelillo et al., 2014]. The non-linear response of the joints, which is then controlled by the unit-mortar interface, is one of the most relevant features of masonry behaviour. Two different phenomena occur in the unit-mortar interface, one associated with tensile failure (mode I) and the other associated with shear failure (mode II) [Angelillo et al., 2014]. Refer Figure 2.9.

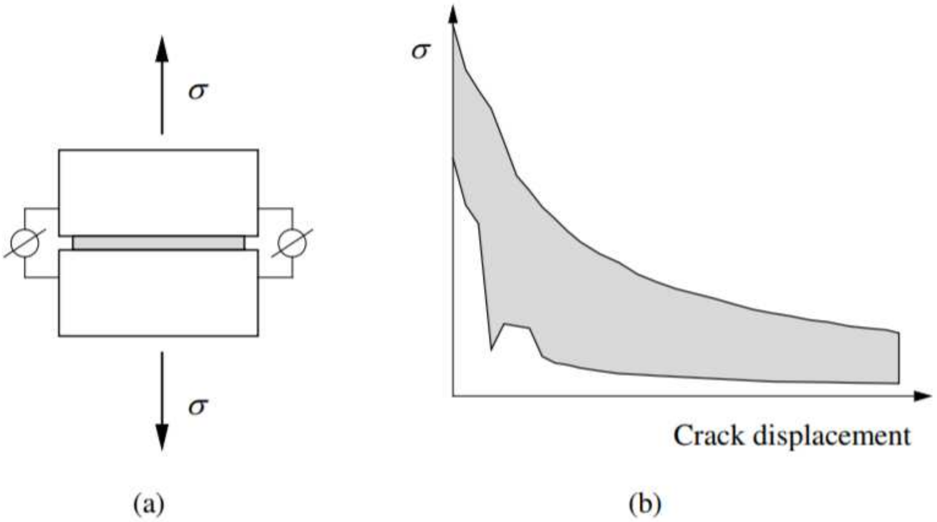

Figure 2.9: Tensile bond behaviour of masonry: (a) test specimen (direct tension); (b) typical experimental stress-crack displacement results for solid clay brick masonry (the shaded area represents the envelope of four tests), [Angelillo et al., 2014]

The parameters needed for the tensile mode (Mode I) are similar to the previous section, namely the bond tensile strength ft and the bond fracture energy Gf . The factors that affect the bond between unit and mortar are highly dependent on the units (material, strength, perforation, size, air dried or pre-wetted, etc.), on the mortar (composition, water contents, etc.) and on workmanship (proper filling of the joints, vertical loading, etc.) [Angelillo et al., 2014]. A recommendation for the value of the bond tensile strength based on the unit type or mortar type is impossible, but an indication is given in Eurocode 6 for the characteristic value (95% fractile), in the range of 0.1 to 0.4N/mm2 [Angelillo et al., 2014].

Uni-axial behaviour of masonry

In masonry, there is relatively low tensile strength between the bed joint and the unit. This joint easily fails when tensile loading perpendicular to the bed joint is applied. As a consequence, the masonry tensile strength can be considered as equal to the tensile bond strength between the unit and the joint [Lourenco, 1996]. In some masonry, the units may have numerous small perforations and the joints made up of high-strength mortar, resulting in a dowel effect. In such cases with low strength units and greater tensile bond strength between the bed joint and the unit, failure may occur as a result of stresses exceeding the unit tensile strength [Lourenco, 1996]. ”As a rough approximation, the masonry tensile strength in this case can be equated to the tensile strength of the unit” [Lourenco, 1996]. For tensile loading parallel to the bed joints the failure can occur in two different ways as shown in the Figure 2.10 [Lourenco, 1996].

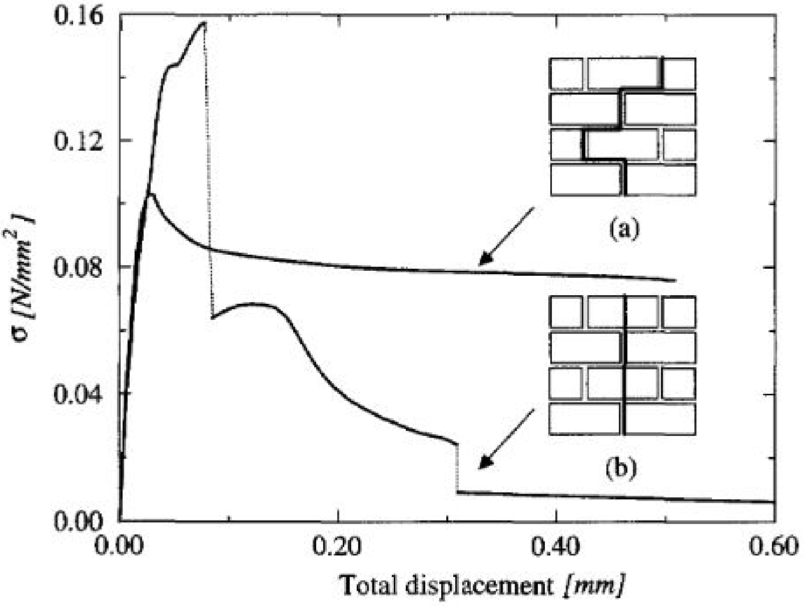

Figure 2.10: Experimental stress-dispalcement graph for tension parallel to the bed joint (a) failure occurs with a stepped crack through head and bed joints (b) failure occurs vertically through head joints and units [Lourenco, 1996]

Bi-axial behaviour of masonry

Masonry is an anisotropic material. The influence of bi-axial stress state cannot be described solely in terms of principal stresses [Lourenco, 1996]. Hence the constitutive behaviour of masonry under bi-axial stress state cannot be completely derived from the uni-axial constitutive behaviour. Therefore, the bi-axial strength envelope must be described in terms of the full stress vector in a fixed set of material axes or, in terms of principal stresses and the rotation angle θ (see Figure 2.11) between the principal stresses and the material axes. The strength envelopes are unique to a certain type of masonry [Lourenco, 1996]. Different strength envelopes for different failure modes are likely found for different materials, unit shapes and geometry [Lourenco, 1996]. Some important points regarding the distinction between uni-axial and bi-axial stress states are listed below.

- For uni-axial tension, cracking and sliding of head and bed joint leads to failure. Whereas, in bi-axial stress state with tensile stress and a lateral compressive stress the tensile strength decreases, which is due to the micro-slip of the joints and micro-cracking of the unit [Lourenco, 1996].
- Uni-axial compression also shows similar failure modes and bi-axial compression failure typically occurs by splitting of the specimen at mid-thickness, in a plane parallel to its free surface. The increase of compressive strength under bi-axial compression is due to the friction in the joints and internal friction between unit and mortar [Lourenco, 1996].

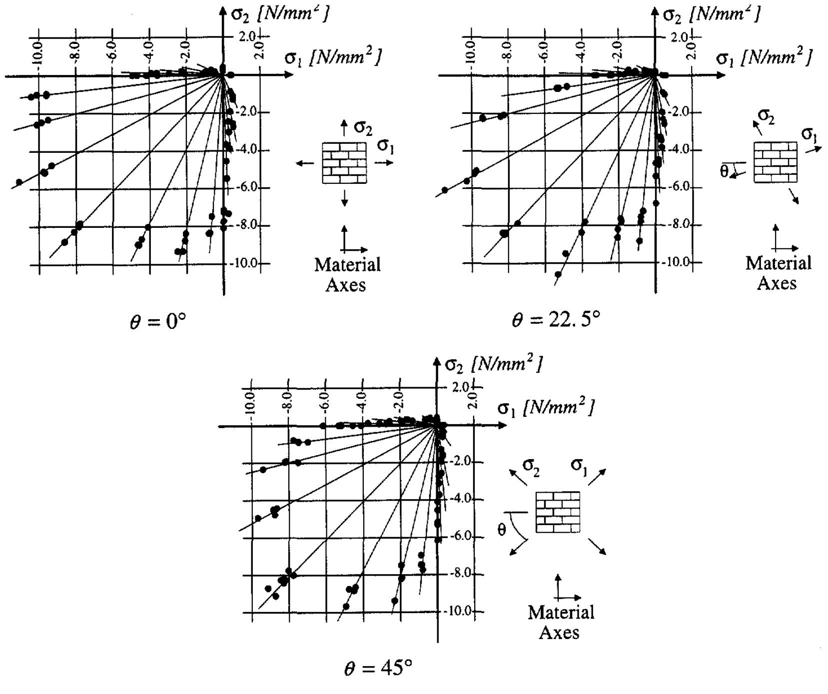

$\theta = 0°$

$\theta = 22.5°$

$\theta = 45°$

Figure 2.11: Bi-axial strength of solid clay unit masonry [Lourenco, 1996].

2.1.4 Shear

An important aspect in the determination of the shear response of masonry joints is the ability of the test set-up to generate a uniform state of stress in the joints [Angelillo et al., 2014]. This objective is difficult because the equilibrium constraints introduce non-uniform normal and shear stresses in the joint. Different test set-ups have been used for the characterisation of the shear behaviour of the unit-mortar interface. These include direct shear or couplet test and triplet test as shown in Figure 2.12 [Angelillo et al., 2014].

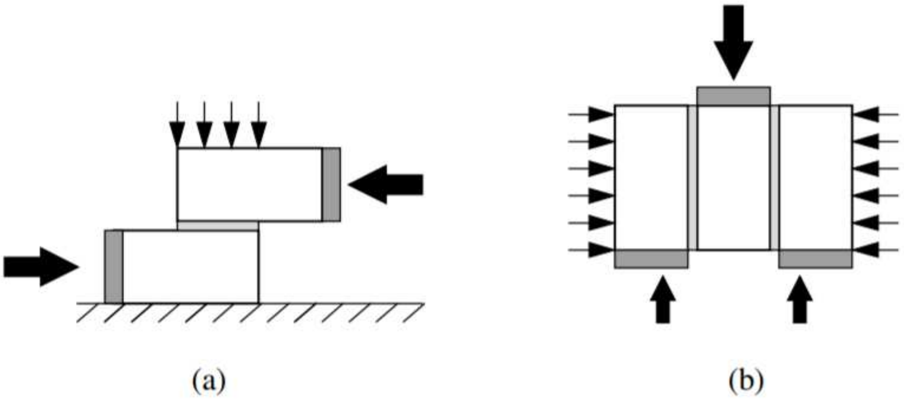

Figure 2.12: Test set-up for shear strength tests [Angelillo et al., 2014]

Experimental results yield typically an exponential shear softening diagram with a residual dry friction level and the envelop of the shear strength for different normal stress values provides the cohesion and the friction angle for a Coulomb type friction model as shown in Figure 2.13. [Angelillo et al., 2014]

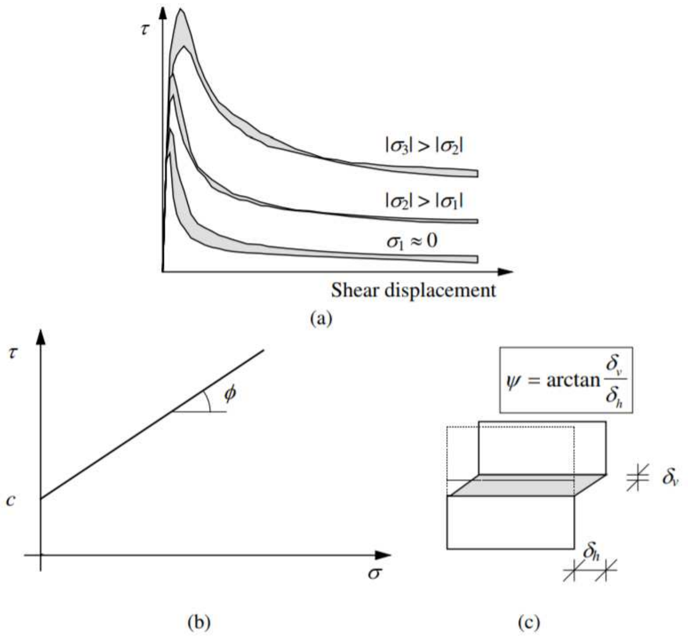

Figure 2.13: Shear bond behaviour: (a) typical stress-displacement diagram for different normal stress levels (b) cohesion and friction angle, (c) dilatancy angle [Angelillo et al., 2014]

2.2 Mechanical behavior of Concrete and Timber

Concrete, timber and masonry are very similar, in the sense that all three are composite materials and behave similarly under various loading. The magnitude and strength may be different but the response to different loads are the same. This is helpful in extending some numerical methods originally proposed for concrete or timber to masonry and viceversa.

If the concrete is looked upon as a two–phase material, then one should take irregular stress distribution into consideration. These stress irregularities are due to the difference in Young's modulus between the aggregates and the matrix material and due to existing pores and micro-crack [Hordijk, 1991]. Concrete also can be considered where the irregular stresses can be regarded to be averaged. This is called "macro level". This means that concrete will be considered as a homogenous isotropic continuum [Hordijk, 1991]. In a continuum it is assumed that after reaching the tensile strength, a crack will arise perpendicular to the direction of the maximum tensile stress. The fictitious crack model for fracture of concrete assumes existence of a fictitious crack ahead of a visible crack (a crack that cannot transfer tensile stresses) while the fictitious crack or process zone has crack-closing stresses ahead of crack tip as shown in Figure 2.14 [Hordijk, 1991].

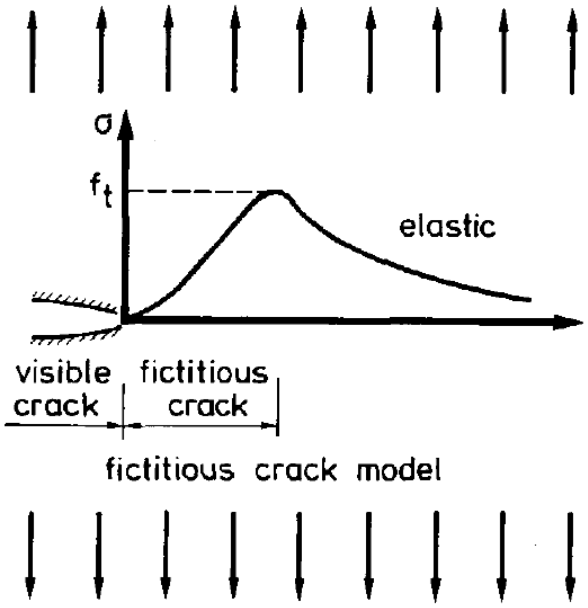

Figure 2.14: Fictitious crack model for concrete cracking [Hordijk, 1991]

2.2.1 Concrete in Tension

When a concrete bar is strained in uniaxial tension it first reacts elastically. A linear load deformation relation almost up to the peak load will be obtained. At peak load the strain starts to localize within a narrow zone of micro-cracks after which a continuous macro-crack develops [Hordijk, 1991]. If the process zone develops in the measuring length whose deformation is used as a control parameter, then the load-deformation relation as indicated by I occurs [Figure 2.15]. The load that can be transferred decreases with an increase in deformation. As a result of this the concrete outside this region unloads (line II) as shown in Figure 2.15 [Hordijk, 1991].

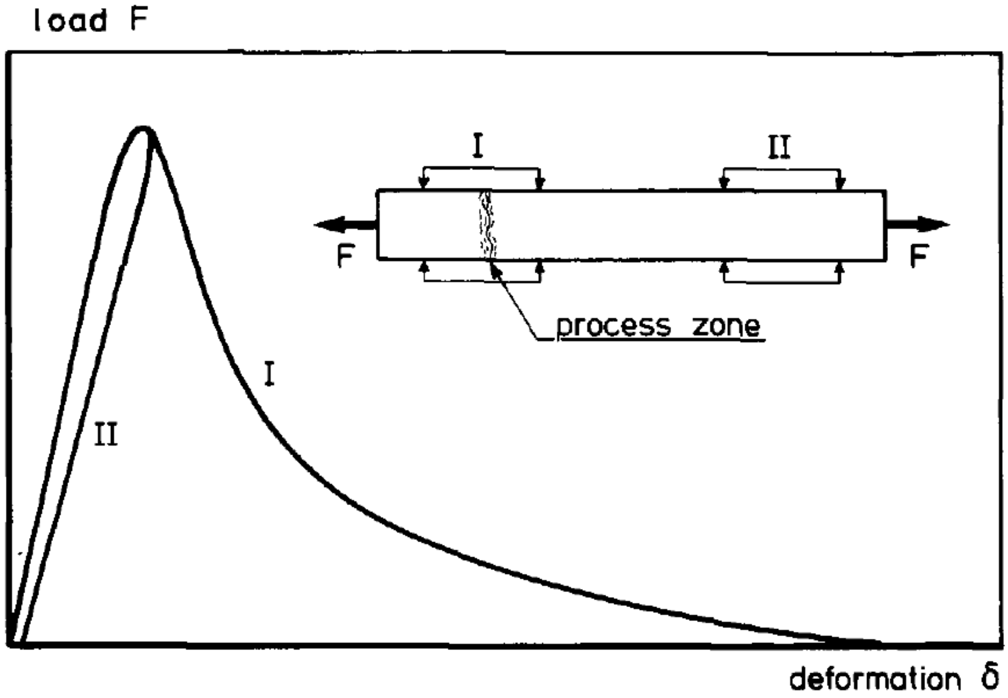

Figure 2.15: Concrete in tension [Hordijk, 1991]

According to this model the concrete under tensile loading can be split into a stress-strain relation for the concrete outside a crack and a stress crack opening relation for the crack itself [Figure 2.16] [Hordijk, 1991].

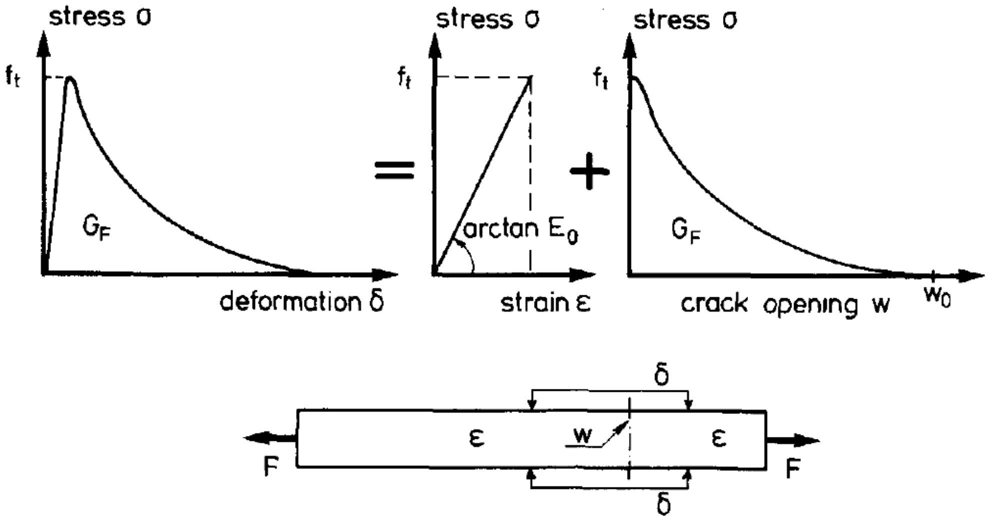

Figure 2.16: Tensile loading split into a stress-strain relation for the concrete outside crack and in the crack [Hordijk, 1991]

Concrete under cyclic loading in tension is based on the fictitious crack model in combination with a non linear description in the softening zone. From deformation- controlled uniaxial tensile tests on concrete, it is known that a loading cycle in the post-peak region of the stress-deformation relation displays a behavior as shown below [Hordijk, 1991]. It appears that after an unloading-reloading cycle, the curve will not return to the same point of the envelope curve where it started from, but to a point which belongs to a lower stress. This is due to the damage which is caused in such a loading loop as shown in Figure 2.17. Some mismatch of the micro-cracks may occur when unloading resulting in the propagation [Hordijk, 1991].

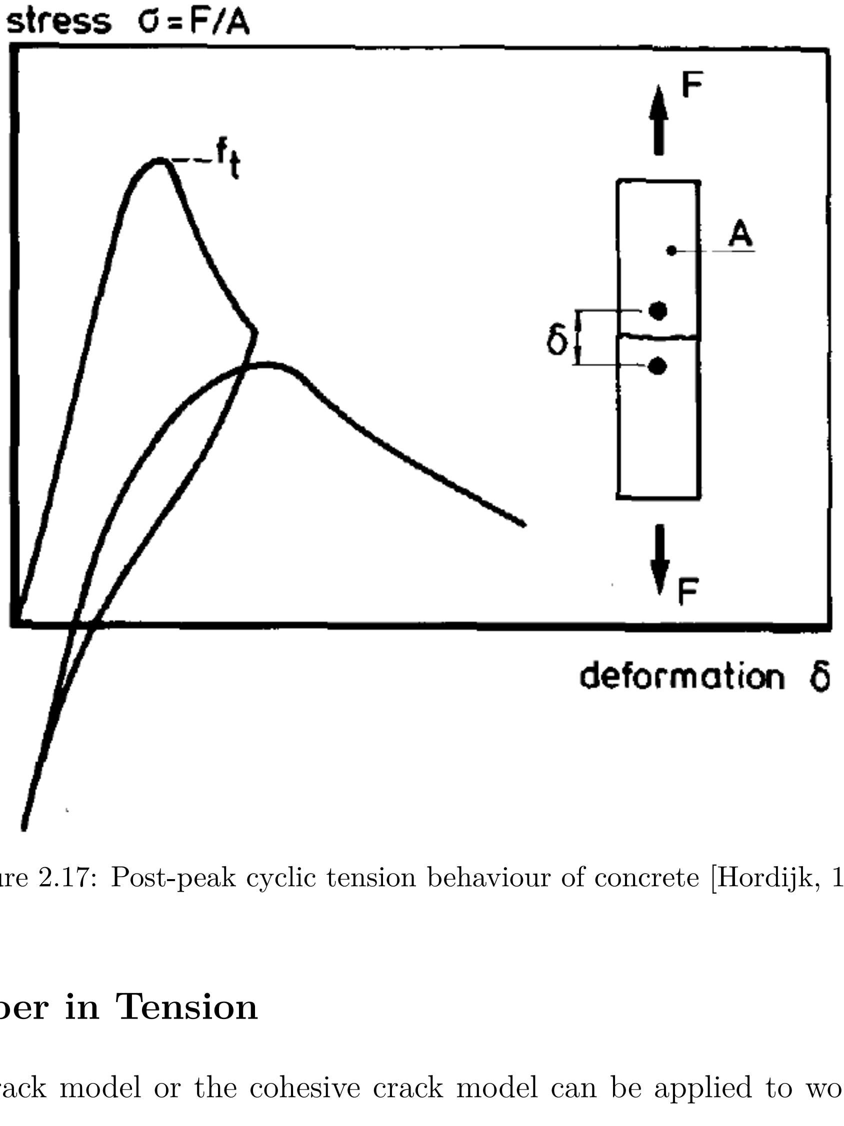

Figure 2.17: Post-peak cyclic tension behaviour of concrete [Hordijk, 1991]

2.2.2 Timber in Tension

The fictitious crack model or the cohesive crack model can be applied to wood as well. The model as explained before, assumes a fracture process zone ahead of the crack tip. In this zone all fracture mechanisms are assumed and localized [Schoenmakers, 2010]. Here the model does not assume an existing crack closing stress distribution, but instead , a constitutive relation is applied in the fracture process zone to model the fracture performance and is represented as shown in Figure 2.18. [Schoenmakers, 2010]

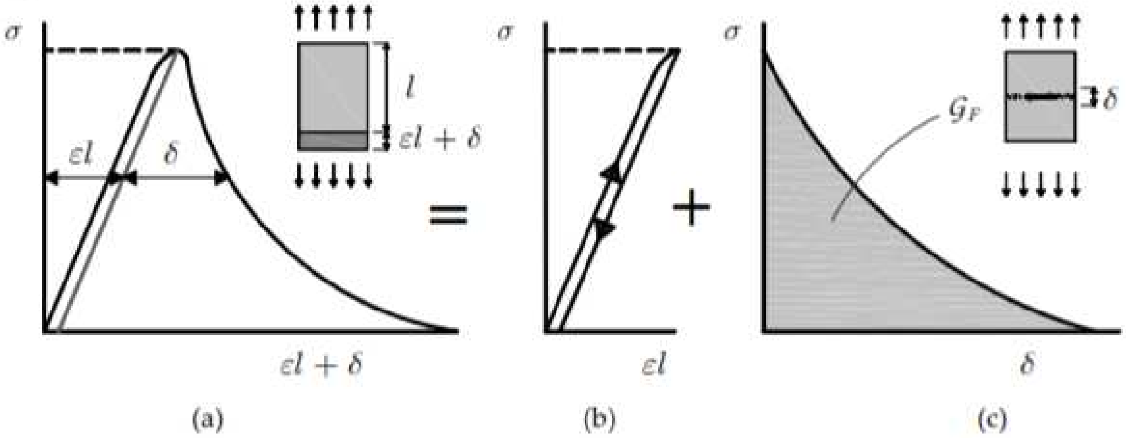

Figure 2.18: Constitutive response in case of uniaxial tension [Schoenmakers, 2010]

Approximate ranges of tensile (pure mode I) and combined tension and shear stress (mode II) vs displacement curves for normal spruce is shown in Figure 2.19.

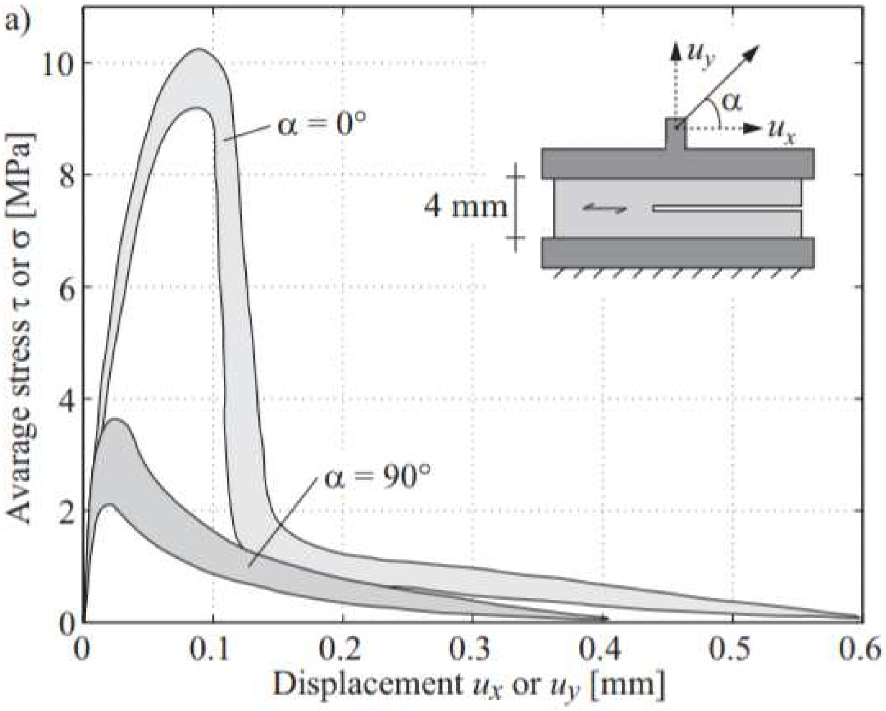

Figure 2.19: Approximate range of stress vs. displacement curves for pure mode I (α= 90) and mode II (α= 0) loading of Norway spruce [Danielsson, 2013]

2.3 Computational Modeling Techniques in Masonry

A number of tests have been conducted on masonry shear walls subjected to seismic type loading either by cyclic push over tests or shake table tests. In order to obtain an understanding of the behaviour in such tests the shear walls are primarily modeled using finite element methods. In the framework of the finite element method and masonry buildings, two different approaches may be described: The micro-modeling of single elements (discrete approach) or the macro-modeling of masonry as a composite material (continuum approach) [Calderini and Lagomarsino, 2008].

2.3.1 Micro-modeling

In the micro-modeling method, no simplifications with respect to discretisation of units, mortar and interface is made and are solved using non-linear finite elements. Such an approach would in principle allow to model and analyze any masonry structure, but there are actually several considerations that significantly limit the field of applicability of these models to small substructures, typically bi-dimensional [Penna et al., 2014]. The parameters required to define these models are derived from micro experiments in units, joints and small masonry samples. Many researchers have provided complex micro-mechanical models with extensive detail and accuracy when predicting the behaviour of masonry to seismic loading. The main drawback of these models is the complexity, efficiency and the high computational time required for obtaining the result. For further information the reader is directed to the following papers [Lotfi and Shing, 1994, Gambarotta and Lagomarsino, 1997, Zucchini and Lourenço, 2002, Lourenço and Rots, 1997].

2.3.2 Macro-modeling

In order to achieve good results with optimum time and effort, equivalent continuum models based on homogenized material derived from the mechanical properties of the components is used. This type of models are called macromodels as given by many authors for masonry [Pegon and Anthoine, 1997, Lourenco et al., 1998, Calderini and Lagomarsino, 2008] but was found to be limited in application to small structures under static monotonic loading. Other intermediate approaches which allow for reasonable compromise between accuracy and computational effort such as a macro-element approach implemented in an equivalent-frame model for walls is worth mentioning [Magenes and Della Fontana, 1998, Penna et al., 2014].

2.4 Engineering masonry model (EMM)

The new anisotropic total strain model or the EMM as introduced before includes the orthotropic behavior of masonry, by using different values for the elastic and inelastic properties in the two principal directions. In the elastic phase, anisotropy is considered. Poisson's ratio is set to zero for reasons of simplicity and robustness. Three pre-defined crack directions in the plane of the element are considered: two of them are set along the local x- and y-axes of the element, whereas a third one (t) is aligned to the diagonal direction determined by the pattern of the bed- and head-mortar joints [Rots et al., 2016]. Tensile cracking is assessed in the three directions normal to the crack planes (i.e. local x-, y- and n- directions); a secant nonlinear unloading and re-loading behavior, similar to that adopted in traditional total strain crack models, is assumed. Compressive crushing is assessed in the directions normal to the local x- and y-directions only (i.e. normal to head and bed-joints, respectively); a nonlinear non-secant unloading and reloading behavior is considered [Rots et al., 2016]. The in–plane shear stresses are limited by a standard Coulomb friction failure criterion, based on the stress normal to the bed-joint. Different elastic parameters are set in the direction of the bed- and head-joints. In order to improve the stability of the numerical procedure, the model assumes that there is no coupling between the stiffness of the normal components in the x- and y-directions and that of the in–plane shear component; any interaction between the normal components is also neglected [Figure 2.20] [Rots et al., 2016]

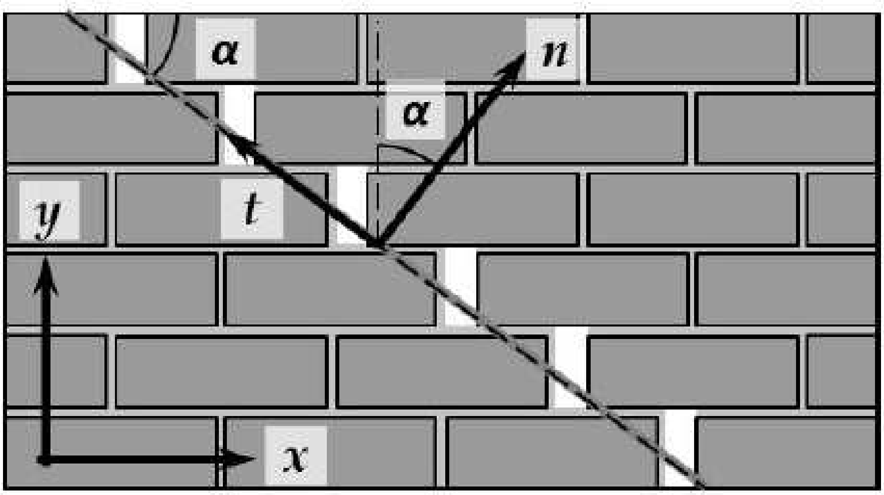

Figure 2.20: Pre-defined crack direction (x, y, n) included in the constitutive model[Rots et al., 2016]

2.4.1 Tension constitutive model

In the element local x- and y-directions, positive tensile stresses are computed according to an uniaxial relation, based on the respective strain component (ϵ_i), the value of the maximum strain that has ever been experienced during the loading history (ϵ_{ti}) and the corresponding stress (σ_{ti}), where i takes the value 1 for the x-direction, and 2 for the y-direction. The tensile uniaxial stress – strain curve for each local direction is defined by the Young's modulus (Ei), the tensile strength (fti), and the crack fracture energy (Gfti) as shown in Figure 2.21 [Rots et al., 2016].

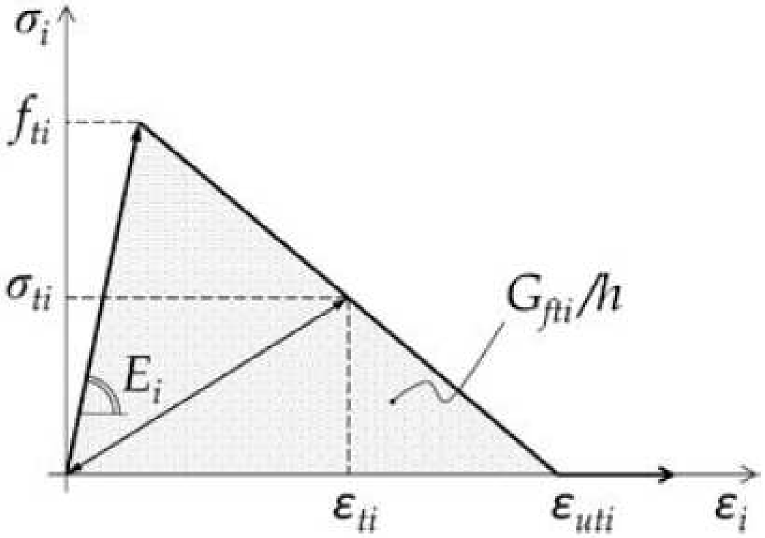

Figure 2.21: Uniaxial tensile stress-strain curve normal to the local axes (x,y)[Rots et al., 2016]

A linear softening curve is assumed, and the ultimate tensile strain is defined as the strain value at which the crack is fully open and no stress can be transferred. Consequently, it can be computed according to the following equation [Rots et al., 2016].

$$\varepsilon_{uti} = 2G_{fti} / (h f_{ti})$$

where h is the crack bandwidth of the element, over which the crack is smeared, related to the size of the finite element. Secant unloading and reloading is assumed. If head-joints are assumed to be unable to transfer any tensile strength, masonry failure can occur when either bricks fail in tension (mechanism a), or shear slip takes place along the bed-joints (mechanism b) [Rots et al., 2016]

2.5 Degradation

Degradation, in the context of civil engineering degradation is defined as a loss of the relevant properties of materials which proceeds gradually due to exposure to in-service conditions [Krzysztof et al.]. In masonry, it is usually the gradual disintegration of unit and mortar and the interface under the effect of different types of loading. Usually when masonry is subjected to cyclic loading so as to simulate the effect of earthquakes on such a structure the first cracks that appear are due to masonry being weak in tension [Naraine and Sinha, 1989]. The masonry may ultimately fail due to progressive cracking or by rocking or crushing mechanisms but the primary reason for these failure is the growing loss of strength and stiffness [Naraine and Sinha, 1989]. This is of particular interest when the loading is not strong enough to cause complete failure of the structure , but is strong enough to cause cracking.

2.5.1 Cyclic degradation in Concrete

The cyclic behaviour and the fatigue behaviour of concrete have been studied for decades by many researchers and many models have been proposed to represent the different aspects of repeated unloading-reloading behaviour.

One of such significant research is that of Otter et al. [Otter and Naaman, 1989], who provides a complete overview of all the mathematical models present for accounting for the cyclic behavior and provides a continuous function model for reloading and unloading based on compressive tests performed on concrete. This model is based on a combination of linear and exponential terms as shown in Figure 2.22 and also takes into account the change in plastic strain due concrete subjected to random cyclic loading [Otter and Naaman, 1989].

$$\frac{f}{f_{hi}} = (1-p)\left(\frac{\epsilon-\epsilon_p}{\epsilon_{hi}-\epsilon_p}\right) + p\left(\frac{\epsilon-\epsilon_p}{\epsilon_{hi}-\epsilon_p}\right)^{n_{uc}} \quad \ldots\ldots\ldots\ldots\ldots\ldots\ldots\ldots\ldots \quad (8)$$

Figure 2.22: Continuous function for unloading-reloading behaviour [Otter and Naaman, 1989]

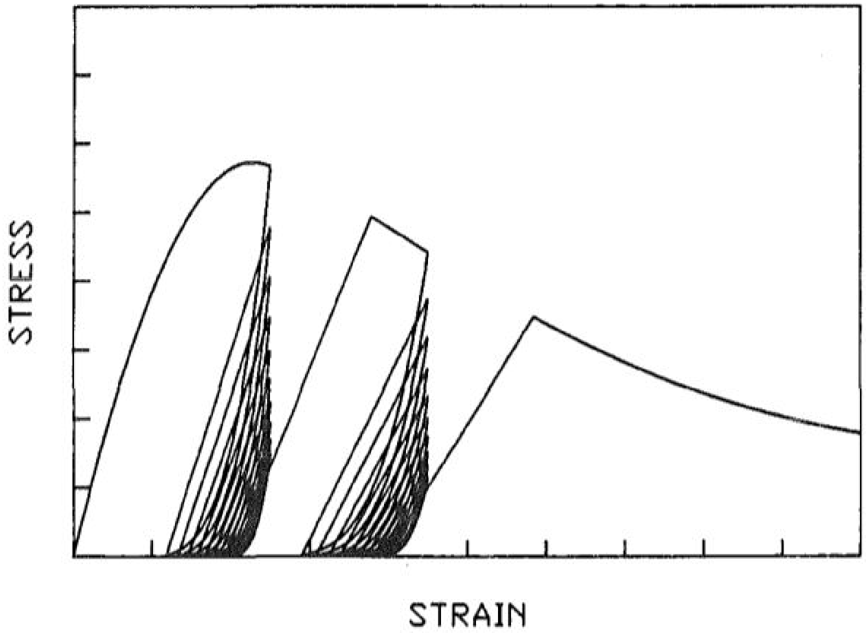

Figure 2.23: Model generated response to cyclic loading for a cylindrical sample to specified strain [Otter and Naaman, 1989]

The experimental campaign done by Greco et al on three concrete specimens with and without reinforcements also show similar results of degradation. The results show a curved reduction of strength as the number of cycles increases as shown in Figure 2.23 to Figure 2.25[Greco et al., 1996].

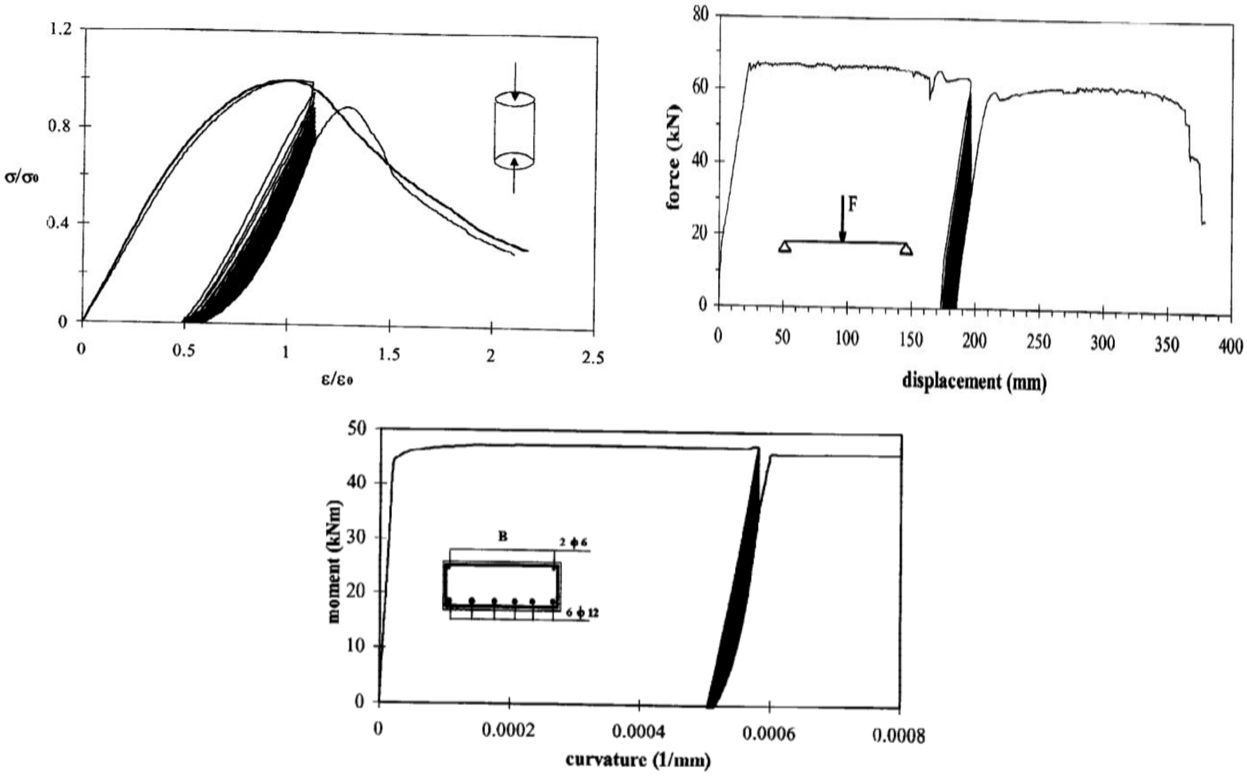

Figure 2.24: Experimental results for a cylindrical specimen, slab and a box beam [Greco et al., 1996]

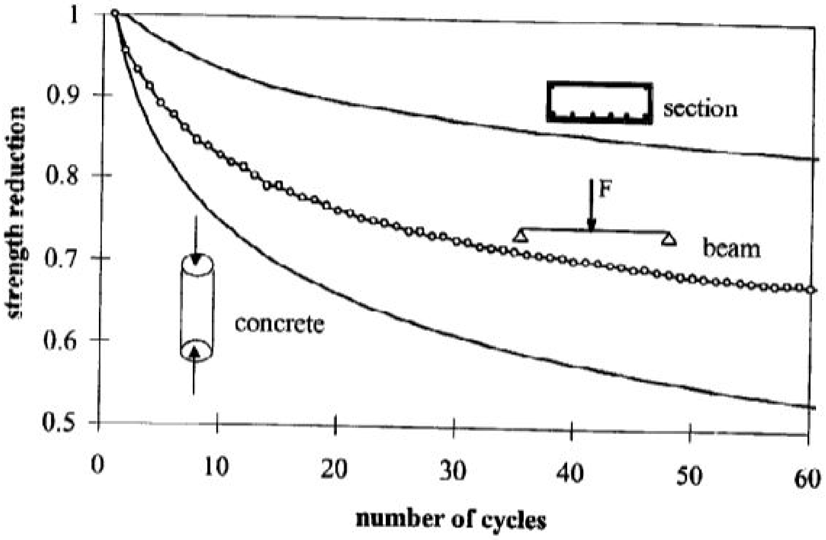

Figure 2.25: Strength reduction for the three specimens [Greco et al., 1996]

Naraine and Sinha proposed analytical expressions for the stress - strain envelope curve, the common point curve and the stability point curve based on experimental results of brick masonry under cyclic compression. Refer Figure 2.26.

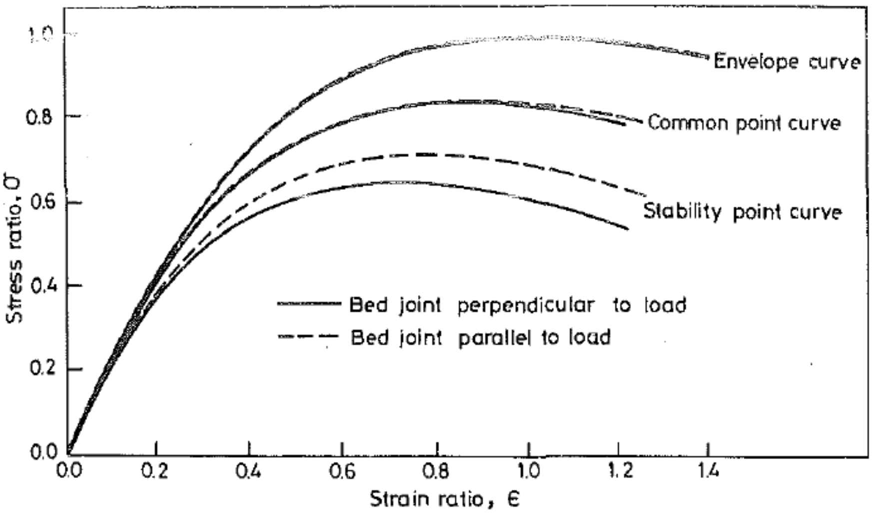

Figure 2.26: Envelope curve, common point curve and stability point curve for cyclic comprresive tests [Naraine and Sinha, 1989]

There are a number of finite element models available for representing tension softening as shown in Figure 2.27, but none of them consider the gradual degradation aspect of the composite material when subjected to unloading-reloading.

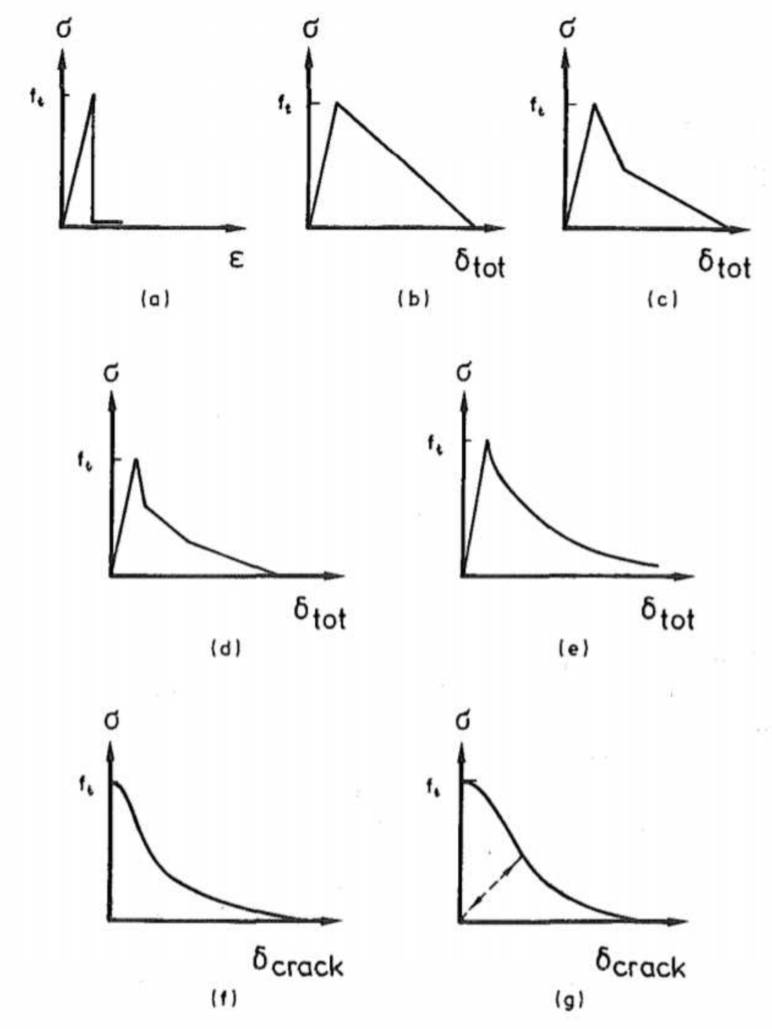

Figure 2.27: Finite element models available for tension softening [Yankelevsky and Reinhardt, 1989]

Focal point model

Yankelevsky and Reinhardt considered 4 different types of unloading-reloading curves for uniaxial cyclic tension of concrete and formulated a mathematical model called as focal point model [Yankelevsky and Reinhardt, 1989]. The model is based on geometrical properties of cyclic stress-strain curves as shown in Figure 2.28, and defines focal points which are used to reproduce the complete unloading-reloading cycles. This model takes into account the degradation and loss of stress experienced by the concrete during unloading and reloading cycles. For further information regarding the model details, the reader is directed to [Yankelevsky and Reinhardt, 1989].

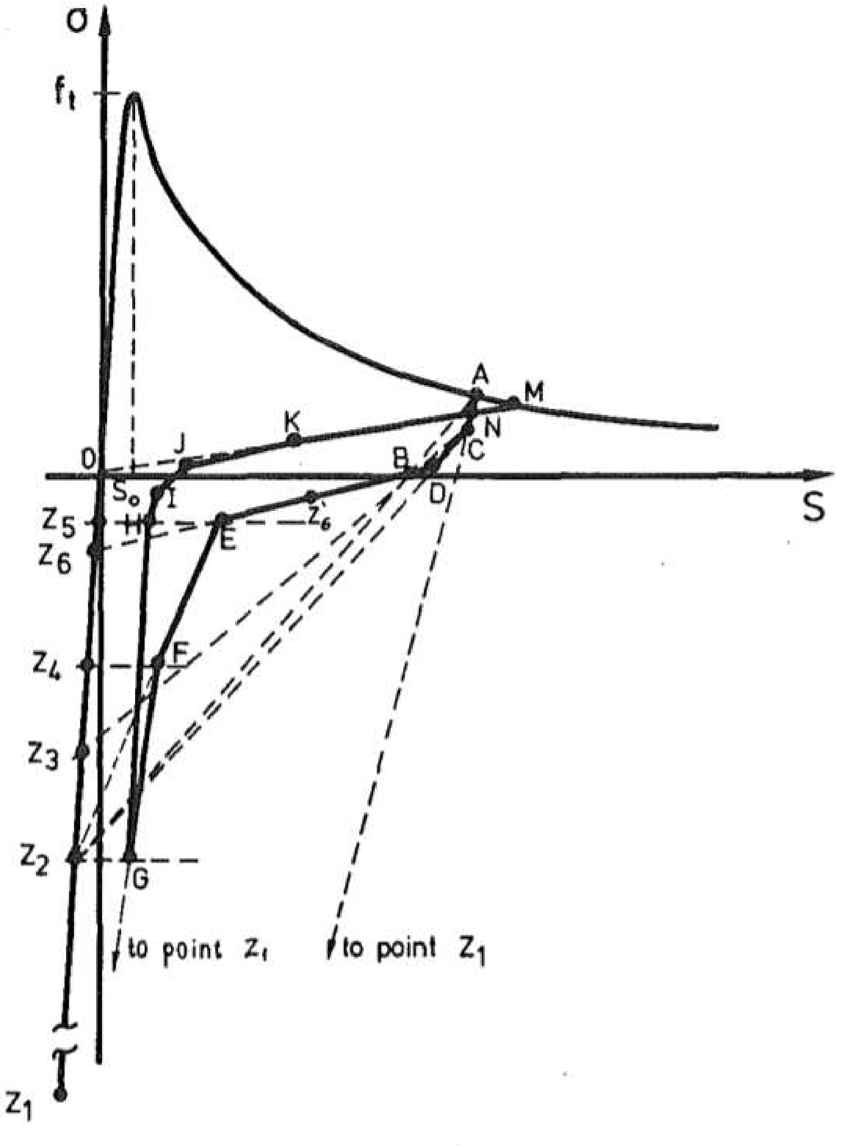

Figure 2.28: Focal point model scheme [Yankelevsky and Reinhardt, 1989]

2.6 Conclusion from literature review

From the examination of literature, it is clear that, although promising work has been done to represent the degradation aspect of concrete using mathematical models and micro mechanical models, there is still a gap for developing a complete macro model which is reliable and robust for analysis of masonry structures.

The model proposed by Yankelevsky and Reinhart (1989), Greco et al (1996), Naraine and Sinha (1989) and the huge compilation of mechanics of masonry structures given by Angelillo (2014) provides a good starting point for the work. The following steps are performed step by step to realize the main objective of implementing degradation in EMM.

1. Framing constitutive equations based on a unloading reloading model in tension mode I.
2. Transforming the equations into step-by-step FORTRAN code for user supplied subroutines.
3. Implementing the code in the latest user supplied subroutines.
4. Modeling in DIANA and checking if the model works and troubleshooting.
5. Validating and calibrating the model with window bank tests.

Chapter 3

Model for the Implementation of Degradation

In the last section of chapter two, various models to depict the cyclic degradation in finite element modeling(FEM) of concrete and masonry structures have been discussed. Although these models are robust, they are highly complicated for macro-modeling of masonry and do not consider the effects of light repetitive loading which are very important for earthquake loading. A masonry unit is generally made up of bricks glued together with mortar. This increases the variability of material properties in every direction. Formulating the characteristics at a micro level is time consuming, expensive and not suitable for global analysis. Hence masonry is generally modeled as a continuum element with smeared crack property. Recently, more and more researchers have recognized that micro-modeling techniques are not suitable to analyse the response of masonry on a global level because of the computational burden [Nobel, 2017]. In this section, a new mathematical model for implementing degradation of masonry structures is presented along with the constitutive equations suitable for the EMM in DIANA. Further, the proposed new model is implemented in the User Supplied Subroutine (USS) for EMM.

3.1 Mathematical model

The mathematical model for implementing strength degradation is based on the concept of hyperbola. The idea stems from the fact that, the experimental results of force reduction per displacement set as seen in Figure 1.1 closely follows the shape of a hyperbola. Hence, a small introduction and a mathematical background related to hyperbolic functions is given in the following sections.

“Hyperbola”

Conic sections are generated by the intersection of a plane with a cone. If the plane is parallel to the axis of revolution (the y-axis), then the conic section is a hyperbola [OpenStax, 2018].

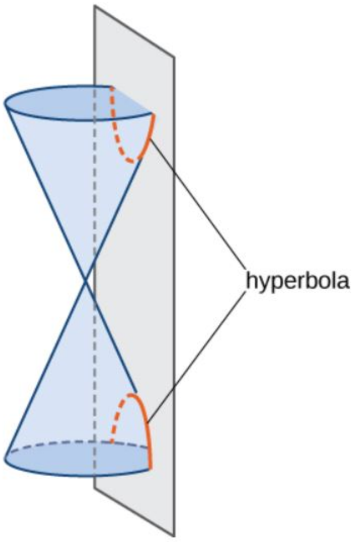

“Hyperbolic function”

Functions of the form $f(x) = (a/x) + q$ are called hyperbolic functions, where a and q are constants . Further, the hyperbolic function $y = (a/(x + p)) + q$ is considered and the effects of each term on the shape of the graph is studied [Siyavula, 2018].

The domain is $x : x \in R, x \neq -p$. If $x = -p$, the denominator is equal to zero and the function is undefined.

We see that

$$y = (a/(x + p)) + q$$
$$y - q = a/(x + p)$$
$$(y - q)(x + p) = a$$

The range is therefore $y : y \in R, y \neq q$.

These restrictions on the domain and range determine the vertical asymptote $x = -p$ and the horizontal asymptote $y = q$.

Effect of a, q and p on vertical shift

The effect of ‘q’ on vertical shift [Siyavula, 2018].

- For $q > 0$, f(x) is shifted vertically upwards by q units.
- For $q < 0$, f(x) is shifted vertically downwards by q units.

- The horizontal asymptote is the line $y = q$.
- The vertical asymptote is the y-axis, the line $x = 0$.

The effect of ‘a’ on shape and quadrants [Siyavula, 2018].

- For $a > 0$, f(x) lies in the first and third quadrants.
- For $a > 1$, f(x) will be further away from both axes than $y = x$.
- For $0 < a < 14$, as a tends to 0, f(x) moves closer to the axes than $y = x$.
- For $a < 0$, f(x) lies in the second and fourth quadrants.
- For $a < -1$, f(x) will be further away from both axes than $y = -x$.
- For $-1 < a < 0$, as a tends to 0, f(x) moves closer to the axes than $y = -x$.

The effect of p is a horizontal shift because all points are moved the same distance in the same direction (the entire graph slides to the left or to the right) [Siyavula, 2018].

- For $p > 0$, the graph is shifted to the left by p units.
- For $p < 0$, the graph is shifted to the right by p units [Siyavula, 2018].

Figure 3.1 gives a detailed overview of different forms of hyperbola based on the above explanation.

	$p > 0$		$p < 0$	
	$a < 0$	$a > 0$	$a < 0$	$a > 0$
$q > 0$	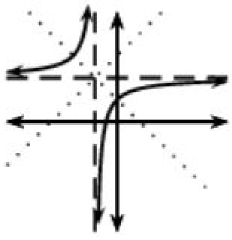	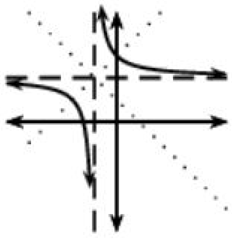	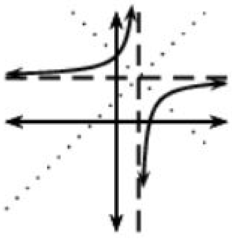	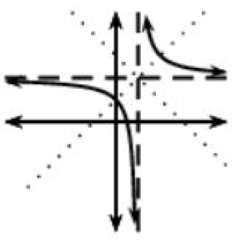
$q < 0$	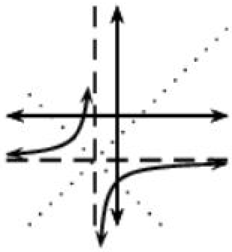	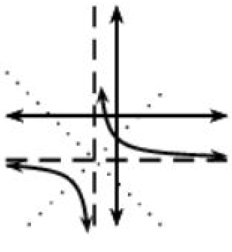	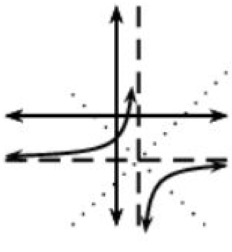	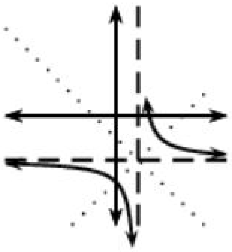

Figure 3.1: Different forms of hyperbola [Siyavula, 2018]

3.2 Constitutive model

The reduction in the stress at certain constant strain is obtained by the use of a degradation factor λ_{tj} which is dependent on the tensile strength, the unloading point and the point up to which it is unloaded and is given as follows.

$$\lambda_{tj} = 0.85^{(P_f)} - \left\{ \frac{f_{ti} - \sigma_{uj}}{\xi_d * f_{ti} + \sigma_{rj}} \right\} \tag{3.1}$$

where, P_f is the partial unloading factor given by,

$$P_f = \left(1 - \frac{\epsilon_{r1}}{\epsilon_{u1}}\right) \tag{3.2}$$

ϵ_{r1} = Strain at the first reloading point, i.e. the first reloading point of the first cycle.

ϵ_{u1} = Strain at the first unloading point on the envelope curve.

λ_{tj} = Degradation factor. Where, j = 1,2,3...n

f_{ti} = Tension strength of masonry.

i = 1,2 for x, y directions respectively.

σ_{uj} = Stress at unloading point for j^{th} cycle. Where, j = 1,2,3...n

σ_{rj} = Stress at reloading point for j^{th} cycle. Where, j = 1,2,3...n

n = number of unloading-reloading cycles.

ξ_d = Calibration constant.

The existing tension stress-strain behaviour in the EMM is shown in Figure 2.21 and the proposed change to the unloading and reloading branch is given in Figure 3.2.

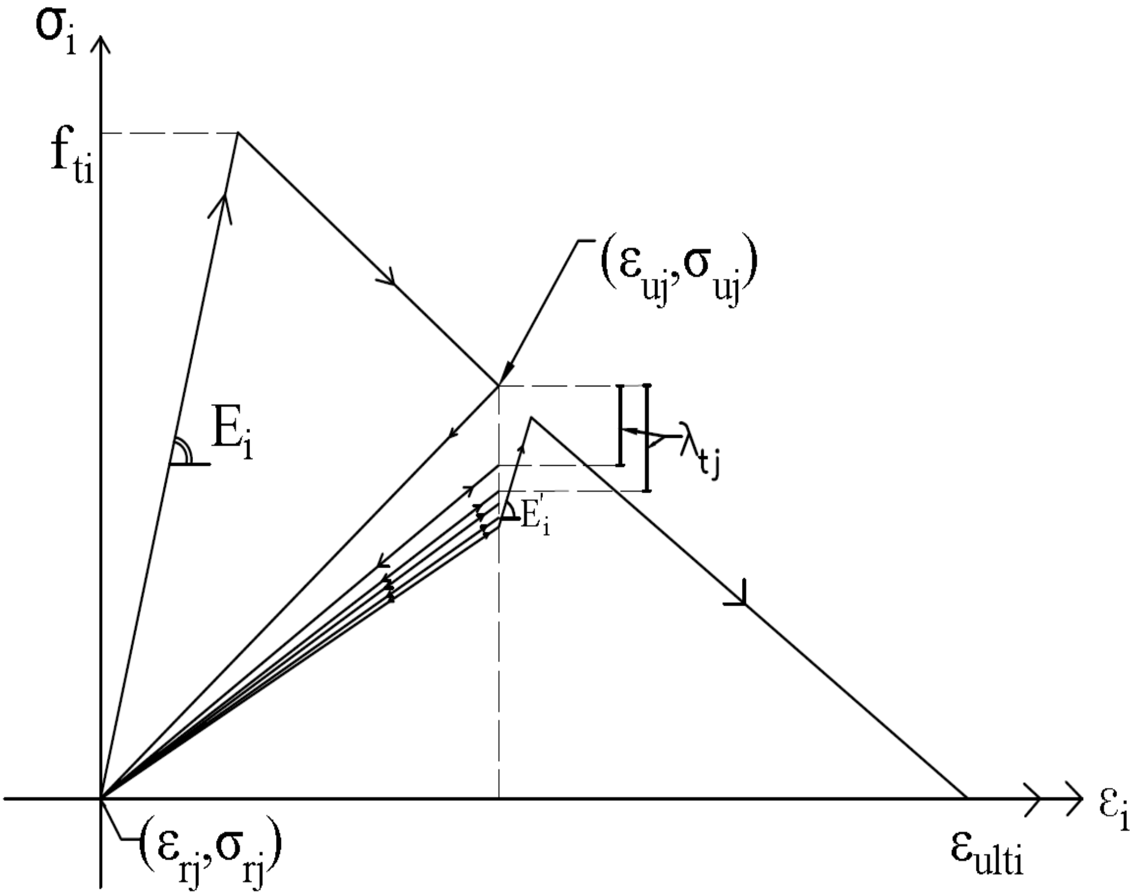

Figure 3.2: New Uniaxial tensile stress-strain curve normal to the local axes (x,y)

The value of 0.85 for complete unloading cycle is chosen based on the experimental observations made by Yankelevsky et al.[Yankelevsky and Reinhardt, 1989], Hordijk et al. [Hordijk, 1991] and Naraine et al. [Naraine and Sinha, 1989]. They observed that the first reduction for a complete unloading cycle will be in the range of 0.7 to 0.9 depending on the type and direction of loading, which is widely accepted. This is reflected in the mathematical equations proposed by each author, with Yankelevsky's focal point model assuming 0.85, Hordijk's continuous function model taking value of 0.75 and Naraine's model considering 0.83 and 0.87 depending on the direction of loading.

The partial unloading factor is introduced to take into account the effect of partial unloading from the unloading point and the subsequent change in the amount of stress reduction. The exact change in values of unloading and reloading points are dealt with in chapter 5 in detail. The factor is dependent on unloading strain and the strain upto which it is unloaded.

The slope of the line joining the envelope curve after cyclic degradation [see E'_i (Figure 3.2)] has been chosen based on the experimental observations and models proposed by Otter and Naaman [Otter and Naaman, 1989] and Greco et al [Greco et al., 1996]. Otter et al. gave a model taking into account the energy dissipation during unloading- reloading cycles of concrete under uni-axial compressive loading. The model considers key end points which depend on the envelope unloading strain and the initial elastic slope. He observed that although the energy loss and stress reduction were due to the crack propagation during repetitions, it was not sufficient to categorically say that the structure was damaged. Further, Greco et al. observed that the stress reduction after every repetition cannot be considered as the effective strength degradation as the cyclic curve can return up to the monotonic one. He also outlines that stress reduction is observed because there is an increment of the plastic strain at the reloading point. Following these observations, for the new model, the slope of the line from the final reloading branch joining the envelope curve is considered to be parallel to the elastic branch (i.e. $E_i' = E_i$).

From the above equation, let f_{ti} = x, σ_{uj} = p, σ_{rj} = q, λ_{tj} = y and P_f = 1.0 (complete reloading)

We get

$$
\begin{gathered}
y = 0.85 - ((x-p)/(x-q)) \\
y = 0.85 - ((x-q+q-p)/(x-q)) \\
y = 0.85 - (1 + (q-p)/(x-q)) \\
y = -0.15 + ((q-p)/(x-q)) \\
(y+0.15)(x-q) = (q-p) \qquad (3.3)
\end{gathered}
$$

This equation represents a hyperbola.

3.2.1 Limitation of the model

- The main limitation of this model is the absence of plastic strain at the reloading point.

  This in-turn results in, the slope E_i' of the line joining the last repetition and the envelope curve to be equal to the Young's modulus of masonry. Intuitively, this line must continue with the same slope as that of the last repetition so that the stress reduction is also carried forward. But in this proposed model the slope E_i' has been assumed to be equal to the elastic branch i.e. E_i.

  An improved version of this model by introducing the plastic strain at the reloading point has been proposed in the appendix B by which, the slope of the last repetition can be extended till the envelope is reached.

NOTE:-

Three different slopes E_i' for the line joining the last unloading point to the envelope curve has been tested as shown in Figure 3.3: (1) parallel to elastic region (2) parallel to first secant unloading (3) continuing the slope of last repetition.

It was found that the slope parallel to elastic region gives the most accurate results. The problem with the other two methods is that the successive repetitions show large amount of degradation and fail easily (sometimes not even completing 10 repetitions). This can be explained in two ways:

(a) If the slope of the last repetition of a displacement set is carried forward (type 3), then there is a high energy loss(area under the stress-strain curve) which cannot be accounted for. This means that, for a large structure, the successive displacement set has lower internal energy to resist the loading. This results in failure of the specimen easily.

(b) Every point on the softening branch represents a magnitude of damage, i.e. a point closer to the peak strength has low damage(or high capacity) and a point closer to the ultimate strength has high damage (or low capacity). Hence, if the slope is carried over from the last repetition then the point at which it intersects the envelope curve is closer to ultimate strength, meaning low capacity. This makes the rest of the repetition sets to fail easily. It was also seen that when the loading reached the next repetition set, the crack jumped few elements and continued with further increase in loading. Degradation at a certain point along the softening branch results in crack propagation of an already existing crack, but does not generate new cracks.

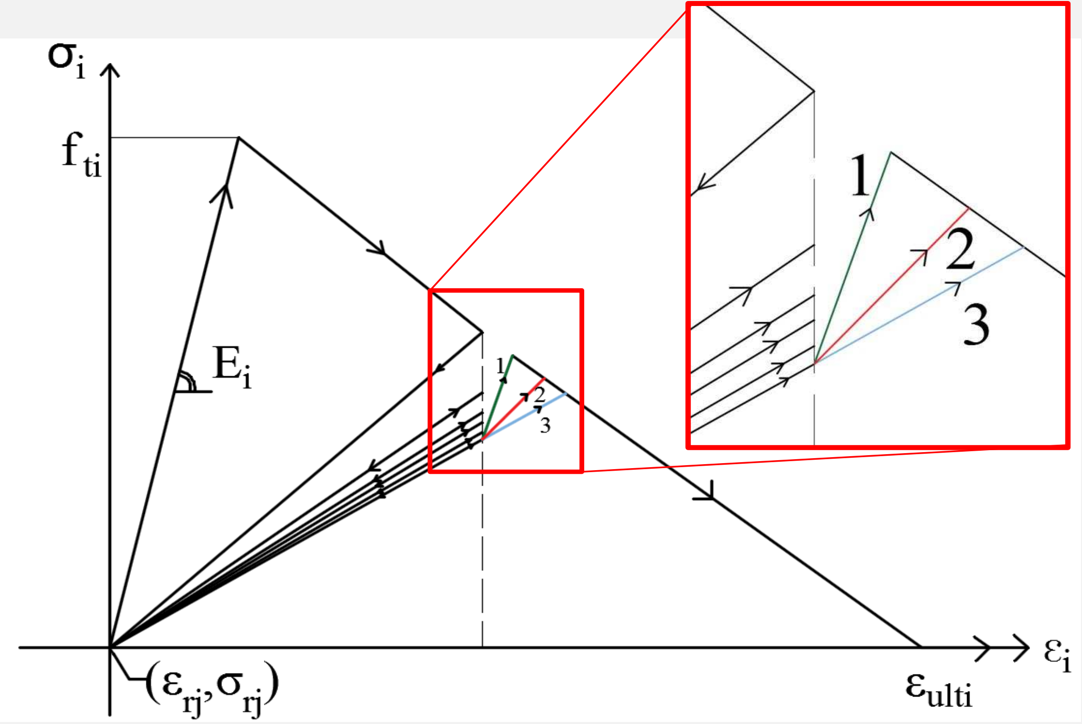

Figure 3.3: Different reloading slopes

The degradation factor for every unloading-reloading cycle is shown in the Figure 3.4. All degradation factors are measured from the first unloading point. Hence λ_{tj} always lies between 1.0 and 0.

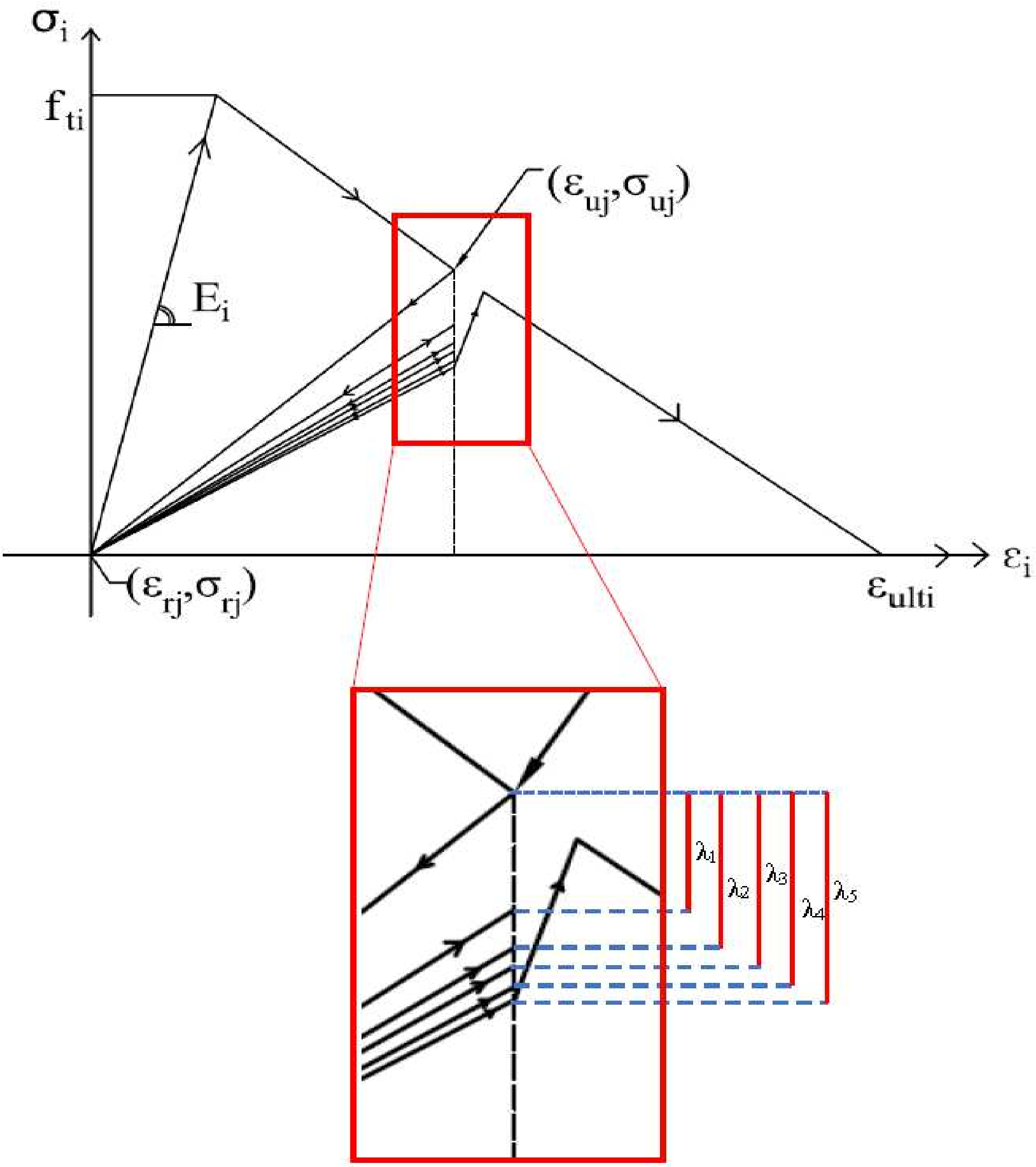

Figure 3.4: Degradation factor after every unloading-reloading cycle

The stress σ_{u1} for the first unloading cycle starts from the envelope curve which is the first unloading point in the stress-strain plot. The unloading follows along a secant slope to reach the reloading point with coordinates as (ϵ_{r1},σ_{r1}). This point is (0,0) for complete unloading. As the strain starts to increase, the reloading cycle begins, with the λ_{t1} value calculated based on equation 3.1. The reloading branch ends when the strain at first unloading point is reached. Further, the second unloading point σ_{u2} is given by (σ_{u1} * λ_{t1}). The second unloading cycle follows the previous reloading path to reach the second reloading point with co-ordinates (ϵ_{r2},σ_{r2}). For full unloading, these co-ordinates are always the origin, but for partial unloading it is updated after every unloading branch. The process repeats for n number of unloading-reloading cycles. The unloading points, the reloading points and the value of degradation factor are stored and updated in every cycle. The stress value σ_{rj} is the point upto which each cycle is unloaded. This value always lies between 0 and σ_{uj}.

3.3 Flowchart for the User Supplied Subroutine

DIANA offers the end user the opportunity to supply FORTRAN source code of some predefined subroutines[DIANA, 2010]. USRMAT is the user supplied subroutine containing the material properties and the post-processing data for EMM and is written in FORTRAN 77 language style. The complete USS for the Engineering Masonry Model including the new degradation model is given in appendix A. The part of this USS detailing the tension stress-strain behaviour of masonry with the new unloading-reloading branch is presented below.

The step by step progress of the new code is represented in the form of a flow chart in Figure 3.5. Refer also Figure 3.6 and Table 3.2 for a representative example along with the procedure. Before the unloading - reloading cycle of tension constitutive model starts, the values of λ_{tj}, σ_{uj} and σ_{rj} are set to 1.0, 0 and 0 respectively. This is represented by the point 1 in Figure 3.6.

In order to differentiate between the unloading and reloading branch, the current updated strain is checked with the strain at the beginning of the increment. If the current strain is less than the first increment, unloading loop begins and if it is greater, then reloading starts. The first unloading point on the envelope is represented by point 2 in Figure 3.6.

First the unloading cycle starts from the envelope curve. Since λ_{t0} is equal to 1.0 for the first branch, the curve has a secant slope to zero in the case of full unloading. The values at the end of the unloading branch representing the reloading point (ϵ_{r1},σ_{r1}) are stored as user state variables. This point is represented as 3 in Figure 3.6.

At this point the current updated strain is larger than the strain at the beginning of increment, which represents the start of the reloading branch. In the reloading cycle λ_{t1} is first calculated based on the equation 3.1 as given before (refer Table 3.2). This updated λ_{t1} is multiplied with the slope of the first unloading branch ($\sigma_{u1}/\epsilon_{u1}$) to obtain the reduced stress at the unloading strain (σ_{u2}). The values of λ_{t1}, σ_{u2} are stored as user state variables. This point is represented as 4 in Figure 3.6.

The next unloading branch follows the slope of the previous reloading branch since the value of λ_{t1} is now updated and does not change. This point is 5 in Figure 3.6. This process is repeated for 'n' number of cycles until the current updated strain exceeds the first unloading point (ϵ_{u1},σ_{u1}). This point is represented as 6 in Figure 3.6.

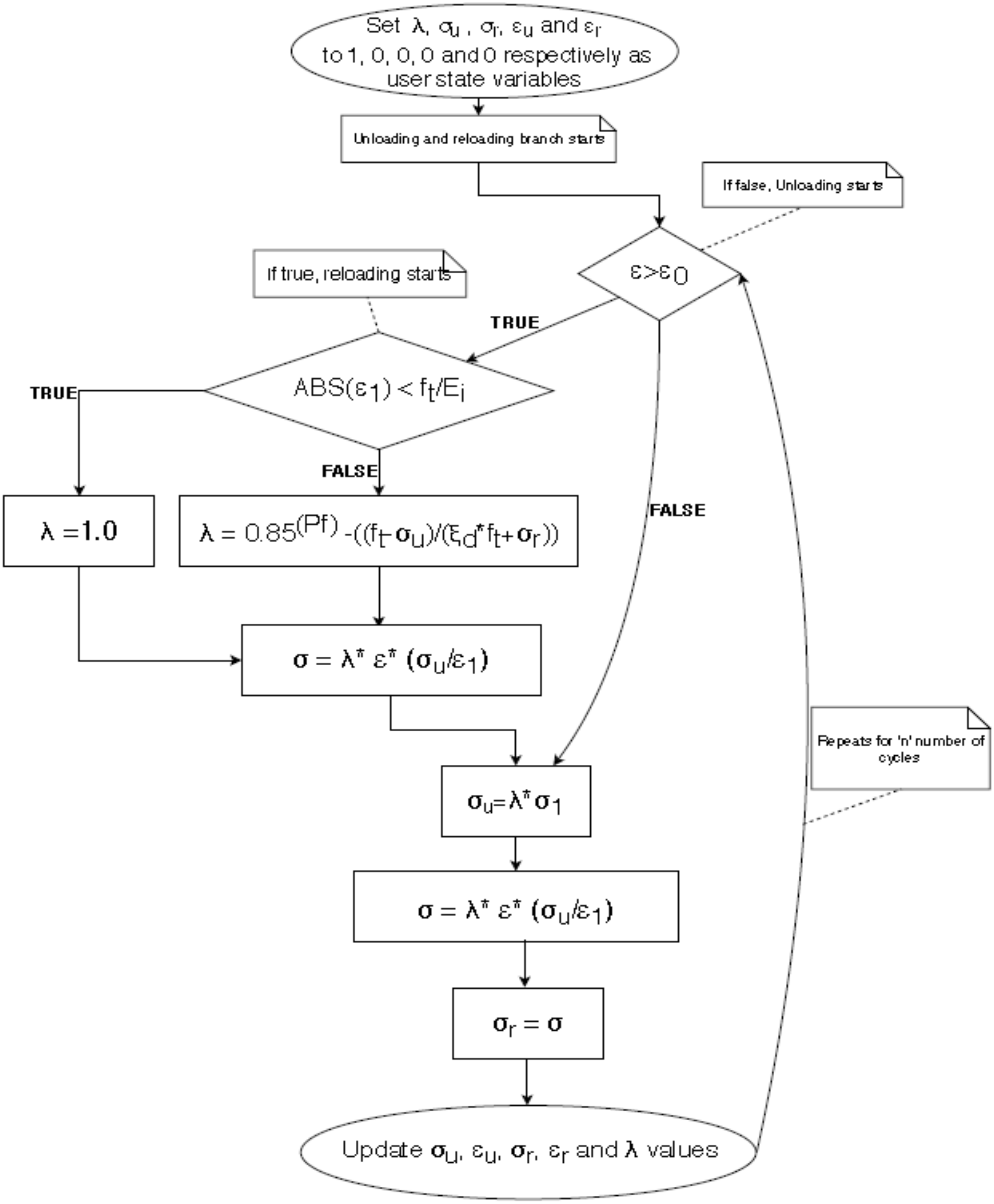

Figure 3.5: Flowchart for the unloading-reloading branch of the EMM subroutine

Table 3.1: List of symbols used in the flow chart

Symbol	Definition
λ	degradation factor
ϵ	new updated strain
ϵ_0	strain at first increment
P_f	partial unloading factor
ξ_d	calibration factor
ϵ_u	strain at unloading point
ϵ_r	strain at reloading point
σ_u	stress at unloading point
σ_r	stress at reloading point
ϵ_1	strain at first unloading point

The line after point 6 towards the envelope follows with slope E_i' until it intersects the envelope at point 7 as shown in Figure 3.6. From here, the curve follows the original envelope curve to reach $\epsilon_{ultimate}$, which is represented as point 8 in Figure 3.6.

To understand the working of USS, an example is presented in Figure 3.6. The code flows from 1 to 8 in order. Refer Table 3.2 for a representative example showing how the program stores and updates different values.

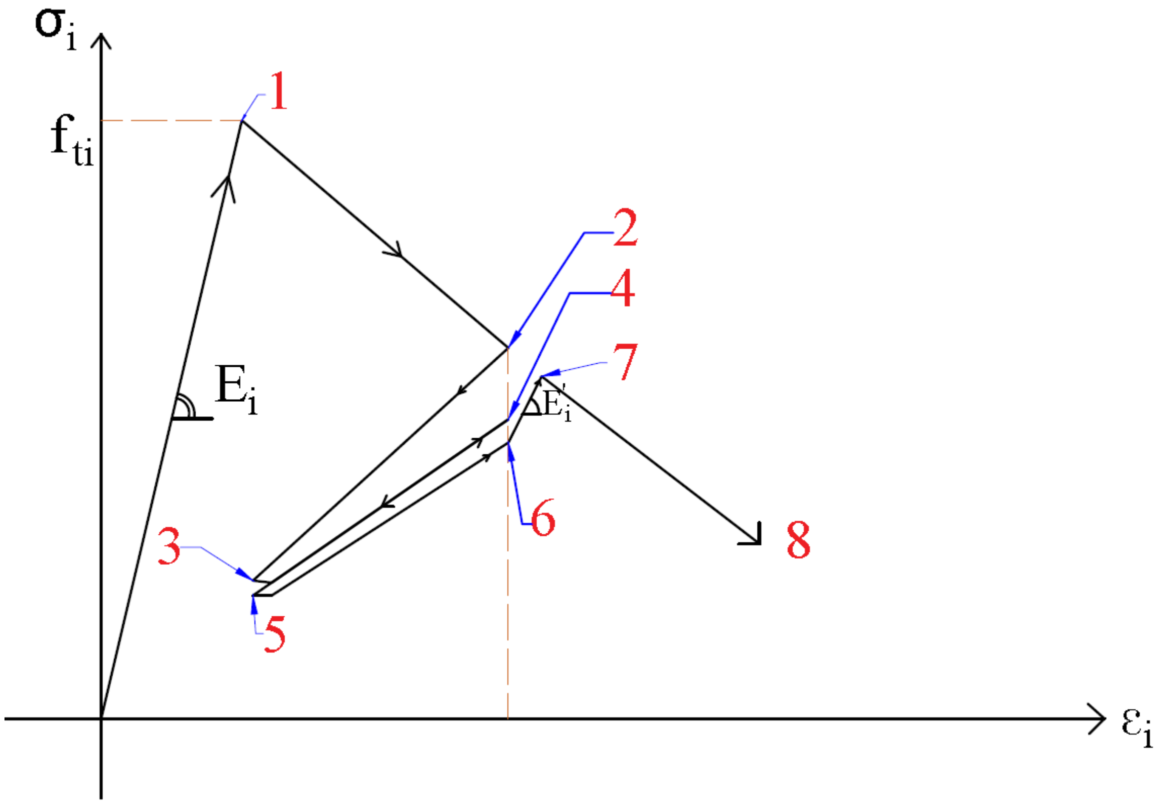

Figure 3.6: Flow of USS for unloading-reloading branch

Table 3.2: Representative example showing the flow of USS

Index from figure	f_t	j	σ_{uj}	ϵ_{uj}	σ_{rj}	ϵ_{rj}	P_f	λ_{tj}	ξ_d
1	0.2	-	0	0	0	0	0	1.0	0
2	0.2	1	0.141	8e-4	0	0	0.9	1.0	1.5
3	0.2	1	NC	NC	0.101	8e-5	0.9	0.96	1.5
4	0.2	2	0.136	8e-4	NC	NC	0.9	0.96	1.5
5	0.2	2	-	-	0.100	8e-5	0.9	0.943	1.5
6	0.2	3	0.133	8e-4	NC	NC	0.9	0.943	1.5
7	Depends on the point of intersection of E_i' and envelope								
8	Towards $\epsilon_{ultimate}$								
NC - No Change									

The portion of the code representing the unloading and reloading branch of tension constitutive model before implementation is shown in Figure 3.7. The changes applied to this code after implementing the degradation model as given in the flowchart are shown in Figure 3.8. Initially the logical operator RECRACKED is set to false. Once the new degradation code is completed, it changes to true indicating that the repetition has ended.

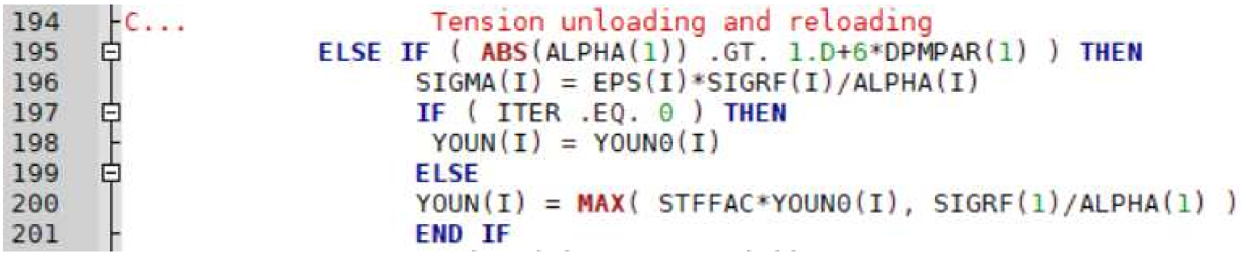

```
C...                 Tension unloading and reloading
               ELSE IF ( ABS(ALPHA(1)) .GT. 1.D+6*DPMPAR(1) ) THEN
                     SIGMA(I) = EPS(I)*SIGRF(I)/ALPHA(I)
                     IF ( ITER .EQ. 0 ) THEN
                      YOUN(I) = YOUN0(I)
                     ELSE
                     YOUN(I) = MAX( STFFAC*YOUN0(I), SIGRF(1)/ALPHA(1) )
                     END IF
```

Figure 3.7: User supplied subroutine showing unloading-reloading part of tension constitutive model before implementation

```
C...                Tension unloading and reloading
                 IF (EPS(I) .GT. EPS0(I)) THEN
                   IF (SIGUE(I) .LE. SREP(I)) THEN
                     SIGMA(I)= LAMBDA(I)*EPS(I)*SIGRF(1)/ALPHA(1)
                   ELSE
                     LAMBDA(I) =(0.85D0)**(1.D0-(EPSLR(I)/ALPHA(1)))-
     $                        ((FT(I)-SIGUE(I))/(3.D0*FT(I)+SIGUR(I)))
                     IF (LAMBDA(I) .LT. 0.D0) THEN
                     LAMBDA(I) = 0.D0
                     SIGMA(I)= EPS(I)*STFFAC
                     RECRACKD = .TRUE.
                     ELSE
                     SIGMA(I)= LAMBDA(I)*EPS(I)*SIGRF(1)/ALPHA(1)
                     YOUNGN(I) = SIGRF(1)
                     SREP(I) = SIGUR(I)
                     RECRACKD = .TRUE.
                     END IF
                   END IF
                  ELSE
                    SIGUE(I) = LAMBDA(I)*SIGRF(1)
                    SIGMA(I)= LAMBDA(I)*EPS(I)*SIGRF(1)/ALPHA(1)
                    SIGUR(I) = SIGMA(I)
                    IF((LAMBDA(I).EQ.1.D0)) THEN
                     EPSLR(I) = EPS(I)
                    END IF
                    EPSUR(I) = EPS(I)
                    IF (EPSUR(I) .NE. EPSLR(I)) THEN
                     EPSLR(I) = EPS(I)
                    END IF
                    AL(I) = ALPHA(1)
                  END IF
```

Figure 3.8: User supplied subroutine showing unloading-reloading part of tension constitutive model after implementation of new code

The slope of the line joining the last reloading branch and the envelope curve is parallel to the elastic curve (equal to the original young's modulus). This requires few changes in the main tension constitutive model and the User Supplied Subroutine to accommodate this effect is shown in Figure 3.9. Since the last point of the reloading cycle is stored, and the equation of the envelope curve is known, it is possible to find the equation of the line joining these two points from simple algebraic expressions. Here, CRACKED logical operator indicates that the new updated strain has surpassed the strain at tension strength of the material (f_t). Therefore, initially, CRACKED is false for the elastic branch and changes to true for the softening branch.

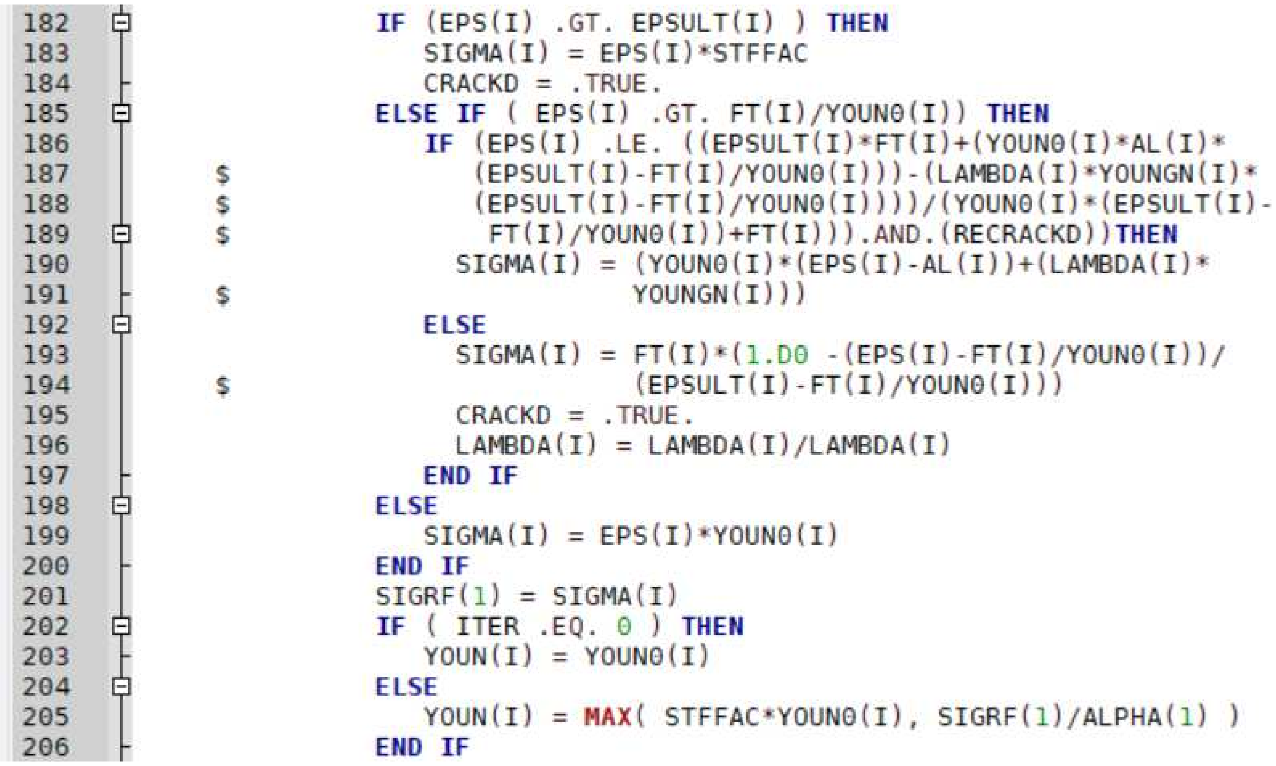

```
               IF (EPS(I) .GT. EPSULT(I) ) THEN
                  SIGMA(I) = EPS(I)*STFFAC
                  CRACKD = .TRUE.
               ELSE IF ( EPS(I) .GT. FT(I)/YOUN0(I)) THEN
                  IF (EPS(I) .LE. ((EPSULT(I)*FT(I)+(YOUN0(I)*AL(I)*
     $               (EPSULT(I)-FT(I)/YOUN0(I)))-(LAMBDA(I)*YOUNGN(I)*
     $               (EPSULT(I)-FT(I)/YOUN0(I))))/(YOUN0(I)*(EPSULT(I)-
     $                FT(I)/YOUN0(I))+FT(I))).AND.(RECRACKD))THEN
                    SIGMA(I) = (YOUN0(I)*(EPS(I)-AL(I))+(LAMBDA(I)*
     $                         YOUNGN(I)))
                  ELSE
                    SIGMA(I) = FT(I)*(1.D0 -(EPS(I)-FT(I)/YOUN0(I))/
     $                         (EPSULT(I)-FT(I)/YOUN0(I)))
                    CRACKD = .TRUE.
                    LAMBDA(I) = LAMBDA(I)/LAMBDA(I)
                  END IF
               ELSE
                  SIGMA(I) = EPS(I)*YOUN0(I)
               END IF
               SIGRF(1) = SIGMA(I)
               IF ( ITER .EQ. 0 ) THEN
                  YOUN(I) = YOUN0(I)
               ELSE
                  YOUN(I) = MAX( STFFAC*YOUN0(I), SIGRF(1)/ALPHA(1) )
               END IF
```

Figure 3.9: User supplied subroutine showing unloading-reloading part of tension constitutive model for slope of line joining the last unloading point and the envelope curve

The total number of lines changed from the original code are 36 including 30 lines from the unloading-reloading branch and 6 lines from the main envelope branch. This does not include the allotment of 5 new user state variables and 1 user indicator. User state variables are used to store certain values for future use cases and the user indicators are logical operators, to let the subroutine know if certain part of the code was run or not.

Table 3.3: User state variables and user state indicators

User state variable	**Number of variables used**
σ_u	2
ϵ_u	2
σ_r	2
ϵ_r	2
λ_t	2
User state indicator	**Number of variables used**
Recracked	2

Chapter 4

Experimental campaign: Window bank Tests

The following tests are not part of the Master thesis but were performed as part of the "Damage sensitivity of Groningen Masonry Structures - Experimental and computational studies " project on behalf of NAM in the year 2017 [Korswagen et al., 2017]. The tests were performed for studying the influence of frequent, light earthquakes on minor, aesthetic damage to masonry structures in Groningen. The goal of the project was to investigate the phenomenon of crack initiation and propagation in masonry for light earthquakes with an in-depth look into crack patterns, crack widths and the effect of repetitive and combined loadings [Korswagen et al., 2017].

For this master thesis, the results of the tests performed on window bank spandrels for 10, 30 and 100 repetitions are considered. The following sections present a short description of the specimen, the loading procedure followed by the experimental results observed. In the next chapter the mechanical representation and the finite element model are described along with the validation of the new USS code including degradation.

4.1 Description of the test

The window bank tests target cracking pattern that are typical and frequently observed in Groningen below or above windows, where cracks follow vertical paths and compressive stresses are minimum. Hence the window bank test can be considered as a four point bending test [Korswagen et al., 2017].

The dimensions of the window bank samples are described in Figure 4.1 and given in

Table 4.1. The window bank sample is the section below the window opening tested to investigate the vertical cracking patterns observed in the Groningen area [Korswagen et al., 2017].

The modified four point bending test will cause tension stresses at the top of the sample. To prevent sudden failure of the sample, the bottom is supported by counterweights; this also allows for repetitive testing of the same sample [Korswagen et al., 2017].

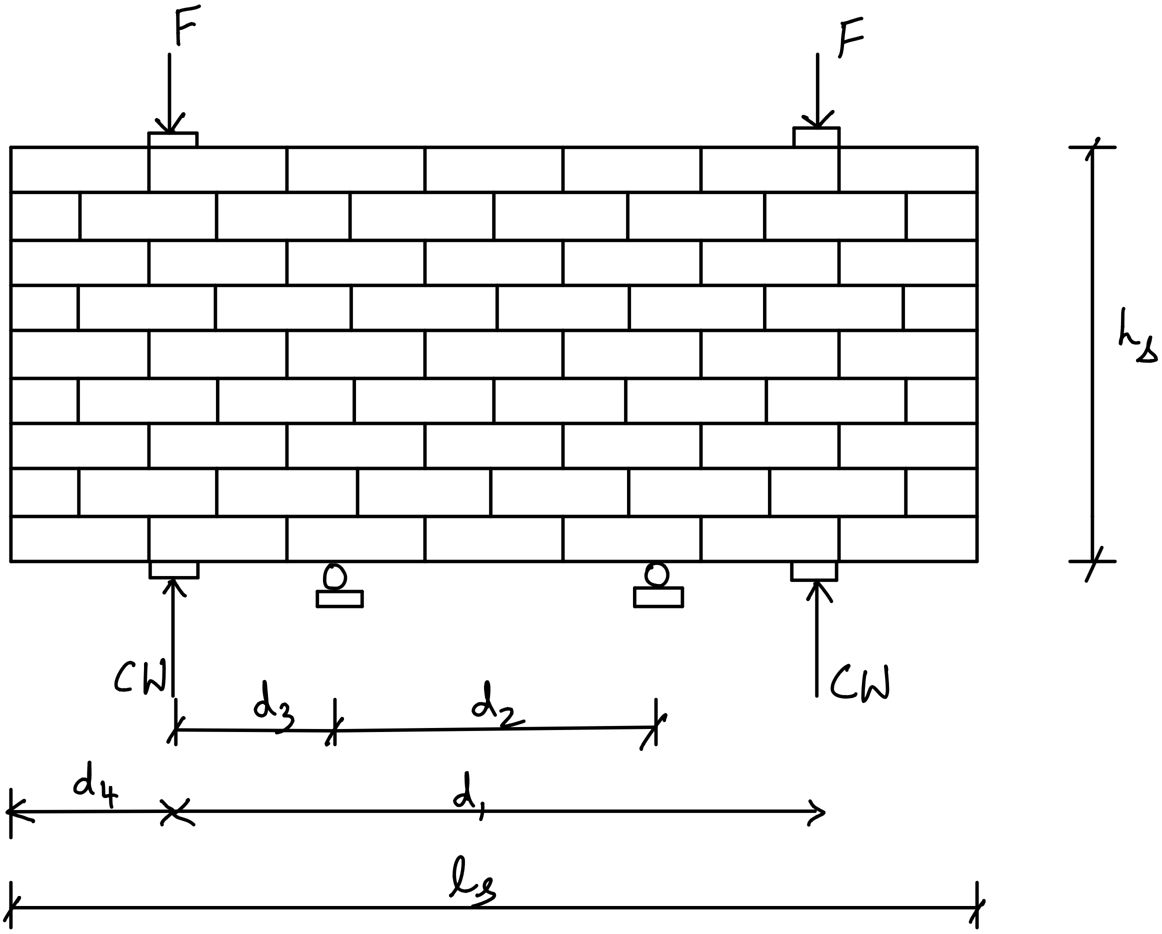

Figure 4.1: Mechanical model based on the experimental setup

Table 4.1: Overview of the repetetive tested window bank samples [Korswagen et al., 2017]

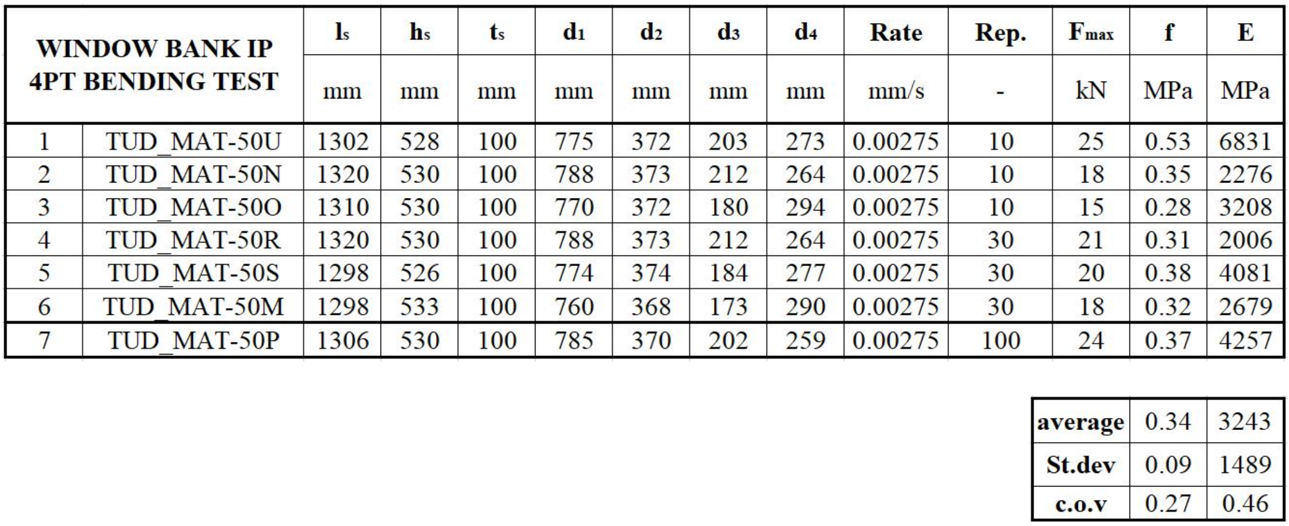

WINDOW BANK IP 4PT BENDING TEST		**l_s**	**h_s**	**t_s**	**d_1**	**d_2**	**d_3**	**d_4**	**Rate**	**Rep.**	**F_{max}**	**f**	**E**
		mm	mm	mm	mm	mm	mm	mm	mm/s	-	kN	MPa	MPa
1	TUD_MAT-50U	1302	528	100	775	372	203	273	0.00275	10	25	0.53	6831
2	TUD_MAT-50N	1320	530	100	788	373	212	264	0.00275	10	18	0.35	2276
3	TUD_MAT-50O	1310	530	100	770	372	180	294	0.00275	10	15	0.28	3208
4	TUD_MAT-50R	1320	530	100	788	373	212	264	0.00275	30	21	0.31	2006
5	TUD_MAT-50S	1298	526	100	774	374	184	277	0.00275	30	20	0.38	4081
6	TUD_MAT-50M	1298	533	100	760	368	173	290	0.00275	30	18	0.32	2679
7	TUD_MAT-50P	1306	530	100	785	370	202	259	0.00275	100	24	0.37	4257

average	0.34	3243
St.dev	0.09	1489
c.o.v	0.27	0.46

Figure 4.2 shows the front of the sample painted with the random patterns necessary for digital image correlation(DIC). The sample is supported by two rollers visible above the red block. Additional support is provided by counterweights (not visible) that are hanging from cables which lift the bottom of the samples. Aligned to the point of application of the counterweight's forces (48kg) are the hydraulic jacks at the top of the specimen. In the middle of the jacks a head joint is left open representing a notch. A sensor is placed across this notch, while at the top of the sample, another sensor runs along three head joints. A total of 12 LVDT sensors are placed as shown in the Figure 4.4 to measure both horizontal and vertical displacement of the specimen. Figure 4.3 shows the sample from the back, without counterweights and with jacks lifted [Korswagen et al., 2017]. For further details the reader is referred to the report " Damage sensitivity of Groningen Masonry Structures - Experimental and computational studies ".

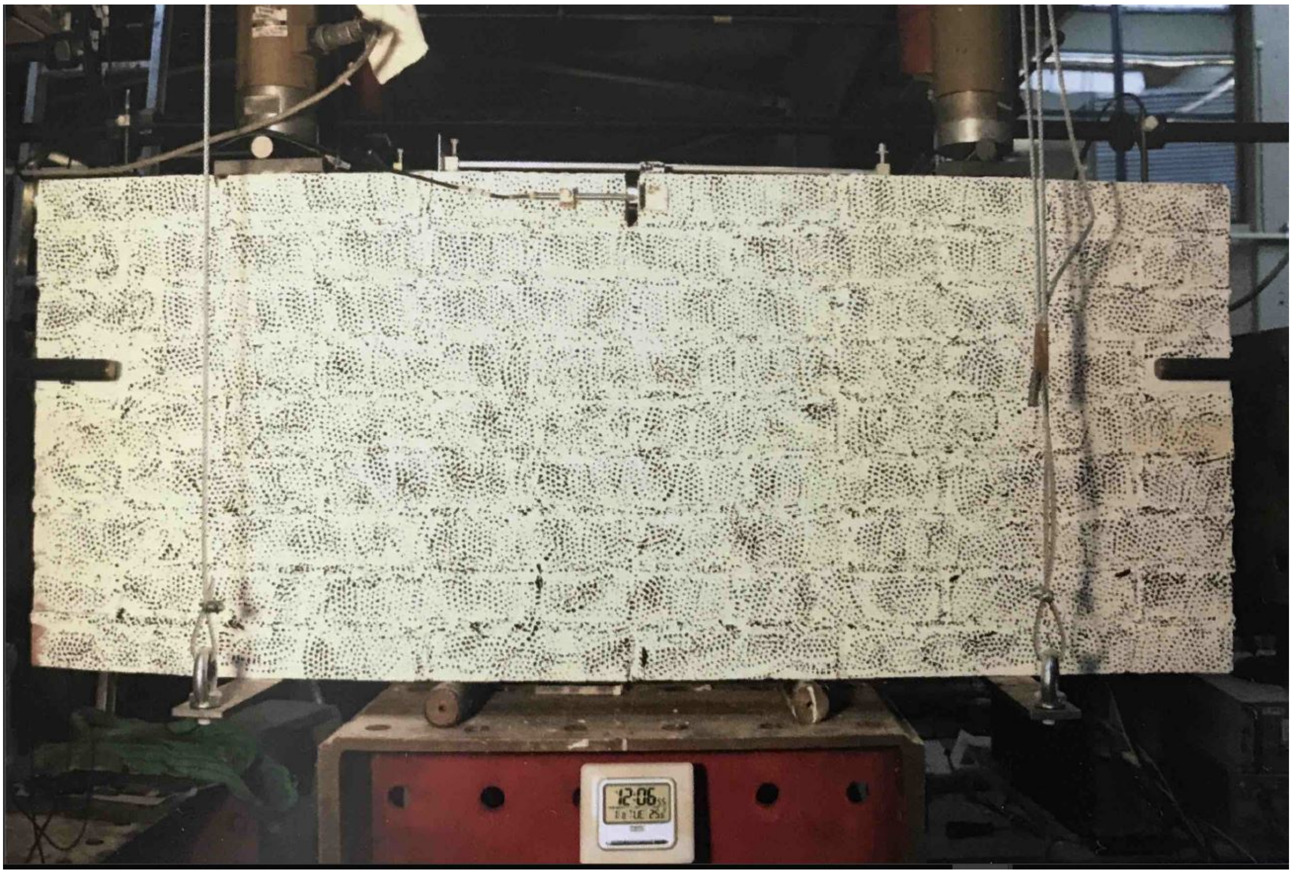

Figure 4.2: Window bank test sample (front side) [Korswagen et al., 2017]

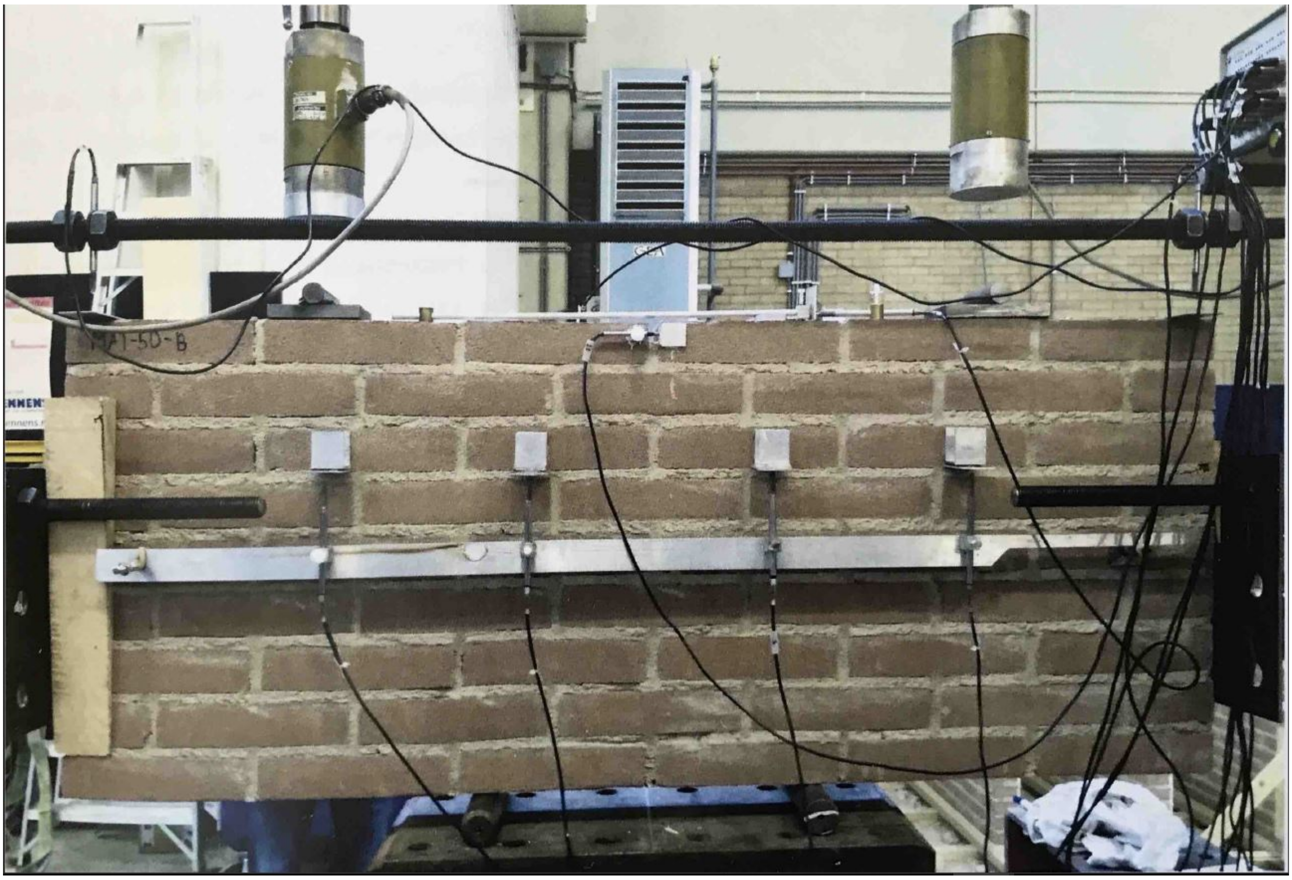

Figure 4.3: Window bank test sample (back side) [Korswagen et al., 2017]

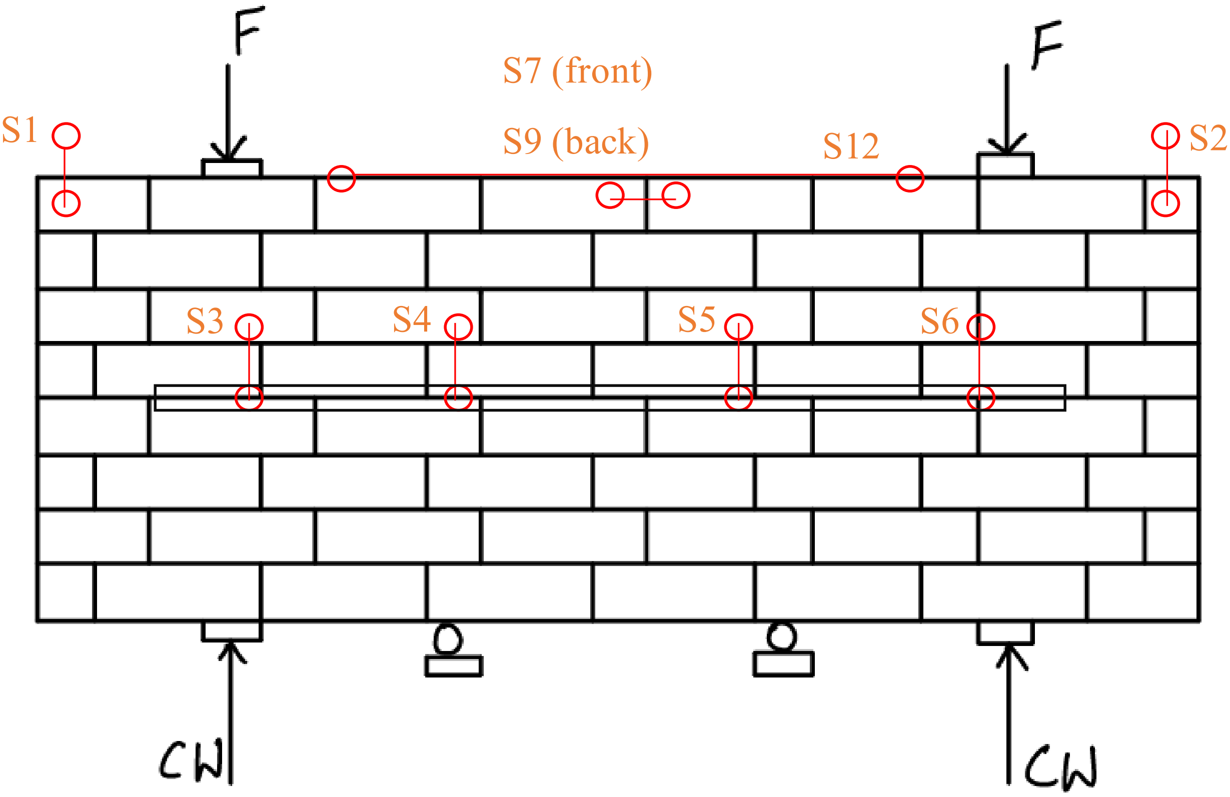

Figure 4.4: Position of Lvdt sensors placed on the specimen [Korswagen et al., 2017]

4.1.1 Results

Two variations of loading were used : monotonic loading which includes variations in the loading rate and the repetitive loading which includes variations in the amount of repetitions. In this report only the repetitive loading case is considered. Further, three different repetition variations of 10, 30 and 100 repetitions on each sample are considered [Korswagen et al., 2017].

Figure 4.5 shows the horizontal displacement measured at the top of the wall for TUD_MAT-50U [Korswagen et al., 2017].

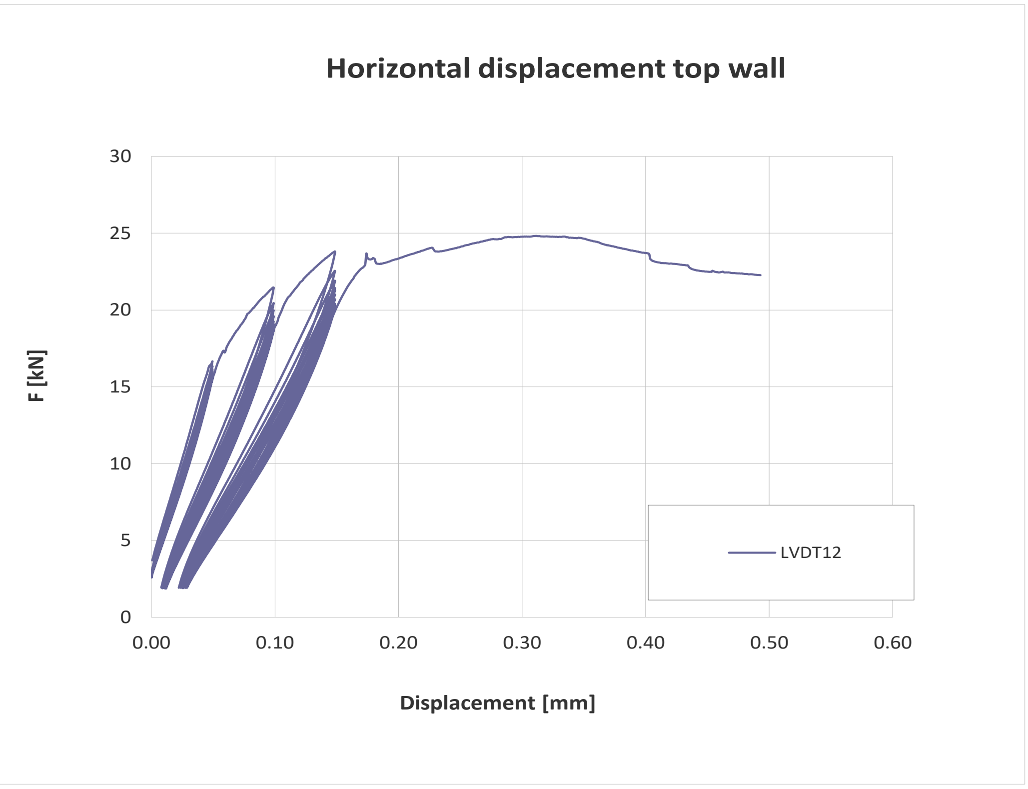

Figure 4.5: Force vs horizontal displacement graph of TUD_MAT-50U [Korswagen et al., 2017]

Figure 4.6 shows the vertical force vs displacement for LVDT number 3(refer Figure 4.4). Figure 4.7 shows the force at each reduction divided in the three repetition displacement steps applied during the test. In the lower repetition displacement steps the reduction force is less if the first repetition is compared with the last repetition within the repetition displacement step [Korswagen et al., 2017].

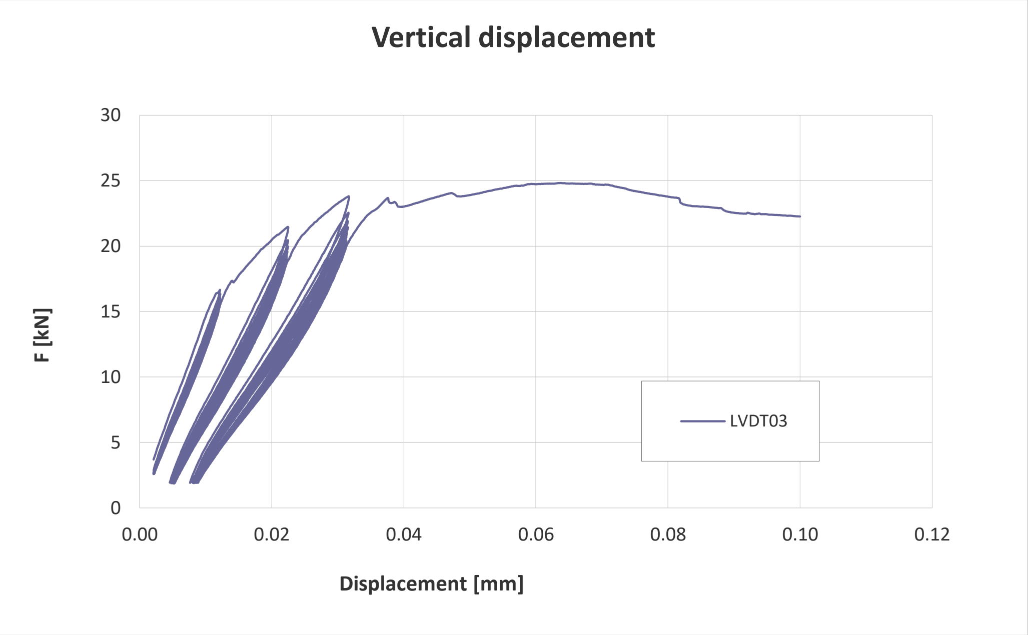

Figure 4.6: Force vs vertical displacement of sensor 3 for TUD_MAT-50U [Korswagen et al., 2017]

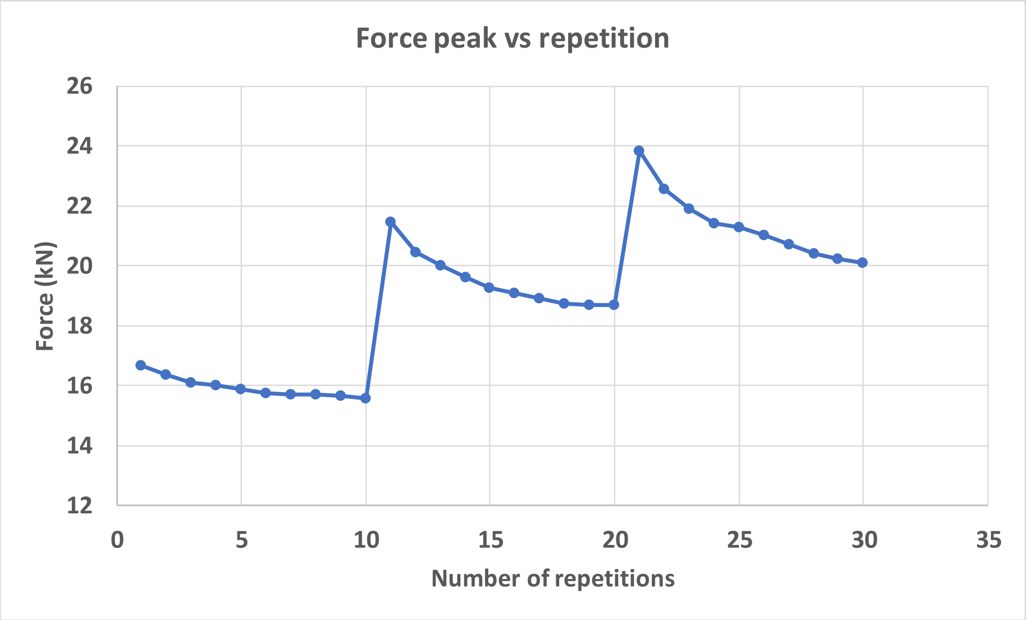

Figure 4.7: Force vs number of repetitions of sample TUD_MAT-50U [Korswagen et al., 2017]

Figure 4.8 shows the force vs horizontal displacement graph of one of the window bank samples that was tested with 30 repetitions TUD_MAT-50M [Korswagen et al., 2017]. Figure 4.9 shows the force vs vertical displacement of sensor 3 for TUD_MAT-50M [Korswagen et al., 2017].

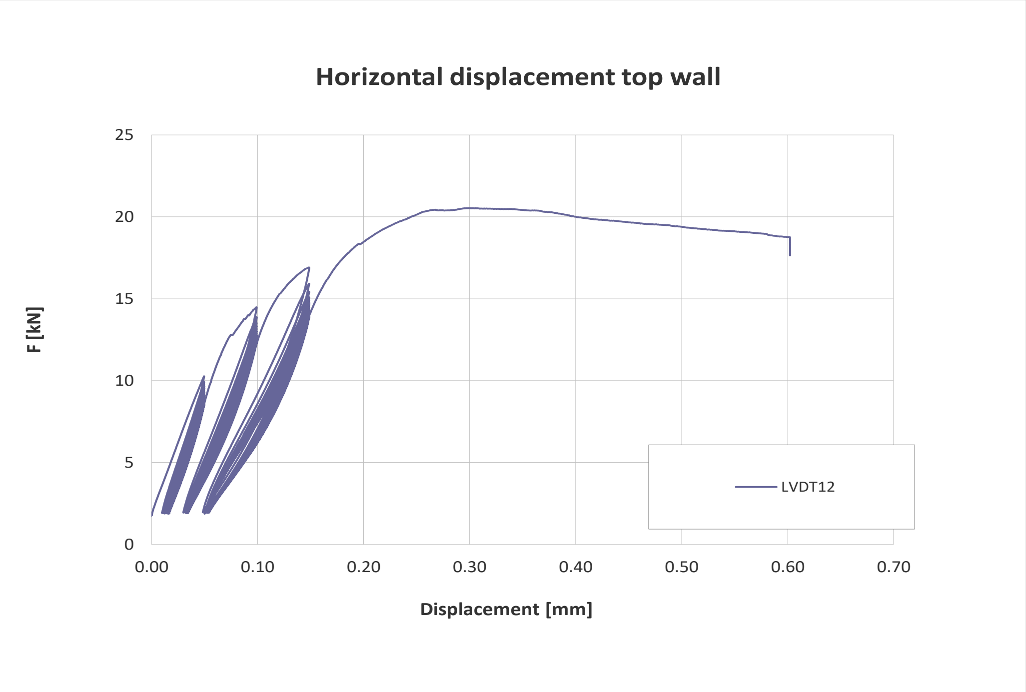

Figure 4.8: Force vs horizontal displacement graph of TUD_MAT-50M [Korswagen et al., 2017]

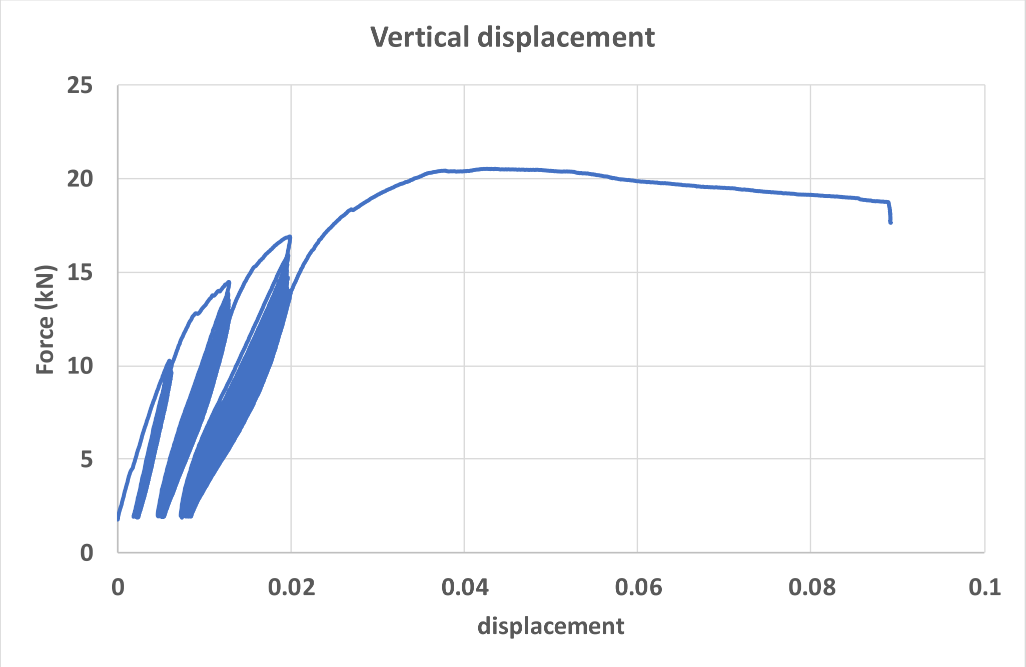

Figure 4.9: Force vs vertical displacement of sensor 3 [Korswagen et al., 2017]

Figure 4.10 shows the force versus the number of repetitions of sample TUD_MAT-50M. The same trend is observed with 30 repetitions as in the 10 repetitions variation.

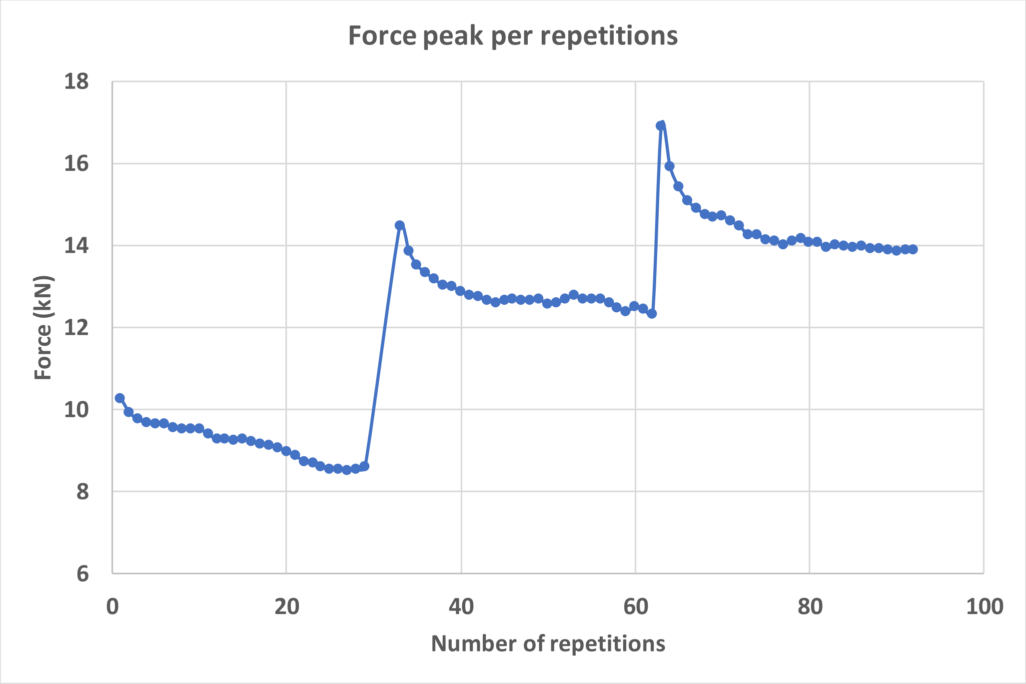

Figure 4.10: Force vs number of repetitions of sample TUD_MAT-50M [Korswagen et al., 2017]

To check the effect of the progressing force reduction and to investigate whether it would stabilize within a repetition displacement, an extra sample was tested with 100 repetitions per set. Figure 4.11 shows the force vs horizontal displacement graph of sample TUD_MAT-50P [Korswagen et al., 2017]. Figure 4.12 shows the force vs vertical displacement of sensor 3 for the same sample [Korswagen et al., 2017]. The vertical displacement plot shows large damage due to which the displacement is not the same for every repetition.

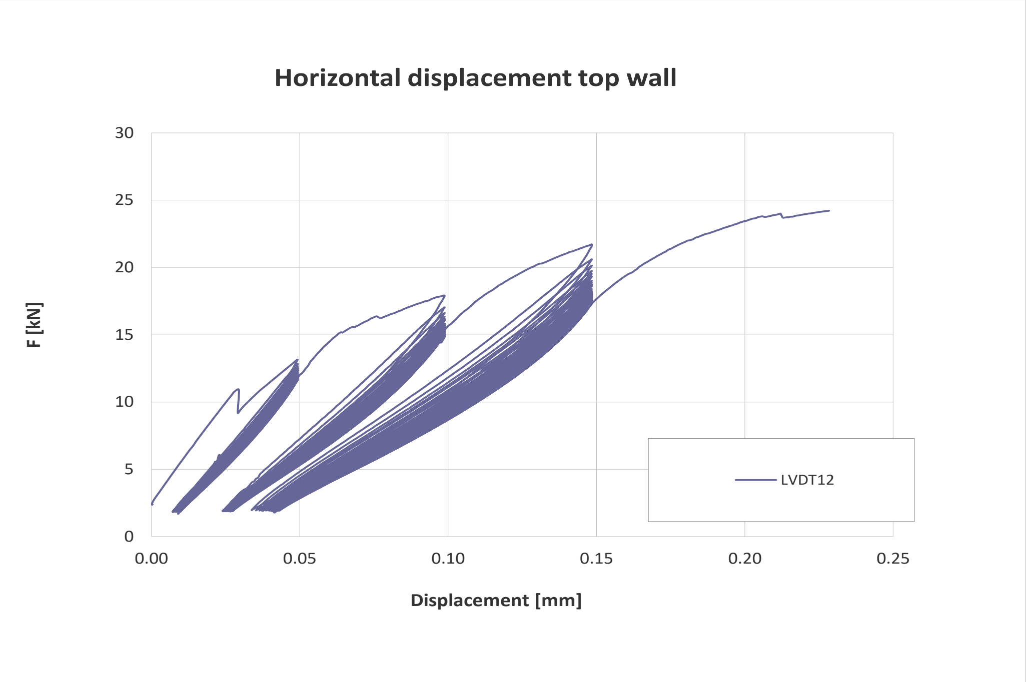

Figure 4.11: Force vs horizontal displacement graph of TUD_MAT-50P [Korswagen et al., 2017]

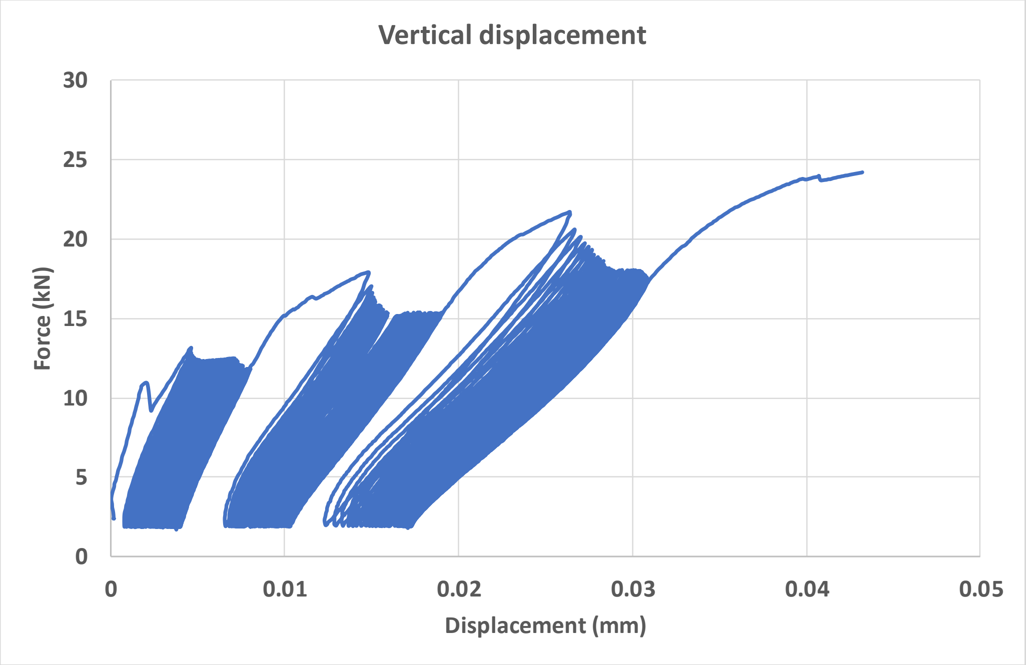

Figure 4.12: Force vs vertical displacement graph of TUD_MAT-50P [Korswagen et al., 2017]

Figure 4.13 shows the force against the number of repetitions and is plotted for TUD_MAT-50P. It is observed that the repetitions eventually go to a stable situation but for the last set the force reduction keeps progressing after 100 repetitions albeit at a slower pace [Korswagen et al., 2017].

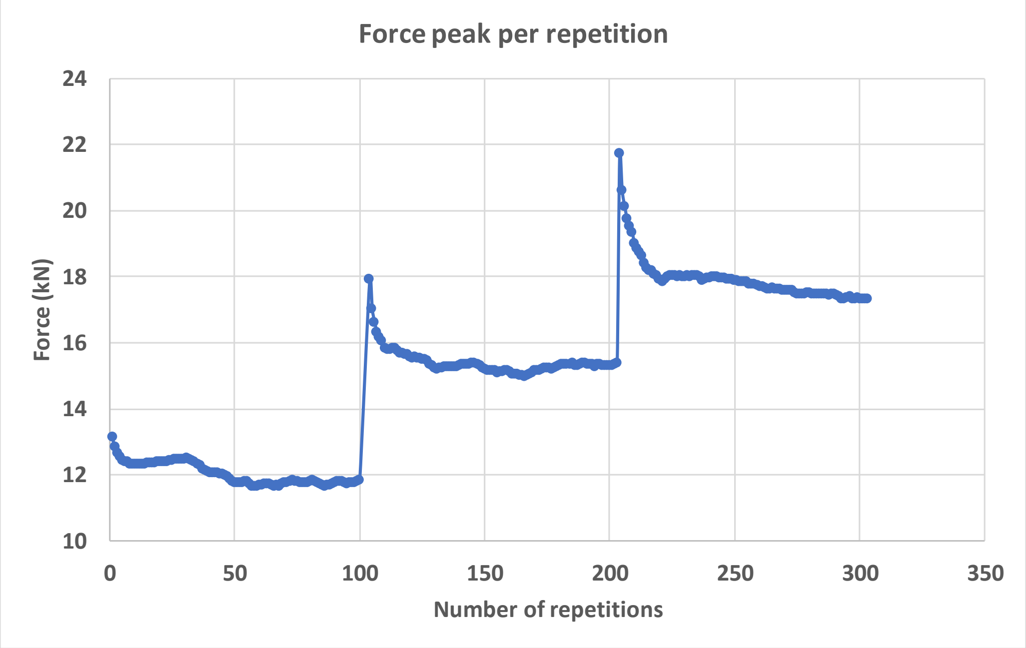

Figure 4.13: Force vs number of repetitions of sample TUD_MAT-50P [Korswagen et al., 2017]

For comparison of the number of repetitions per displacement step the difference in force between the first and last repetition of a repetition displacement step is calculated and expressed as a percentage. Table 4.2 gives the overview of the tested samples with the force reduction per displacement step [Korswagen et al., 2017]

Table 4.2: Force reduction per repetition displacment step expressed in percentage of the force measured in the first repetition in that particular step [Korswagen et al., 2017]

Sample	Number of repetitions	R1	R2	R3	Average
N	10	12.1	17	17.8	15.6
O	10	7.8	16.7	22.9	15.8
U	10	6.6	13	15.6	11.7
M	30	4	14.2	27.2	15.1
R	30	16.4	15	17.8	16.4
S	30	13.8	19	28.9	20.6
P	100	10.1	14.2	20.3	14.9
Average		10.1	15.6	21.5	

In Figure 4.14 the values of Table 4.2 are plotted together with the average of the three repetition displacement steps. It can be seen that in average, the force reduction increases when the repetition displacement step increases. The percentages in Table 4.2 do not show a significant difference between the sample with different number of repetitions. Which means that the degradation mainly takes place in the first 10 repetitions. In other words, the repetitions after the 10th repetition show a lower progress of degradation [Korswagen et al., 2017].

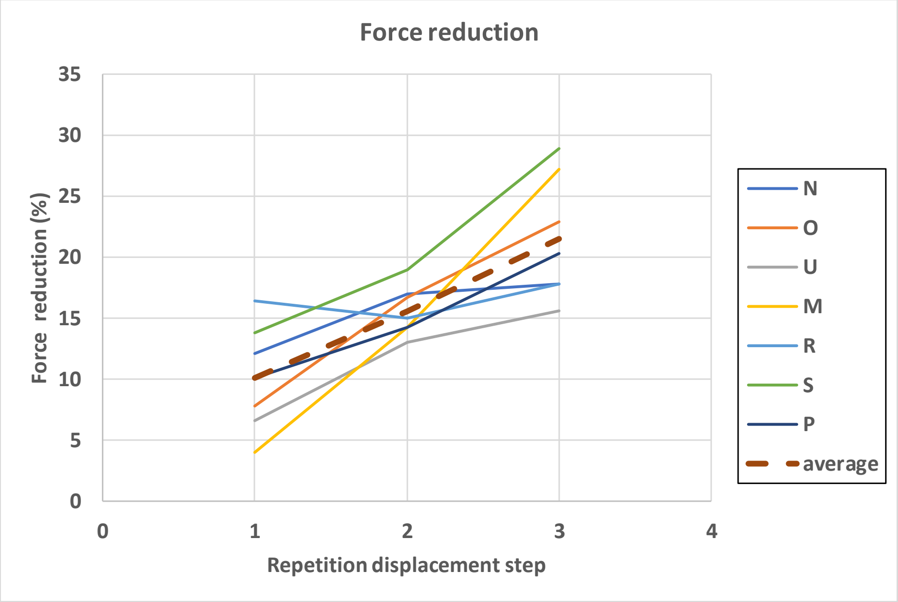

Figure 4.14: Force reduction per repetition displacement step plot of Table 4.2 [Korswagen et al., 2017]

4.2 Conclusions

- The crack propagation or material degradation is the change in resistance of the sample throughout the test [Korswagen et al., 2017].
- Degradation levels out after 10 repetitions, although not completely.
- The material degradation mainly takes place in the first repetitions of a certain applied displacement. [Korswagen et al., 2017].
- A hypothesis for the observed degradation is lengthening of the cracks due to micro-damage of the crack surfaces or redistribution of stresses within the sample[Korswagen et al., 2017].

Chapter 5

Validation and Calibration of the adapted material model using DIANA

In this chapter the new model is tested on a single element followed by the validation based on the window bank (four-point bending) tests and the wall with an opening (pushover analysis). The results of the EMM with and without the degradation model are presented for clear differentiation and better understanding.

5.1 Single element

First the code is tested on a single element of 25x25mm in dimension. A linear 4-node quadrilateral and a quadratic 8-node quadrilateral element are tested under tension loading. The material properties remain the same for both the element types and are given in Table 5.1. The quadratic element gives the same results as the linear element and hence, only the results of linear element are presented in this report.

Table 5.1: Masonry material properties

Clay Masonry properties			
Engineering masonry model			
Density	ρ	Kg/m^3	1680
Young's modulus perpendicular to bed-joint	E_y	MPa	3400
Young's modulus parallel to bed-joint	E_x	MPa	2200
Shear modulus	G_{xy}	MPa	1300
Tensile strength perpendicular to bed-joint	f_{ty}	MPa	0.2
Tensile strenght parallel to bed-joint	f_{tx}	MPa	-
Tensile fracture energy	G_f	N/m	10
Compressive strength	f_c	MPa	14
Compressive fracture energy	G_c	N/m	20000
Friction angle	ϕ	rad	0.6
Cohesion	c	MPa	0.15

5.1.1 Linear 4 node element

Figure 5.1 shows the linear 4-node element (Q8MEM) with the mesh, supports and loads. Here the bottom side and an adjacent side are restricted to move in y and x direction respectively. The tension load is applied at the top as a displacement control upto 2mm.

For the analysis of a single element, the regular Newton-Raphson solution method is used with an energy norm (displacement and force norm at 0.01 tolerances can also be used) with a tolerance of 0.0001 to be satisfied for each load step. The convergence tolerance values are given in Table 5.2 along with the load step sizes used for each test in Table 5.3. Each test is for ten repetitions at an unloading point in the softening zone.

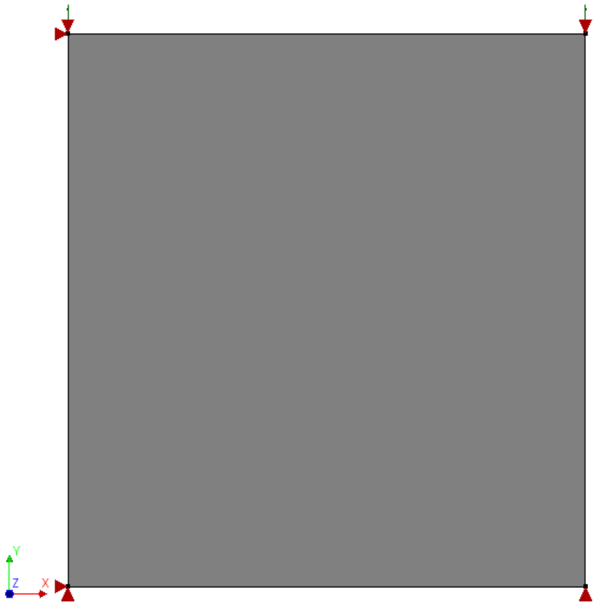

Figure 5.1: Finite element model of a single 4-node linear element

Table 5.2: Convergence criteria and analysis type

Number of repetitions	10
Element type	Linear
Solution type	regular Newton-Raphson
Convergence norm	Energy
Convergence tolerance	0.0001
Simultaneously satisfy all norms	OFF

Table 5.3: Load steps and load step sizes

Analysis	Load step sizes
All variations of ξ_d	0.0005(20), (-0.001(10),+0.001(10))x10, 0.0005(50)
partial unloading (1/2)	0.0005(20), (-0.001(5),+0.001(5))x10, 0.0005(50)
partial unloading (1/4th)	0.0005(20), (-0.0005(20),+0.0005(20))x10, 0.0005(50)
partial unloading (1/8th)	0.0005(20), (-0.0001(10),+0.0001(10))x10, 0.0005(50)
unloading into compression zone	0.0005(20), (-0.001(15),+0.001(15))x10, 0.0005(50)

Figure 5.2 shows the single element test with the original EMM without the degradation model for tension mode-I cracking. The figure on the left shows the stress vs strain and the one on the right shows the stress reduction vs repetition number. It is clearly noticeable that the stress after every repetition shows no reduction for any repetition.

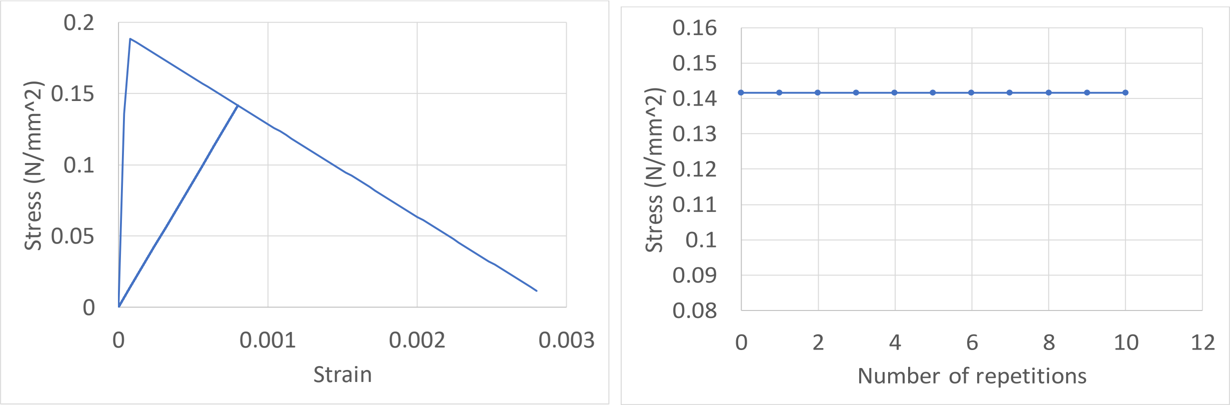

Figure 5.2: Stress vs strain plots(left) and stress reduction(right) for EMM without degradation

Figure 5.3 shows the results after the degradation model is implemented in EMM with varying ξ_d from 1 to 5. Notice that, as ξ_d increases, the curve shifts upward and reaches an asymptote sooner, i.e. becomes linear after a very few repetitions when ξ_d is large. When ξ_d is equal to 1.0, the stress becomes 0 at a certain repetition and continues along the 0 stress line for the rest of the cycles. This means that the material failed at this repetition step and can no longer support any load. These tests are done to give the user an intuitive explanation for the impact of ξ_d value on the degradation factor.

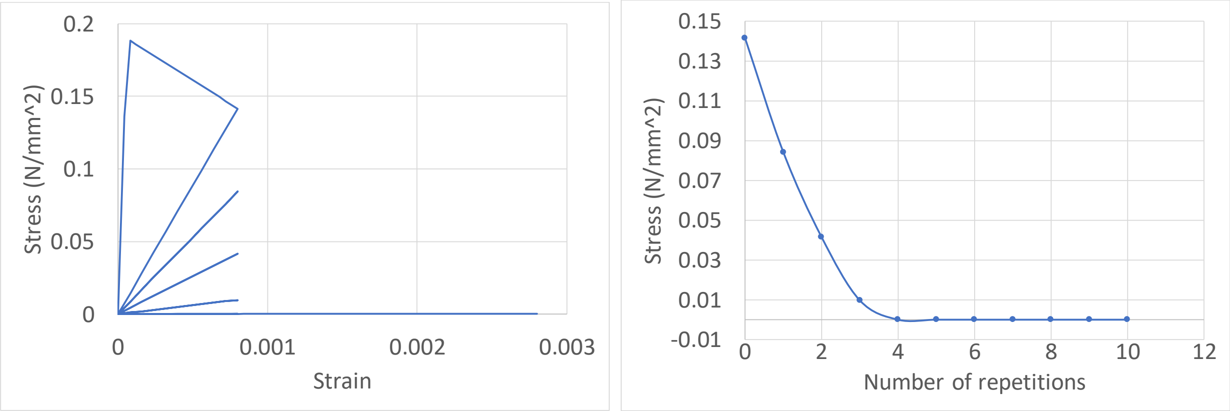

(a) $\xi_d = 1.0$

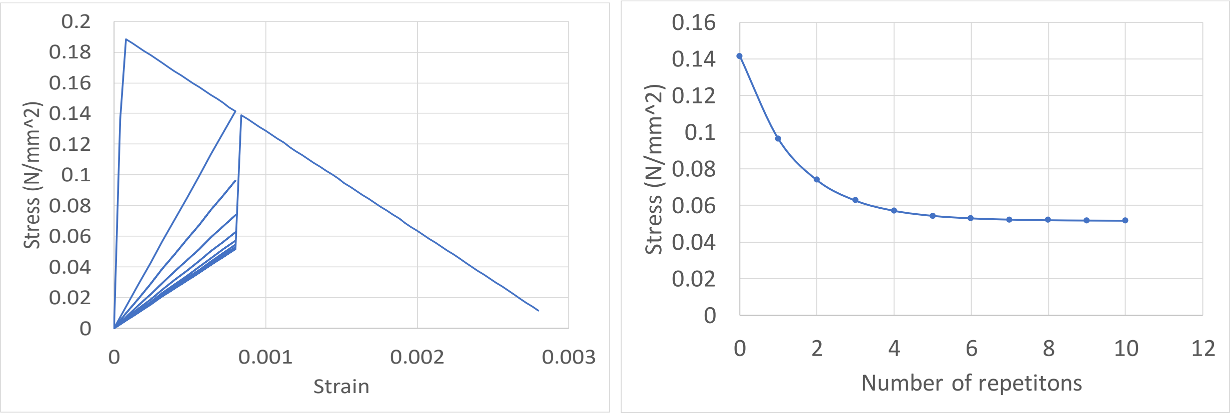

(b) $\xi_d = 1.50$

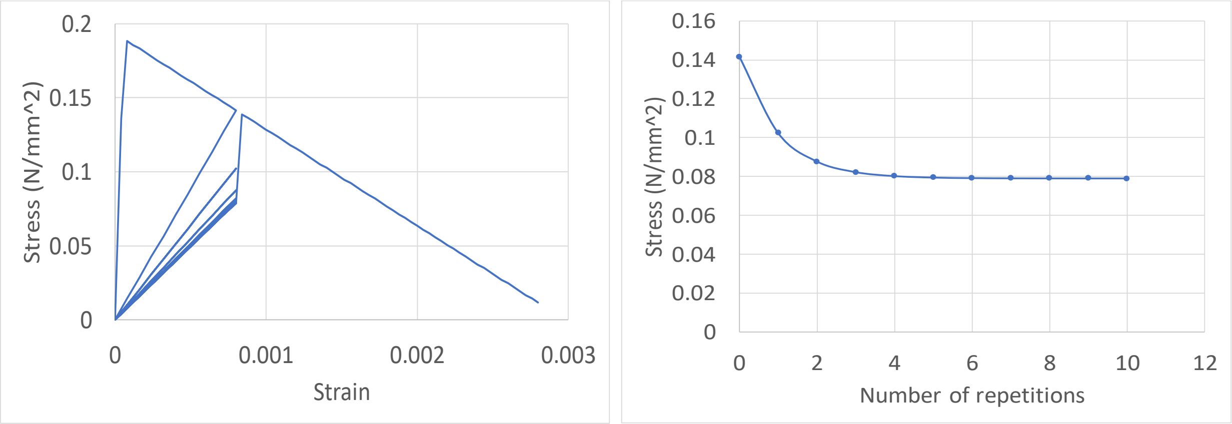

(c) $\xi_d = 2.0$

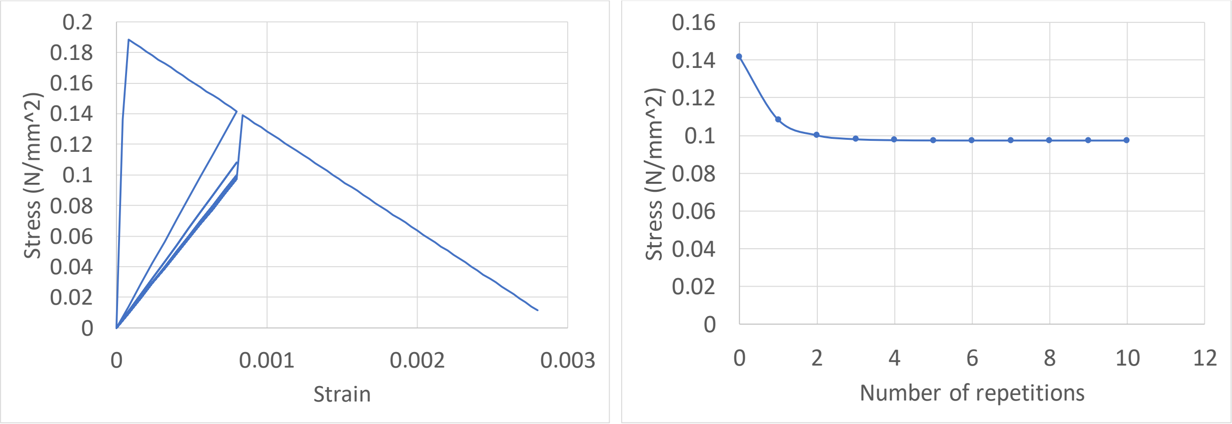

(d) $\xi_d = 3.0$

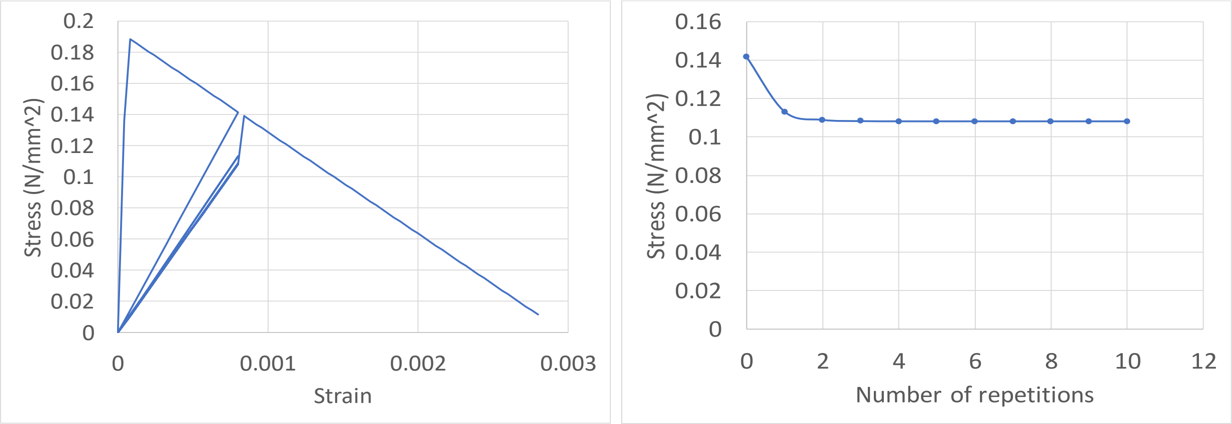

(e) $\xi_d = 5.0$

Figure 5.3: Stress vs strain plots(left) and stress reduction(right) for EMM+degradation model

The parameters such as the σ_{Rj}, σ_{Uj}, λ_t vary after every cycle. For large values of ξ_d the λ_t value is closer to 1.0 and for small values of ξ_d the λ_t value is closer to 0.7. In order to keep a track of the range of λ_t and between 0.7 to 0.85 (based on literature review) the results of different ξ_d values and corresponding formula parameters are tabulated in Table 5.4 below. Here we see that for a ξ_d value of 1.5 and above, the λ_t is in the range of 0.7 to 0.8. Also for extremely high values of ξ_d like 5.0, the stress reduction becomes negligible quickly as the number of repetitions increase. Hence, it is advisable to use a ξ_d value in the range of 1.5 to 4.

Table 5.4: Analysis Parameters for varying ξ_d

repetition number	f_t (N/mm^2)	Load step number	σ_{Rj} (N/mm^2)	ξ_d =1.0		ξ_d =1.5		ξ_d =2.0		ξ_d =3.0		ξ_d =5.0	
				σ_{Uj} (N/mm^2)	λ_t	σ_{Uj} (N/mm^2)	λ_t	σ_{Uj} (N/mm^2)	λ_t	σ_{Uj} (N/mm^2)	λ_t	σ_{Uj} (N/mm^2)	λ_t
0	0.19	20	0	0.141	X	0.141	X	0.141	X	0.141	X	0.141	X
1	0.19	40	0	0.084	0.595	0.0963	0.680	0.102	0.722	0.108	0.765	0.113	0.799
2	0.19	60	0	0.041	0.293	0.0738	0.521	0.0876	0.619	0.100	0.706	0.1089	0.769
3	0.19	80	0	0.009	0.068	0.0626	0.442	0.0822	0.580	0.0980	0.692	0.1082	0.764
4	0.19	100	0	8E-8	5.64E-07	0.057	0.403	0.0802	0.566	0.0975	0.688	0.10818	0.7639
5	0.19	120	0	0	0	0.054	0.383	0.0794	0.561	0.09738	0.6877	0.108168	0.76387
6	0.19	140	0	0	0	0.0529	0.373	0.0791	0.559	0.09735	0.6875	0.1081664	0.76386
7	0.19	160	0	0	0	0.0522	0.369	0.0790	0.558	0.097348	0.68746	0.1081661	0.7638593
8	0.19	180	0	0	0	0.0519	0.366	0.07902	0.558	0.0973467	0.687453	0.108166068	0.763859068
9	0.19	200	0	0	0	0.0517	0.365	0.07901	0.5578	0.0973462	0.687450	0.108166061	0.763859019
10	0.19	220	0	0	0	0.0516	0.364						

The case of partial unloading will be considered. See Figure 5.4. The single element is tested for (a) full unloading, (b) partial unloading upto 1/2 that of full unloading (c) partial unloading upto 1/4th that of full unloading (d) partial unloading upto 1/8th of full unloading. Notice that the total stress reduction for 10 repetitions reduces as the unloading point reduces i.e. the asymptote shifts upward and the amount of reduction for the first repetition also decreases. The ξ_d value was kept constant for all tests, in this case at 3.0. This value is chosen at random for the purpose of explanation of the model only and no particular significance. Table 5.5 gives an overview of the changes in stress and degradation parameters upon partial unloading. Here the first stress reduction for full unloading is about 0.76 that of unloading stress (which is within the range of 0.7 and 0.9 as per literature) and about 0.92 times of unloading stress for partial unloading to 1/8th full unloading (the other extreme case). The material properties, analysis procedure and convergence criteria remain the same as given in Table 5.1, Table 5.9 and Table 5.2 respectively. This shows that the model can be used for partial unloading situations as well.

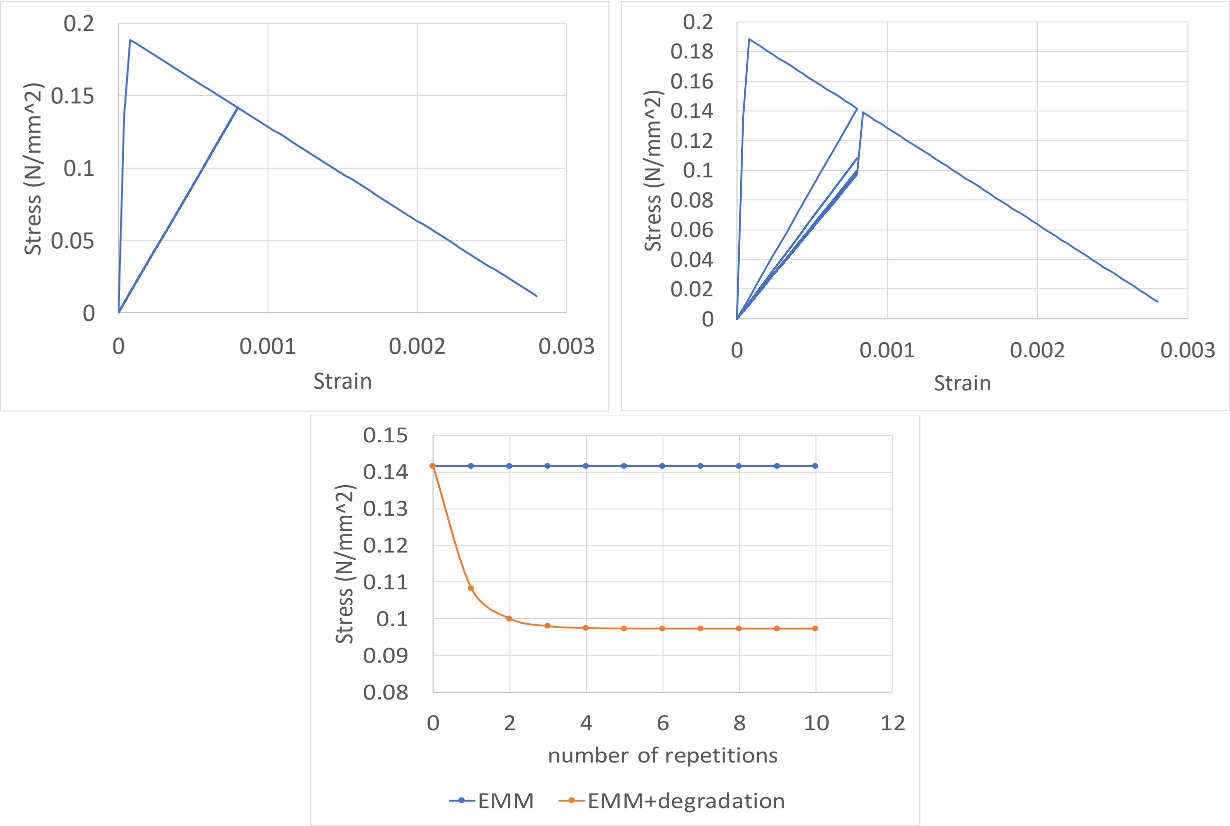

(a) full unloading

Stress vs strain plots EMM only(left), Stress vs strain plots EMM+degradation (right) and stress reduction(middle) for EMM+degradation model ($\xi_d = 3.0$)

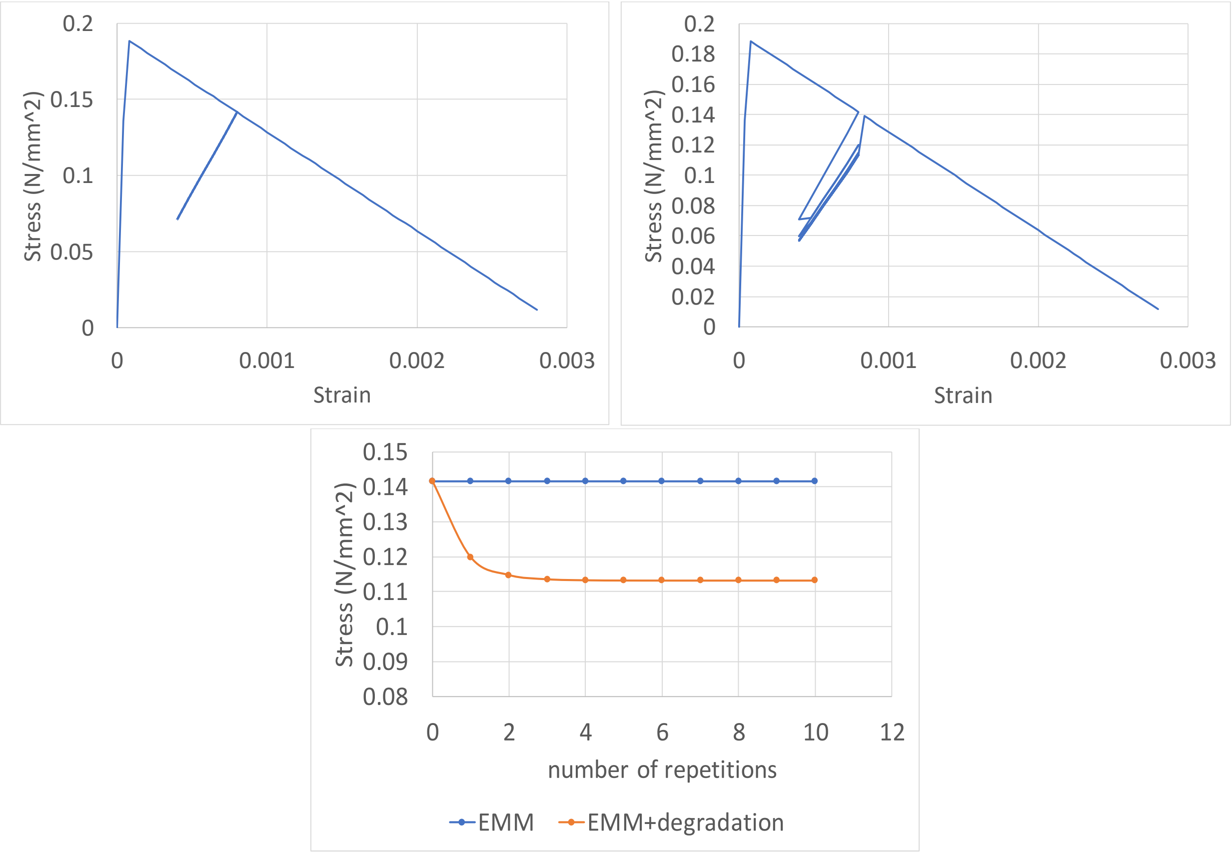

(b) partial unloading 1/2 of full unloading

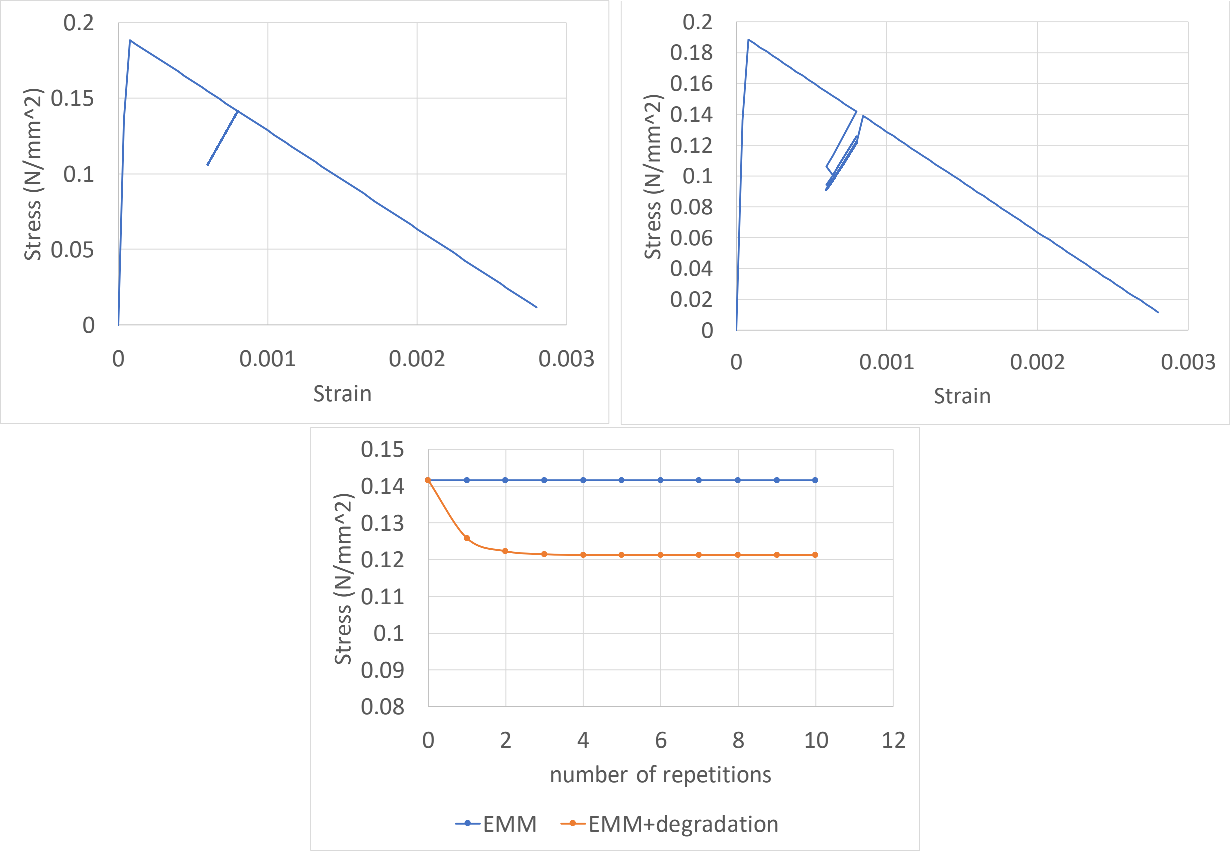

(c) partial unloading about 1/4th full unloaoding

Stress vs strain plots EMM only(left), Stress vs strain plots EMM+degradation (right) and stress reduction(middle) for EMM+degradation model ($\xi_d = 3.0$)

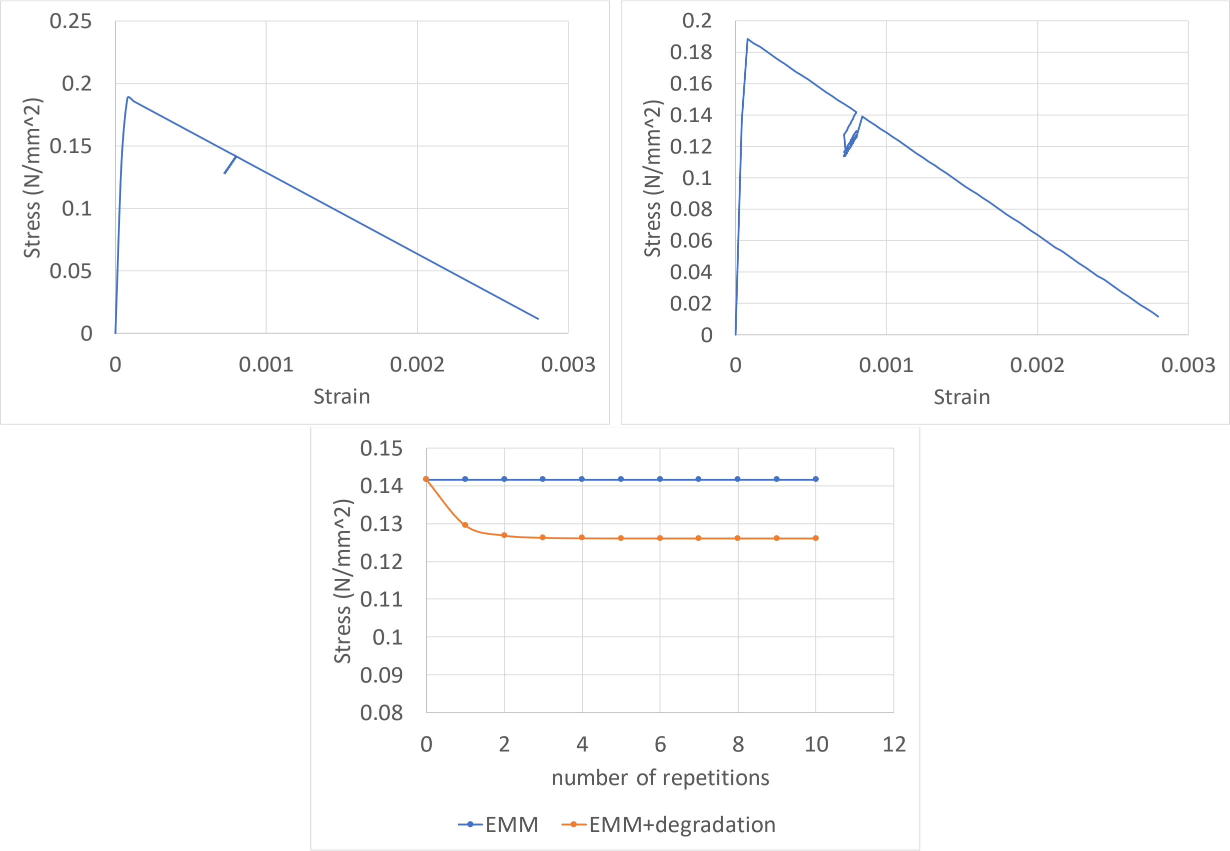

(d) partial unloading 1/8th full unloading

Figure 5.4: Stress vs strain plots EMM only(left), Stress vs strain plots EMM+degradation (right) and stress reduction(middle) for EMM+degradation model ($\xi_d = 3.0$)

Table 5.5: Analysis parameters for varying unloading point

cycle number	f_t (N/mm^2)	ξ_d	Full unloading			Partial unloading (1/2)		
			σ_{Rj} (N/mm^2)	σ_{Uj} (N/mm^2)	λ_t	σ_{Rj} (N/mm^2)	σ_{Uj} (N/mm^2)	λ_t
0	0.19	3	-	0.141	X	-	0.141605	X
1	0.19	3	0	0.108	0.765	0.070	0.119	0.846
2	0.19	3	0	0.100	0.706	0.059	0.114	0.810
3	0.19	3	0	0.098	0.692	0.057	0.1135	0.802
4	0.19	3	0	0.0975	0.688	0.0567	0.113288	0.800
5	0.19	3	0	0.09738	0.6877	0.056644	0.113218	0.799537
6	0.19	3	0	0.097356	0.6875	0.056609	0.113202	0.799419
7	0.19	3	0	0.097349	0.68746	0.056601	0.113198	0.799391
8	0.19	3	0	0.097347	0.687454	0.056599	0.113197	0.799384
9	0.19	3	0	0.097346	0.68745	0.056598	0.113196	0.799382
10	0.19	3	0	0.09734	0.68745	0.056598	0.113196	0.799382

cycle number	f_t (N/mm^2)	ξ_d	Partial unloading (1/4)			Partial unloading (1/8th)		
			σ_{Rj} (N/mm^2)	σ_{Uj} (N/mm^2)	λ_t	σ_{Rj} (N/mm^2)	σ_{Uj} (N/mm^2)	λ_t
0	0.19	3	-	0.141	X	-	0.141605	X
1	0.19	3	0.106	0.125	0.888	0.127	0.129	0.914
2	0.19	3	0.094	0.122	0.863	0.116	0.1268	0.895
3	0.19	3	0.0917	0.1214	0.857	0.114	0.12625	0.891
4	0.19	3	0.0911	0.12129	0.856536	0.1136	0.126117	0.890626
5	0.19	3	0.090967	0.121246	0.85623	0.1135	0.126087	0.890416
6	0.19	3	0.090935	0.121236	0.85616	0.1134	0.12608	0.890368
7	0.19	3	0.090927	0.121234	0.856143	0.113472	0.126079	0.890358
8	0.19	3	0.090925	0.121233	0.856139	0.113471	0.126079	0.890355
9	0.19	3	0.090925	0.121233	0.856139	0.113471	0.126078	0.890355
10	0.19	3	0.090925	0.121233	0.856138	0.113471	0.126078	0.890354

Figure 5.5 shows the stress vs strain plots for which the unloading has been carried out to the compression zone. The purpose of unloading to the compression zone is to see if the compression constitutive model has any effect on the results of the degradation model. It is noted from Table 5.6 and also from the stress reduction plot in Figure 5.5 that the λ_t values for both full unloading and unloading upto the compression zone are the same. The analysis procedure, convergence criteria and loading scheme are as given in Table 5.1, Table 5.9 and Table 5.2 respectively. The value of ξ_d is again kept constant at 3.0. With this, the new model can be applied to large number of elements, where it is subjected to a combination of tension and compression stresses.

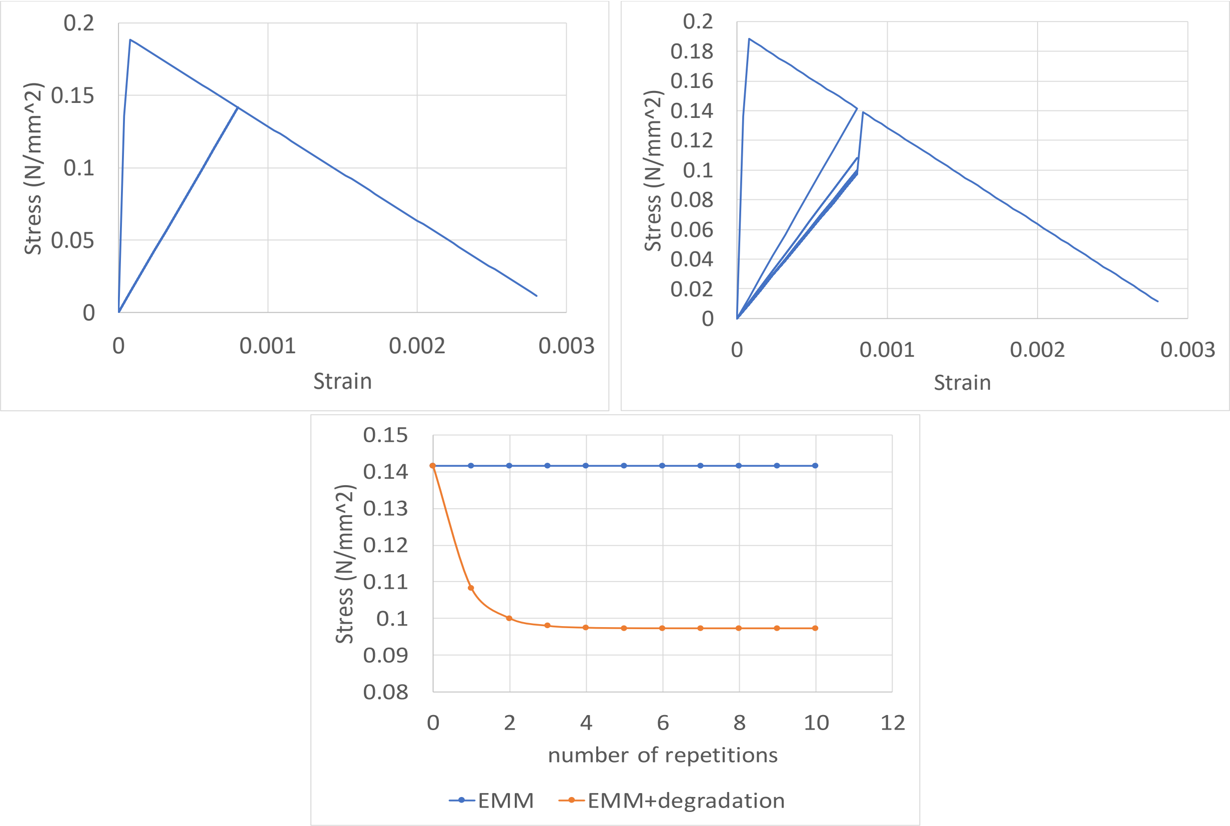

(a) full unloading

Stress vs strain graph for EMM, EMM+degradation and stress reduction for unloading to compression zone ($\xi_d = 3.0$)

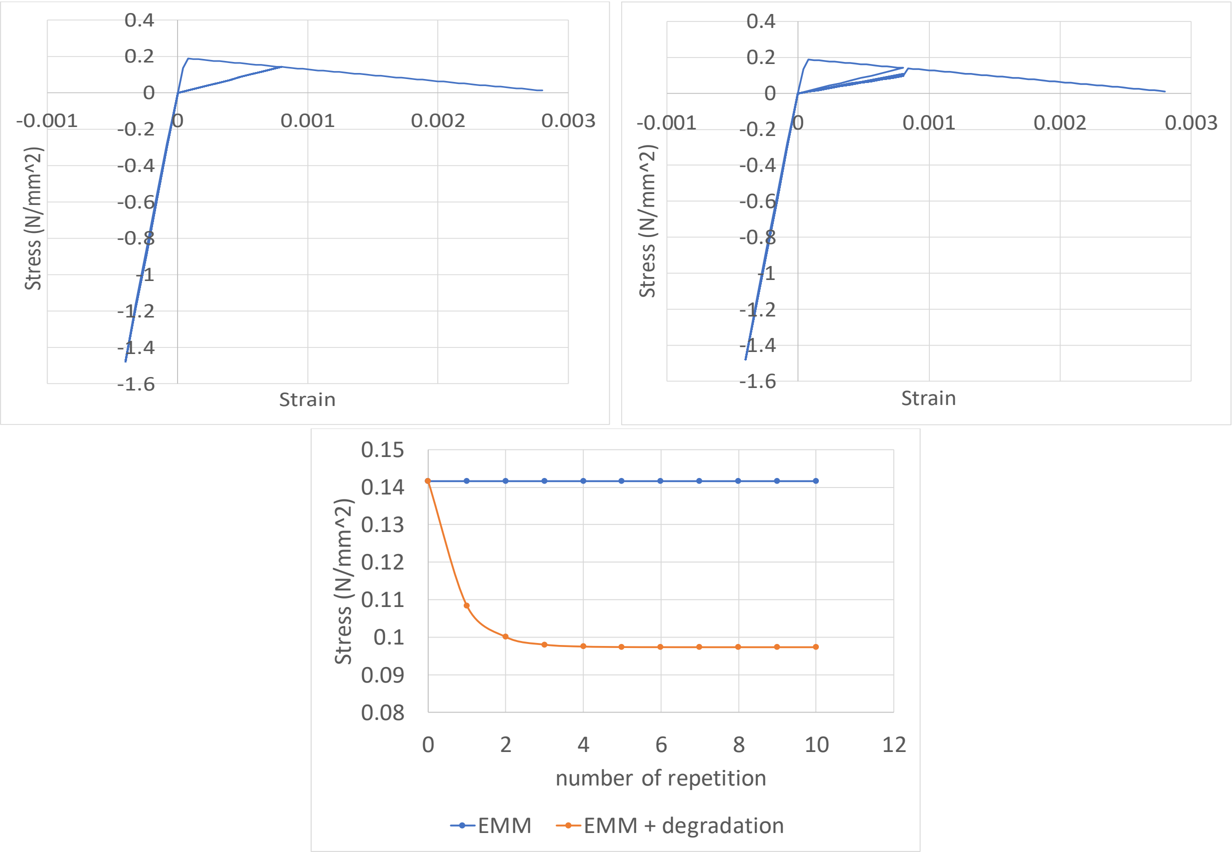

(b) Unloading to compression zone

Figure 5.5: Stress vs strain graph for EMM, EMM+degradation and stress reduction for unloading to compression zone ($\xi_d = 3.0$)

Table 5.6: Analysis parameters for unloading to the compression zone

cycle number	f_t (N/mm^2)	ξ_d	Full unloading			Unloading to compression zone		
			σ_{Rj} (N/mm^2)	σ_{Uj} (N/mm^2)	λ_t	σ_{Rj} (N/mm^2)	σ_{Uj} (N/mm^2)	λ_t
0	0.19	3	0	-	X	-	0.141	X
1	0.19	3	0	0.108	0.765	-1.47928	0.108	0.765
2	0.19	3	0	0.100	0.706	-1.47928	0.100	0.706
3	0.19	3	0	0.098	0.692	-1.47928	0.098	0.692
4	0.19	3	0	0.0975	0.688	-1.47928	0.0975	0.68864
5	0.19	3	0	0.097388	0.687745	-1.47928	0.097388	0.687745
6	0.19	3	0	0.097356	0.687523	-1.47928	0.097356	0.687523
7	0.19	3	0	0.097349	0.687468	-1.47928	0.097349	0.687468
8	0.19	3	0	0.097347	0.687454	-1.47928	0.097347	0.687454
9	0.19	3	0	0.097346	0.68745	-1.47928	0.097346	0.68745
10	0.19	3	0	0.097346	0.68745	-1.47928	0.097346	0.68745

5.2 Finite element model: Window bank

5.2.1 FE modeling

The window bank has been modeled as an isotropic continuum model realized as a four-point bending test under displacement-controlled load.

The finite element model is shown in Figure 5.6. The four-point bending beam is divided into three sheets. The middle sheet is made up of EMM elements with material properties as given in Table 5.7, the two adjacent sheets are linear isotropic with properties as given in Table 5.8. This allows the crack, in the middle sheet to propagate only in this sheet. This concept is based on the experimental observations of a four point bending beam where the crack always follows vertically through the middle of the beam. The six steel plates are linear isotropic with properties as given in Table 5.9. All three window bank specimens are similar in terms of modeling and only vary in dimensions and material properties as given in Table 4.1 and Table 5.7 respectively. In Table 5.7 the superscript 1 represents calibrated value and all other values are obtained from the report “ Damage sensitivity of Groningen Masonry Structures - Experimental and computational studies ” [Korswagen et al., 2017]. The calibration was necessary to suit the modified 4-point bending beam so that the crack propagates only in the mid sheet and also to match the model results with the experiment graphs.

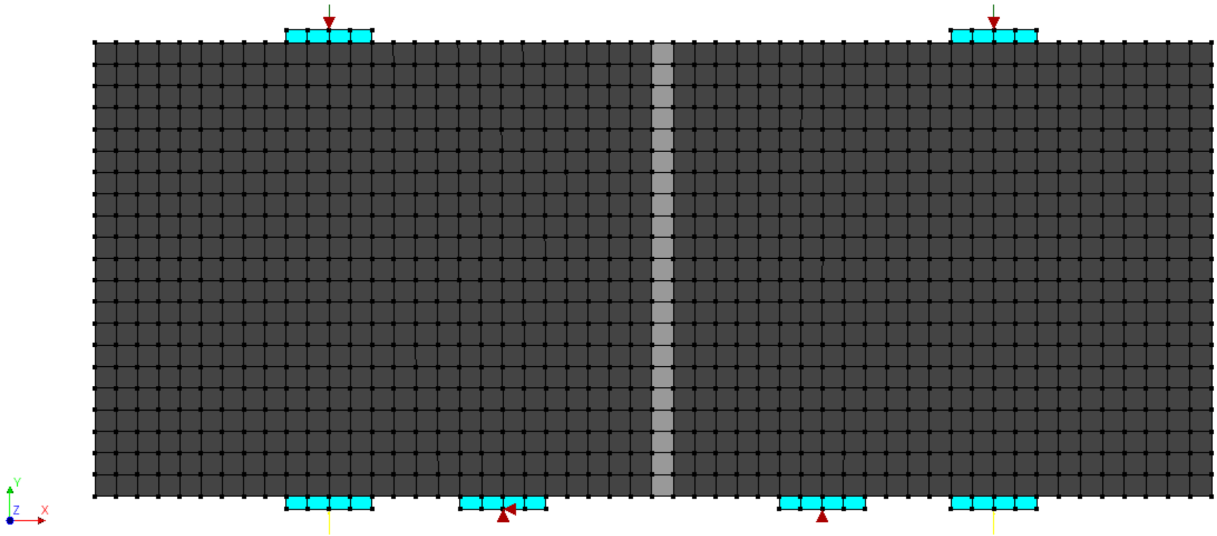

Figure 5.6: Finite element model of TUD_MAT-50U with linear 4-node elements

Table 5.7: Material properties for the three different window bank specimens

Engineering masonry model					
Specimen name			TUD_MAT-50U	TUD_MAT-50M	TUD_MAT-50P
Number of repetitions			10	30	100
Density	ρ	Kg/m^3	1680	1680	1680
Young's modulus perpendicular to bed-joint	E_y	MPa	3400	3400	3400
Young's modulus parallel to bed-joint	E_x	MPa	6831	2006	4257
Shear modulus	G_{xy}	MPa	1300	1300	1300
Tensile strength along the vertical	f_{ty}	MPa	0.55[1]	0.45[1]	0.6[1]
Tensile strength along the horizontal	f_{tx}	MPa	0.183[1]	0.15[1]	0.2[1]
Tensile fracture energy	G_f	N/mm	2[1]	1.2[1]	1.2[1]
Compressive strength	f_c	MPa	14	14	14
Compressive fracture energy	G_c	N/mm	20	20	20
Friction angle	ϕ	rad	0.6	0.6	0.6
Cohesion	c	MPa	0.15	0.15	0.15
1 - Calibrated value					

Table 5.8: Masonry linear isotropic properties

Masonry isotropic properties			
Young's modulus	E	MPa	3400
Poison's ratio	ν	-	0

Table 5.9: Steel properties

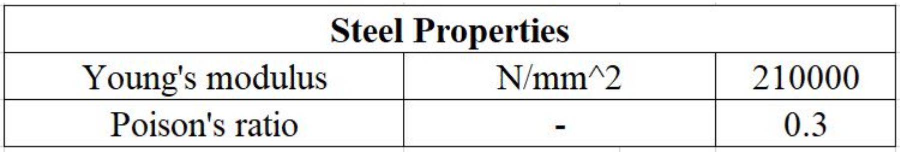

Steel Properties		
Young's modulus	N/mm^2	210000
Poison's ratio	-	0.3

Analysis properties and loading scheme

The supports and loading plates are provided for an uniform distribution of point loads like the counterweights and displacement controlled load. Each element is a plane stress type with square size, 25mm and a thickness of 100mm. The dimensions of the beam and the distance of the support and loading plates are obtained from Table 4.1 from chapter 5. The loading is displacement control with a Newton-Raphson iterative solution method using energy norm as given in Table 5.10. The counterweights are 471N each, which is approximately 48 kg as applied in the experiment. The energy convergence norm with 0.001 convergence tolerance is used for all three window bank samples. Although, it is interesting to note that energy norm with 0.0001 tolerance also gives similar results but takes a lot more computational time and effort. This is due to the tighter tolerance, more number of iterations are required to achieve convergence, which in-turn increases the computational time. The models were also tested to satisfy two norms simultaneously with a combination of (a)energy and displacement and (b)energy and force,and the conclusion is that these too, gave accurate results but took longer computational time. In general, the new degradation model takes 2 to 3 times the computational time when compared to the EMM model without degradation. Refer Table 5.11 for the details related to the computational time required with different tolerances for the energy norm.

Table 5.10: Analysis details for all the window bank samples

Number of repetitions	10, 30, 100
Element type	Linear
Solution type	regular Netwon-Raphson
Convergence norm	Energy
Convergence tolerance	0.001
Simultaneously satisfy all norms	OFF

Table 5.11: Computational time and tolerances used

Sample name	Reptitions	Energy norm Convergence tolerance	Computational time EMM (minutes)	Computational time EMM+degradation (minutes)	Time multiplier
TUD_MAT-50U	10	0.001	2	4	2X
		0.0001	4	15	3.75X
TUD_MAT-50M	30	0.001	7	12	1.7X
		0.0001	11	42	3.8X
TUD_MAT-50P	100	0.001	20	45	2.25X
		0.0001	34	130	3.8X

5.3 Results and Comparison

5.3.1 Window bank tests

The three window bank samples for 10, 30 and 100 repetitions is validated with the new model and the results are presented in this section. Hereafter the commercial version of EMM without degradation is referred to as "EMM" and the one with new degradation model is referred to as "EMM+degradation".

Figure 5.7 shows force vs vertical displacement of TUD_MAT-50U sample with 10 repetitions for (a) EMM+degradation (b)EMM (c)experimental results. It is clearly evident that the EMM model does not show any degradation or force reduction within a displacement set. All the repetitions overlap one on top of each other and return to the same point on the envelope curve. The EMM model does not show any plastic strain at the reloading point. This is because the model has a secant slope for the unloading and reloading branch. This is evident from the force vs displacement graphs of EMM results where all three displacement sets (R1, R2, R3) return to the origin. The EMM+degradation model does take into account the force reduction at the unloading point but does not take into account the plastic strain yet.

The force reduction vs number of repetitions with the new model closely matches the experimental results, both in terms of the hyperbolic shape and the percentage of degradation. The first displacement set R1 does not show much reduction in force when compared to the other two displacement sets which is similar to the experimental results. A normalized combined plot of the force reduction for all three models is shown in Figure 5.8.

The displacements from the computational model slightly deviate from the results of the experiments. This is because, in the experiment, the vertical displacement is measured at sensor 3 which is placed exactly along the force vertical but at the middle of the beam sample and not at the point of application of the force. Hence, the computational results have been matched in terms of the shape of the monotonic curve from the repetitive experiments in order to get a close match. Also, it is worth mentioning that, two sensors data from sensor 3 and sensor 1(see Figure 4.4 for sensor positions) have been compared to get the best match.

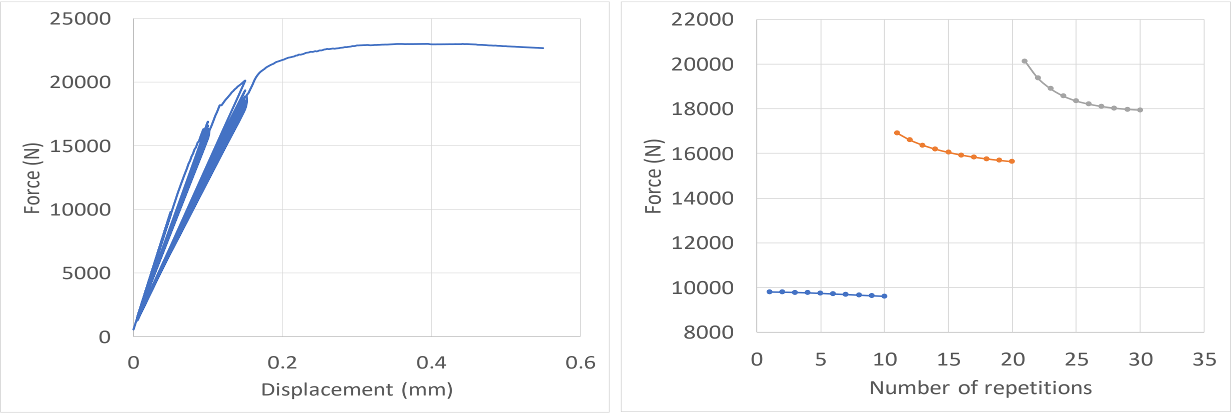

(a) EMM+Degradation model

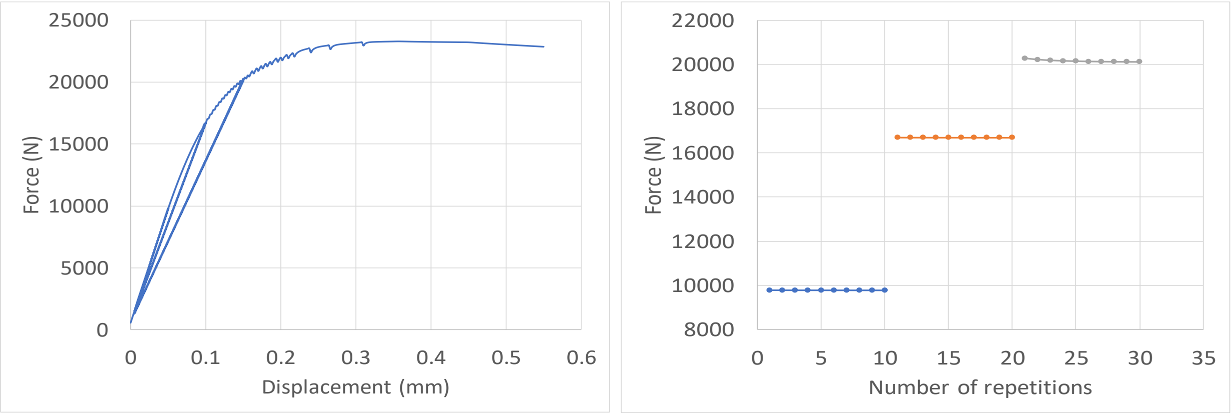

(b) EMM

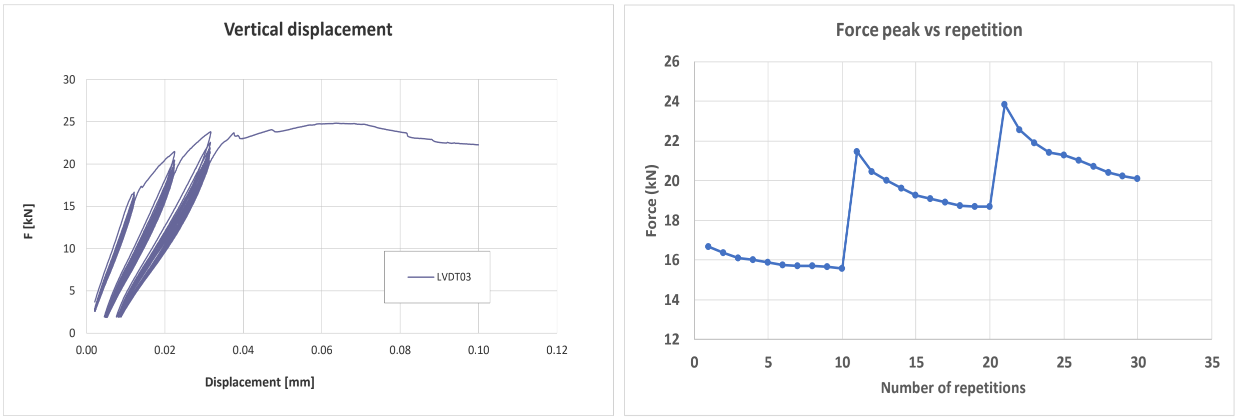

(c) Experimental

Figure 5.7: Force vs displacement (left) and Force vs number of repetitions(right) for window bank sample under 10 repetitions ($\xi_d = 1.5$)

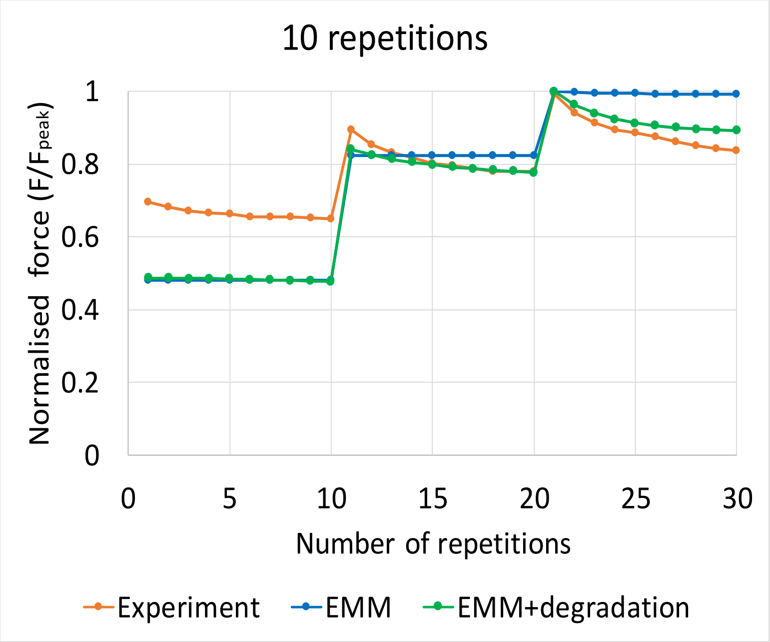

Figure 5.8: Combined normalized force reduction vs number of repetition plot for 10 repetitions sample ($\xi_d = 1.5$)

Refer Table 5.12 for the percentage of force reduction for each displacement set for all three window bank samples. The percentage of force reduction varies for the three displacement sets. This can be explained by the fact that every point on the softening branch of the tension constitutive model represents an amount of damage or in other words capacity of the structure. The higher the point, the closer it is to the tension strength of the material and hence it has larger capacity (minimum damage). The point for R1 displacement set in the softening branch of the stress-strain curve is closer to the tensile strength of the material which means that the amount of damage is very less and the structure has high capacity. Hence the reduction is small. Similar observations are made for 30 and 100 repetition window bank samples and the results are presented below.

Table 5.12: Percentage of force reduction for all three samples

Sample name	Number of repetitions	R1[%]	R2[%]	R3[%]	Average
TUD_MAT-50U	10	2.19	7.81	10.95	6.98%
TUD_MAT-50M	30	11.69	13.25	17.22	14.05%
TUD_MAT-50P	100	12.67	14.38	18.9	15.32%
Average		8.9%	11.81%	15.69%	

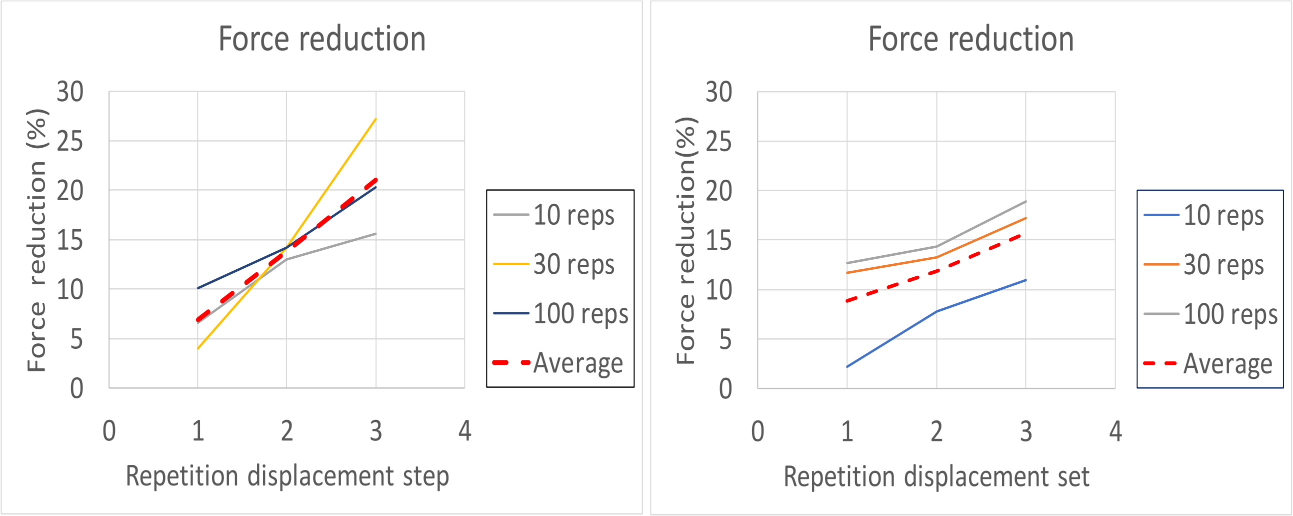

(a) EMM

(b) EMM+Degradation model

Figure 5.9: Force reduction in percentage at every displacement set for all three window bank samples compared with the experimental results

Figure 5.10 shows the force versus displacement plots of TUD_MAT-50M with 30 repetitions for (a) new degradation model (b) EMM without degradation and (c) experimental results. Here the force reduction gradually stabilizes by reaching an asymptote which is synonymous to the experimental results. Also it is seen that the force reduction for the first repetition is larger when compared to the force reduction of the last repetition considerably in a displacement set. This phenomenon was also observed in the experimental results as stated in chapter 5. This shows that the majority of the degradation occurs in the first 10 repetitions and gradually stabilizes with further increase in the repetitions. A normalized combined plot of the force reduction for all three models is shown in Figure 5.11.

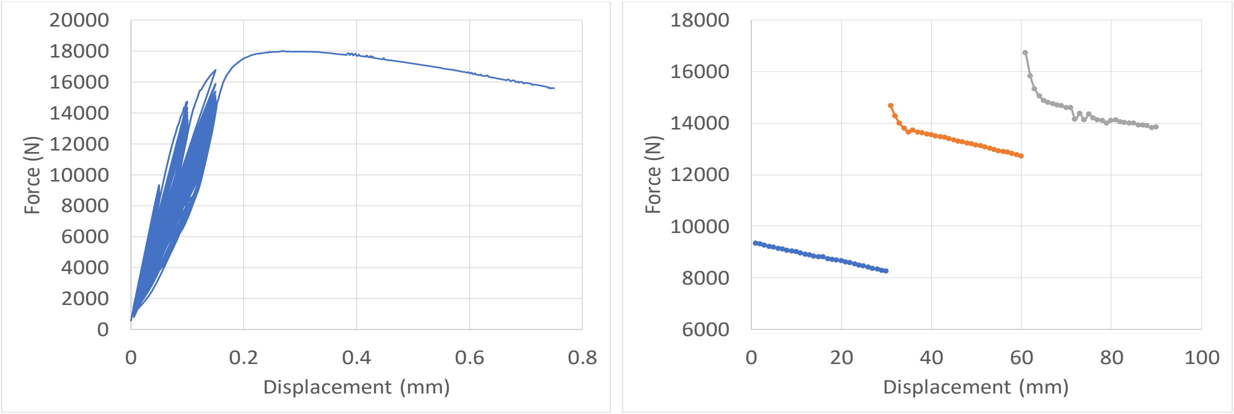

(a) EMM+Degradation model

Force vs displacement(left) and Force vs number of repetitions(right) for window bank sample under 30 repetitions ($\xi_d = 1.5$)

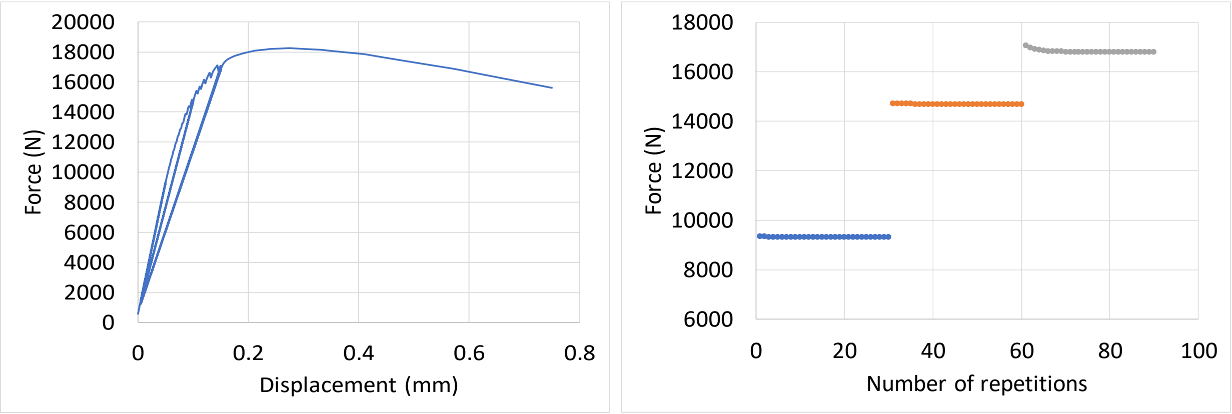

(b) EMM

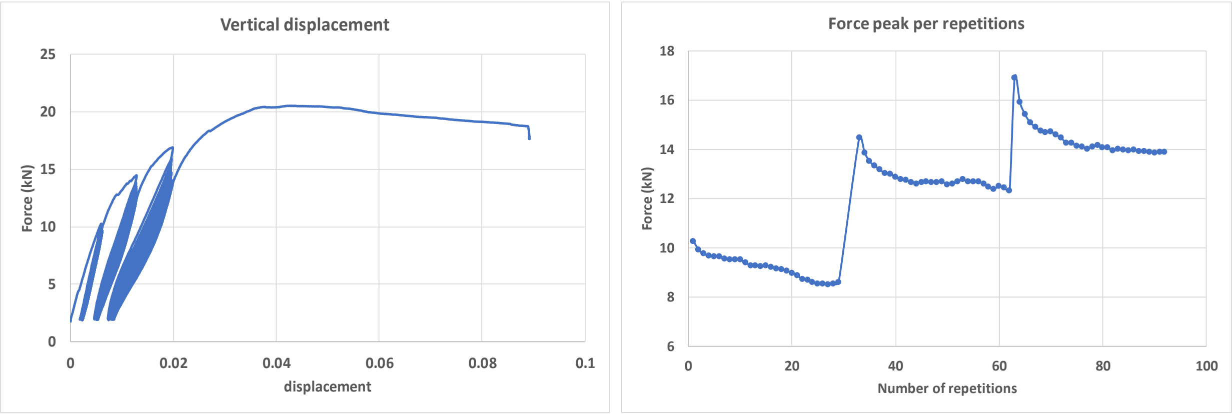

(c) Experimental

Figure 5.10: Force vs displacement(left) and Force vs number of repetitions(right) for window bank sample under 30 repetitions ($\xi_d = 1.5$)

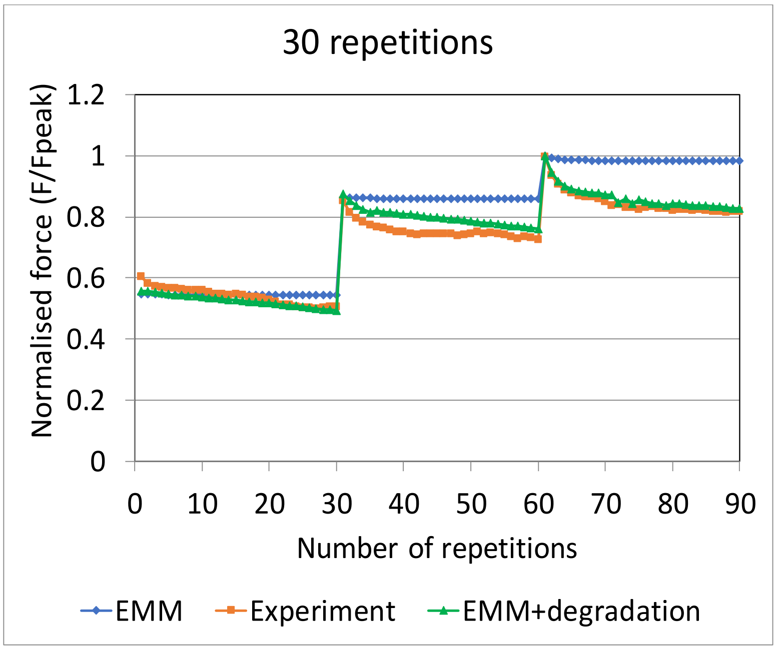

Figure 5.11: Combined normalized force reduction vs number of repetition plot for 30 repetitions sample ($\xi_d = 1.5$)

Figure 5.12 shows the force versus displacement plots of TUD_MAT-50P with 100 repetitions for (a) new degradation model (b) EMM without degradation and (c) experimental results. The force vs vertical displacement for experimental results shows excessive damage close to the sensor for 100 repetitions and hence the graph slightly deviates from that of 10 and 30 repetitions results. But it is verifiable from the horizontal top wall displacement graph in Figure 4.11 as to how the plot should be. Here, again a similar trend of force reduction is seen and the new degradation model can predict the force reduction quite accurately. There are some deviations in the force reduction, above 50 repetitions, which is due to convergence tolerance issues. The same model was run using energy norm with tolerance 0.0001 instead of 0.001 and, clear hyperbolic reduction was obtained, but at a high computational cost. The time consumed by the model with tighter tolerance was 120 minutes more than the fairly accurate results at tolerance of 0.001. Hence, it is only advisable to use tighter tolerances, when there are no restrictions on computational expense and effort. A normalized combined plot of the force reduction for all three models is shown in Figure 5.13.

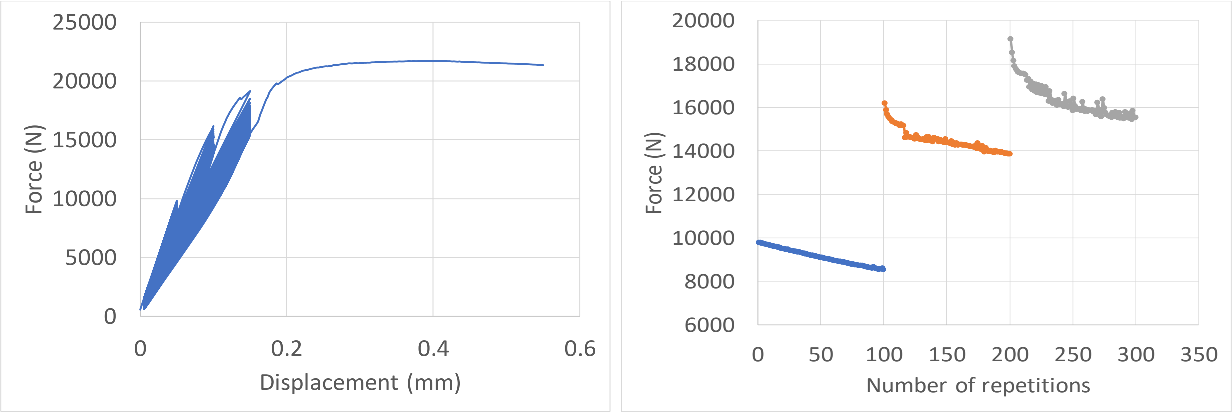

(a) EMM+Degradation model

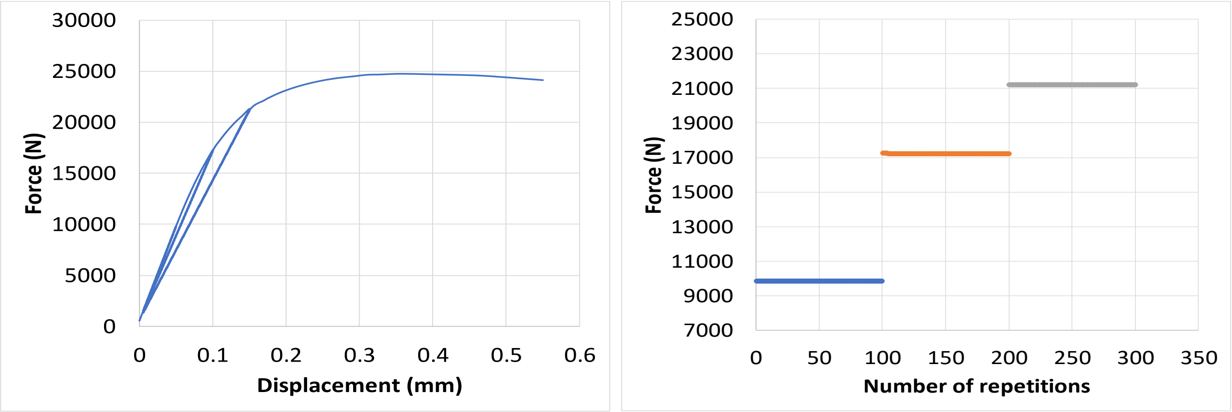

(b) EMM

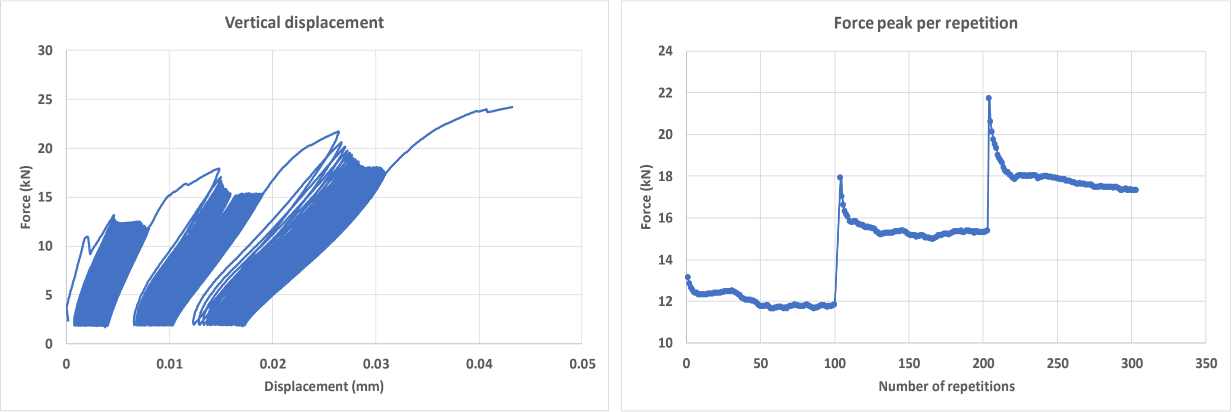

(c) Experimental

Figure 5.12: Force vs displacement(left) and Force vs number of repetitions(right) for window bank sample under 100 repetitions ($\xi_d = 1.5$)

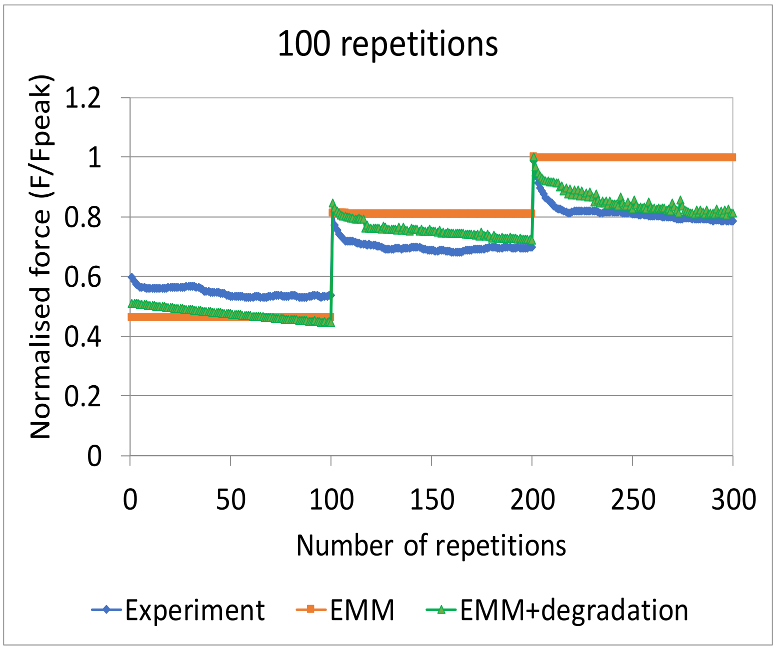

Figure 5.13: Combined normalized force reduction vs number of repetition plot for 100 repetitions sample ($\xi_d = 1.5$)

Table 5.13 shows the percentage change in values for the variations of ξ_d from 1.5 to 5. For 10 and 100 repetition samples the percentage change in force reduction remained in the same range as that of 30 repetition sample and hence are not shown here. For ξ_d value of 1.0 the test does not converge leading to improper answers and hence has been omitted.

Table 5.13: Percentage force reduction for variation of ξ_d values for 30 repetition samples

ξ_d	force reduction for displacement set R1 (%)	force reduction for displacement set R2 (%)	force reduction for displacement set R3 (%)
1.5	11.69	13.25	15.32
2	7.244219	10.10854	14.74412
3	5.833006	9.454809	13.8056
5	4.784195	9.17866	13.36787

Table 5.14 shows the load steps used for each window bank sample. The maximum displacement control load was upto 2 mm as was in the experiment. Figure 5.14 shows the crack width plots without degradation model on the left and with the degradation model on the right. The crack width option is set to calculate at the integration point in DIANA and measured at the top of the window bank sample (mid strip). The crack widths for the EMM model do not show any change within the repetitions, whereas the EMM+degradation model shows an increase in the crack width after every repetition in a displacement set. This shows that force reduction or degradation has indeed an effect on crack propagation and crack widths. Further,it is clearly seen in the contour plots from Figure 5.16, Figure 5.18, Figure 5.20 that there is crack propagation and crack width increase within each repetition displacement set.

Table 5.14: Load steps used for all three window bank samples

Sample name	Number of repetitions	Load steps
TUD_MAT-50U	10	0.001(25), (-0.0045(5), +0.0045(5))x10, 0.001(25), (-0.0095(5), +0.0095(5))x10, 0.001(25), (-0.0145(5), 0.0145(5))x10, 0.005(50)
TUD_MAT-50M	30	0.001(25), (-0.0045(5), +0.0045(5))x30, 0.001(25), (-0.0095(5), +0.0095(5))x30, 0.001(25), (-0.0145(5), 0.0145(5))x30, 0.005(50)
TUD_MAT-50P	100	0.001(25), (-0.0045(5), +0.0045(5))x100, 0.001(25), (-0.0095(5), +0.0095(5))x100, 0.001(25), (-0.0145(5), 0.0145(5))x100, 0.005(50)

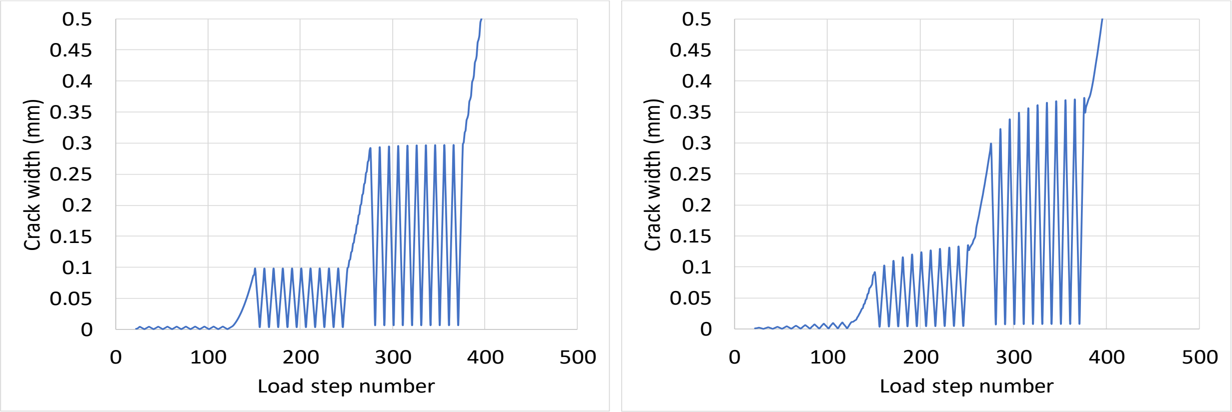

(a) 10 repetitions

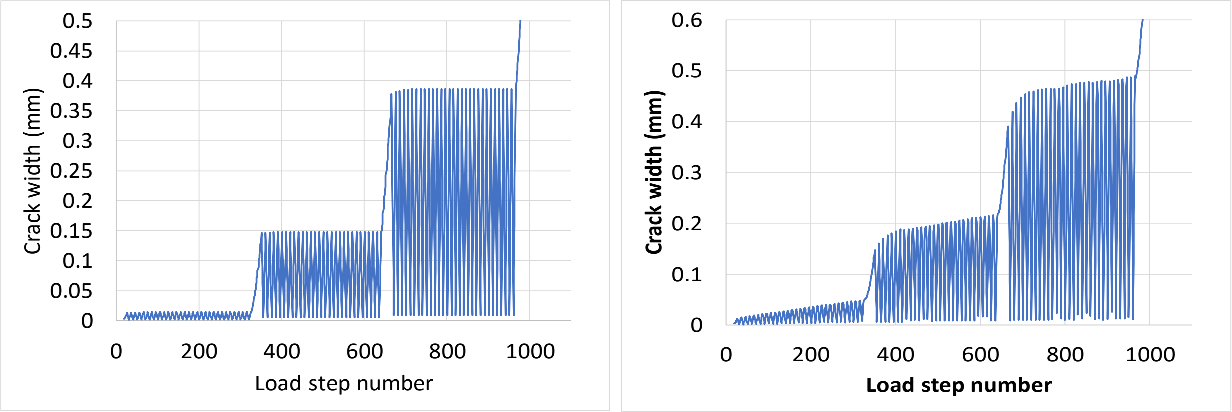

(b) 30 repetitions

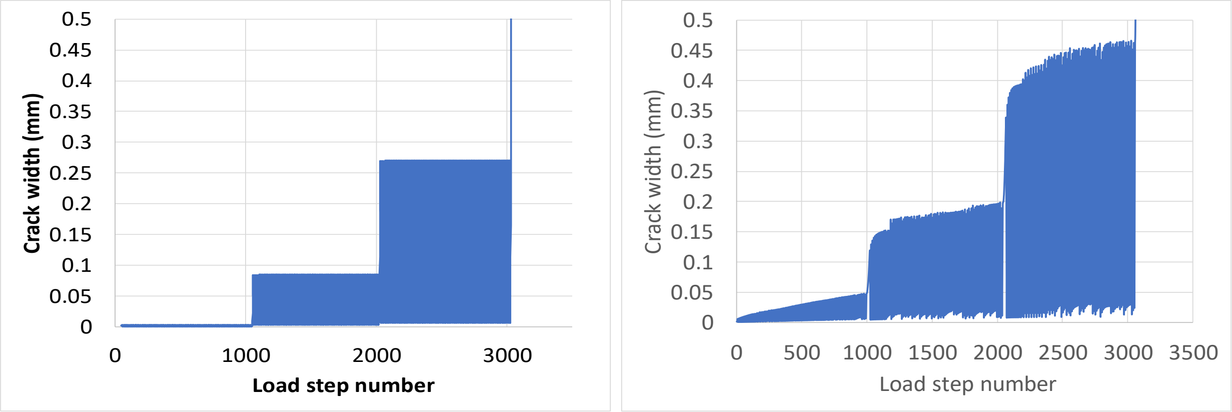

(c) 100 repetitions

Figure 5.14: Crack width variation vs load step number for all three window bank samples without(left) and with(right) degradation model

Figure 5.16 shows contour plots for both EMM, EMM+degradation at the beginning and at the end of each set for 10 repetitions window bank sample. Table 5.15 gives a detailed overview of the load step number at the start and end of each displacement set and also the contour color calibration values used for proper comparison between EMM and EMM+degradation plots. Figure 5.11 shows the contour plots for displacement set R1 of 10 repetition window bank sample. Here we clearly notice that there is crack propagation as well as crack widening from the start and the end of the set. At the start of the displacement set R1 the crack width at the top two elements is about 1.43e-3mm and by the end of the set the crack width increased to 1.14e-2mm at the top element and also has propagated to the third element. This trend can be seen in the other two displacement sets similarly. Also notice that when using the EMM model there is no change in the crack width contours as was verified by the graphs before in Figure 5.14.

Table 5.15: Load steps at the start and end of each displacement set along with minimum and maximum calibrated contour values

Sample name (repetitions)	Displacement set	load step number	Contour color magnitude	Crackwidth (mm)
TUD_MAT-50U (10 reps)	R1	26	min	0
		126	max	1.14e-2
	R2	151	min	0
		251	max	0.13
	R3	276	min	0
		376	max	0.37
TUD_MAT-50M (30 reps)	R1	26	min	0
		316	max	4.85e-2
	R2	351	min	0
		641	max	0.22
	R3	666	min	0
		956	max	0.49
TUD_MAT-50P (100 reps)	R1	26	min	0
		1016	max	9.0e-2
	R2	1041	min	0
		2031	max	0.25
	R3	2086	min	0
		3046	max	0.5

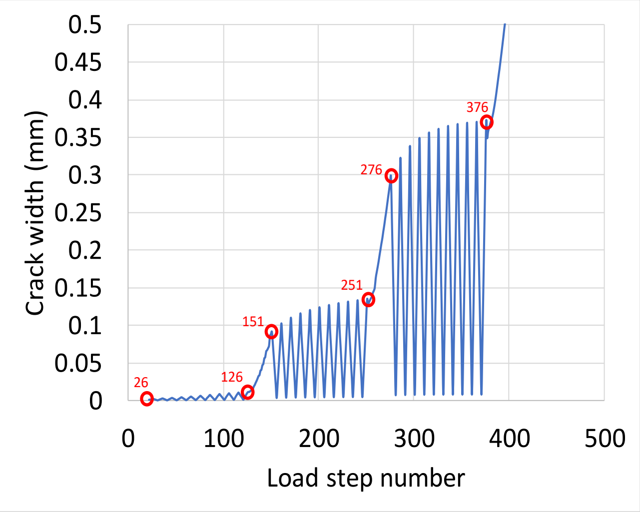

Figure 5.15: Crack width plot showing the load step at start and end of each displacement set

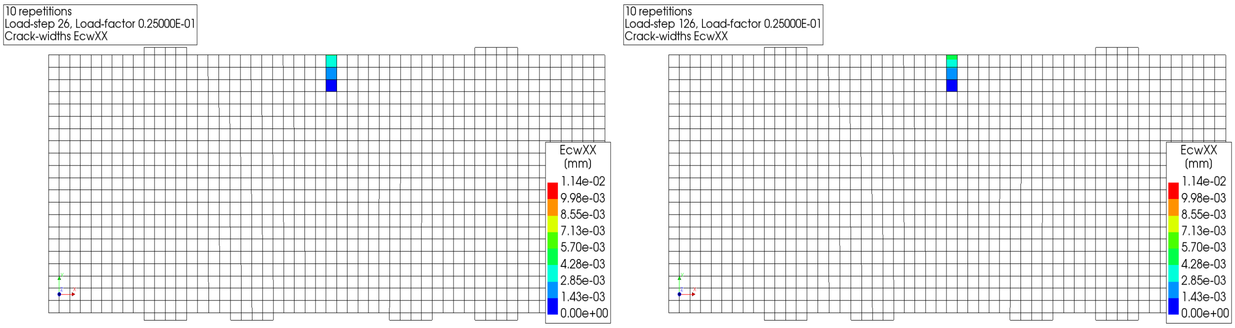

(a) EMM

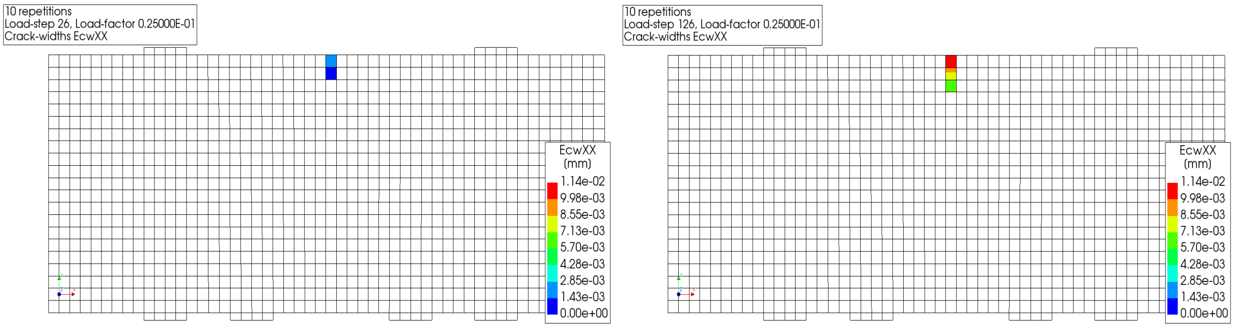

(b) EMM+degradation

Displacement set R1

Crack width plots showing start(left) and end(right) of a repetition set for 10 repetitions sample

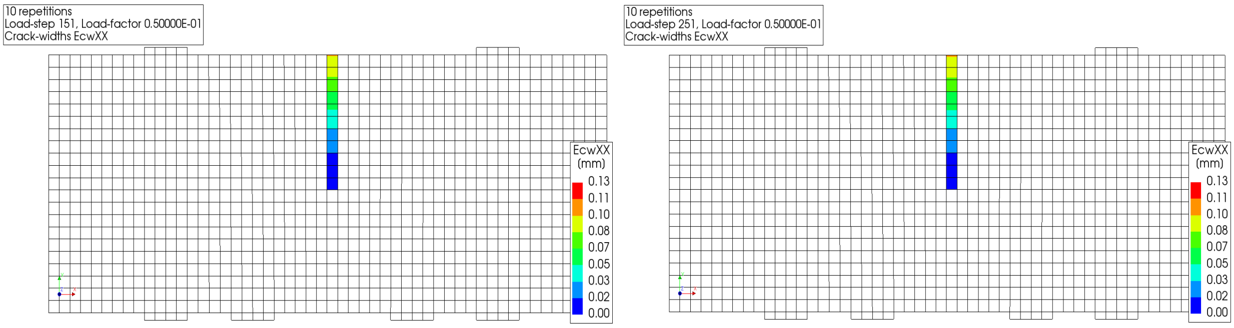

(c) EMM

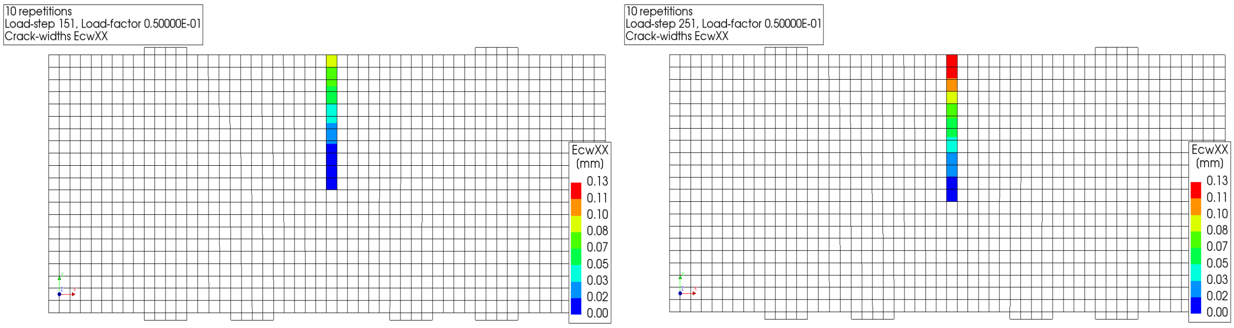

(d) EMM+degradation

Displacement set R2

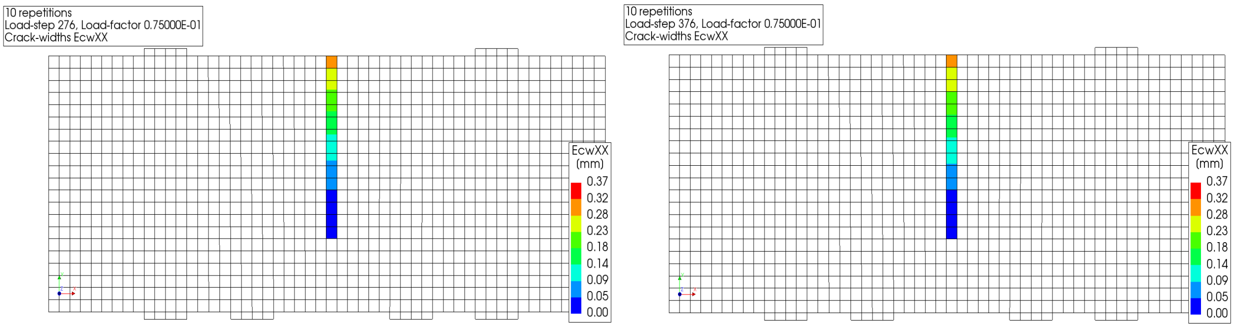

(e) EMM

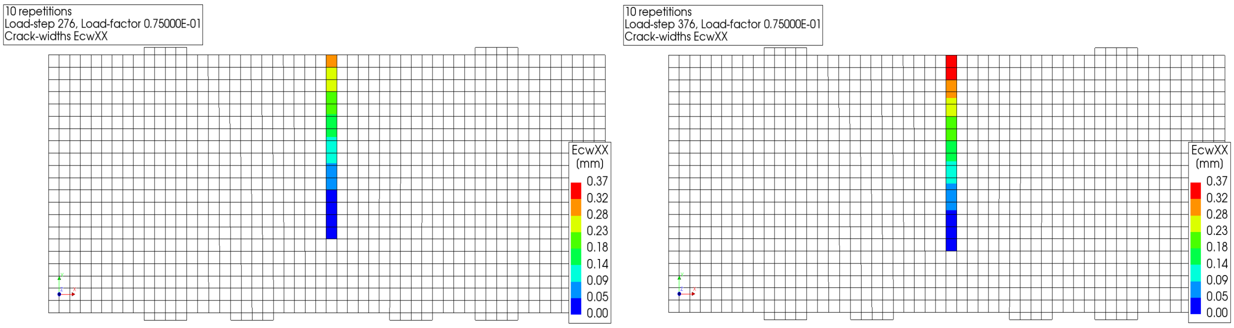

(f) EMM+degradation

Displacement set R3

Figure 5.16: Crack width plots showing start(left) and end(right) of a repetition set for 10 repetitions sample

Figure 5.18 shows contour plots for both EMM, EMM+degradation at the beginning and at the end of each set for 30 repetitions window bank sample. As explained before the crack width contours show a similar trend of crack widening and propagation within each set, the only difference is the magnitude of crack width when the number of repetitions increases which can be seen from Table 5.15. Notice that in Figure 5.17 and Figure 5.13 for displacement set R3 of 10 repetition and 30 repetition sample respectively, the crack width at the top most element is about 0.49mm after 30 repetitions, 0.37 after 10 repetitions. This shows that the major amount of degradation happens in the first 10 repetitions and in the rest of the repetitions there is comparatively lower magnitude of degradation. This confirms the observations and the reason hypothesized in the experimental results as mentioned in chapter 5. Similarly, comparing Figure 5.17 and Figure 5.21 for displacement set R3 of 30 repetition and 100 repetition sample respectively, we see that the crack width stays the same at 0.49mm which means that the degradation has remained almost same after 30 repetitions.

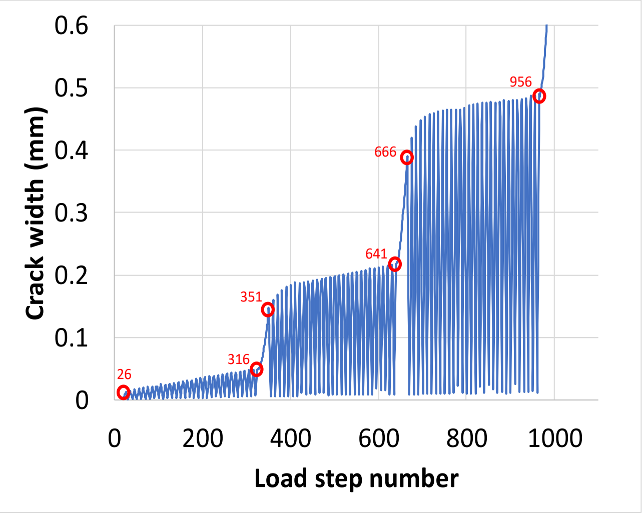

Figure 5.17: Crack width plot showing the load step at start and end of each displacement set

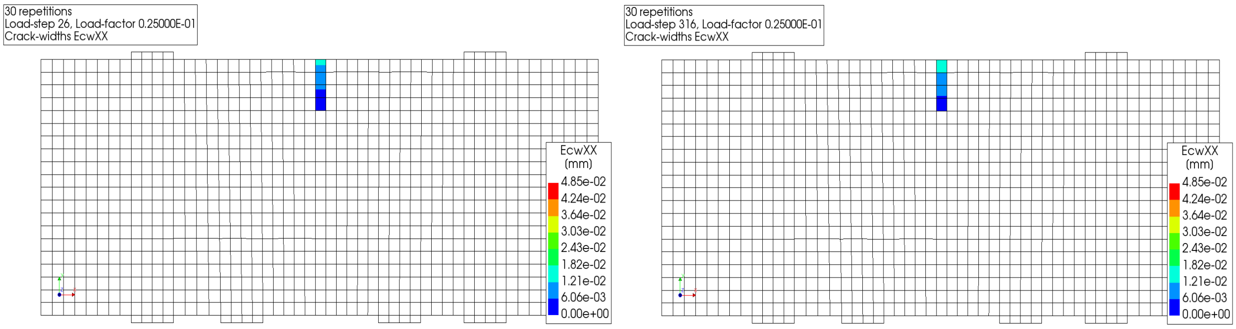

(a) EMM

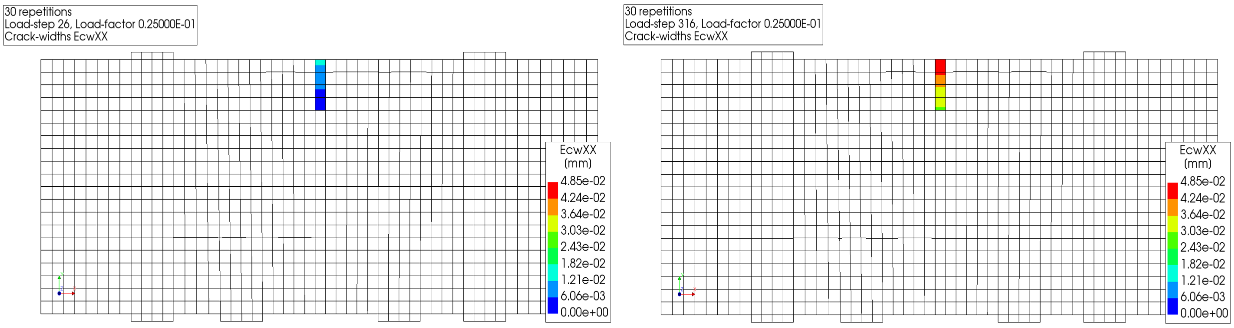

(b) EMM+degradation

Displacement set R1

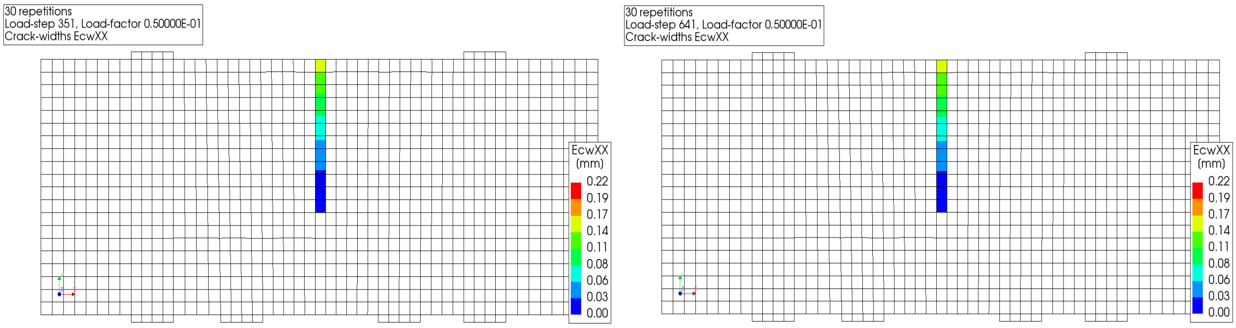

(c) EMM

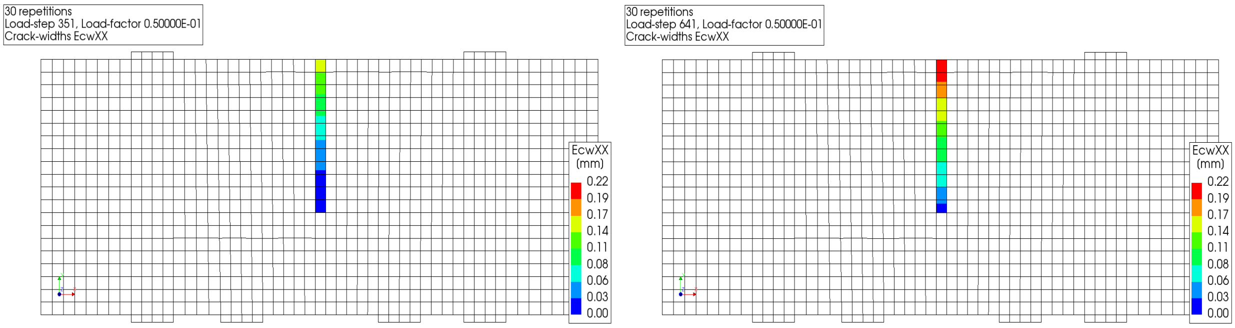

(d) EMM+degradation

Displacement set R2

Crack width plots showing start(left) and end(right) of a repetition set for 30 repetitions sample

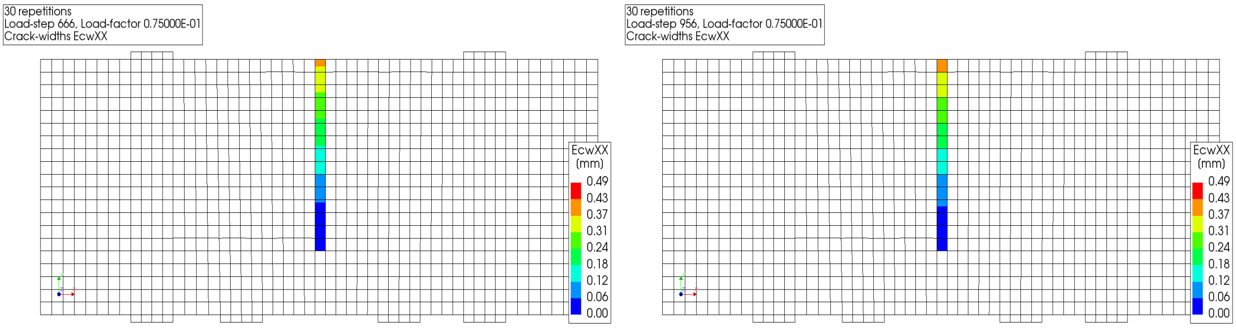

(e) EMM

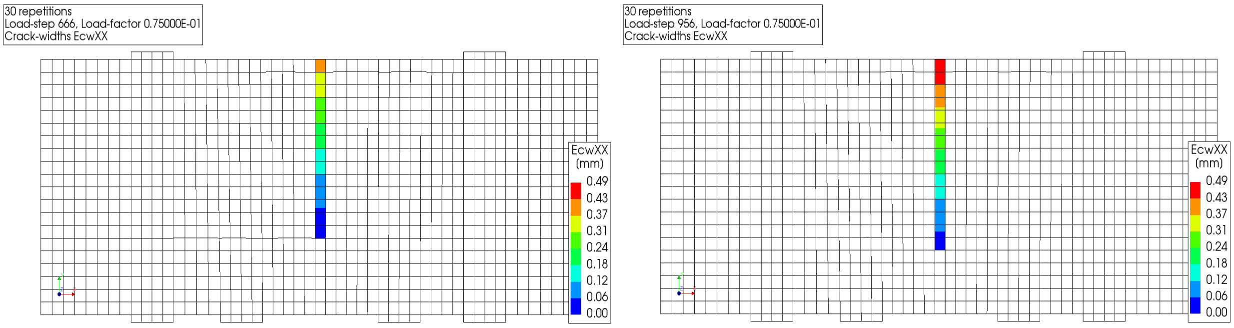

(f) EMM+degradation

Displacement set R3

Figure 5.18: Crack width plots showing start(left)and end(right) of a repetition set for 30 repetitions sample

Figure 5.20 shows contour plots for both EMM, EMM+degradation at the beginning and at the end of each set for 100 repetitions window bank sample.

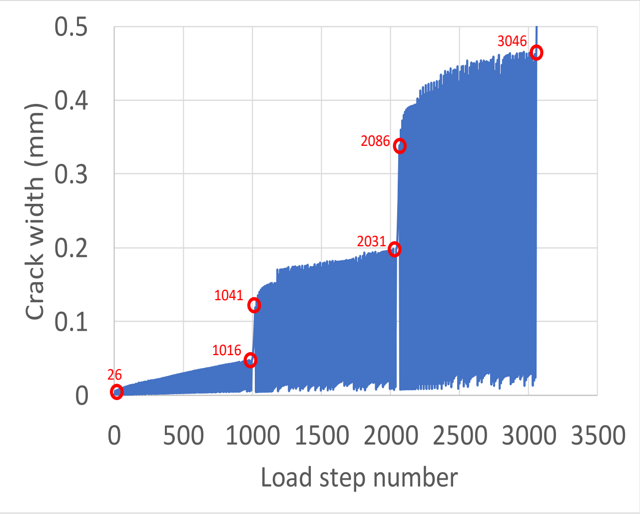

Figure 5.19: Crack width plot showing the load step at start and end of each displacement set

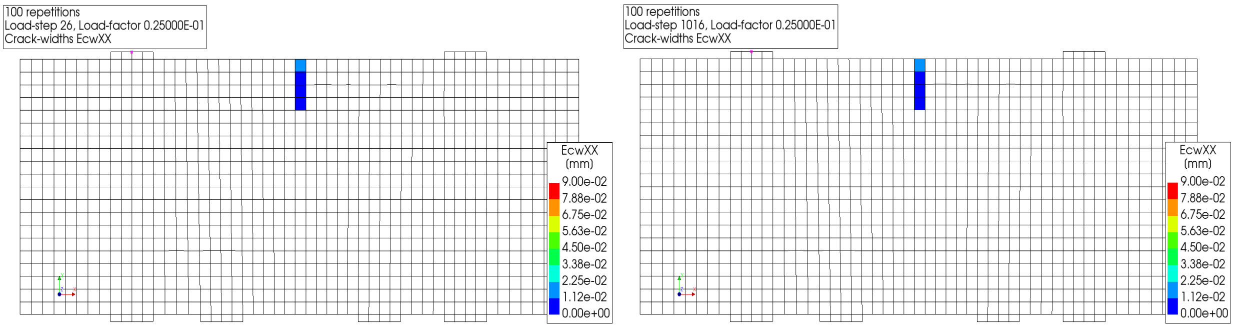

(a) EMM

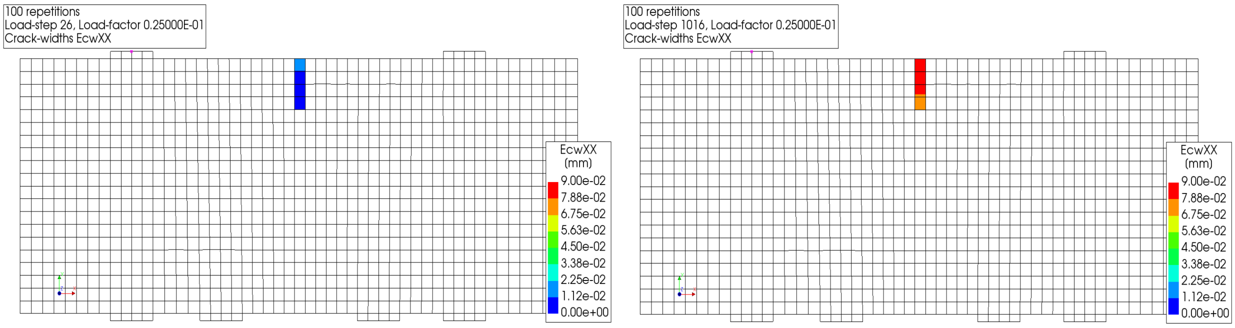

(b) EMM+degradation

Displacement set R1

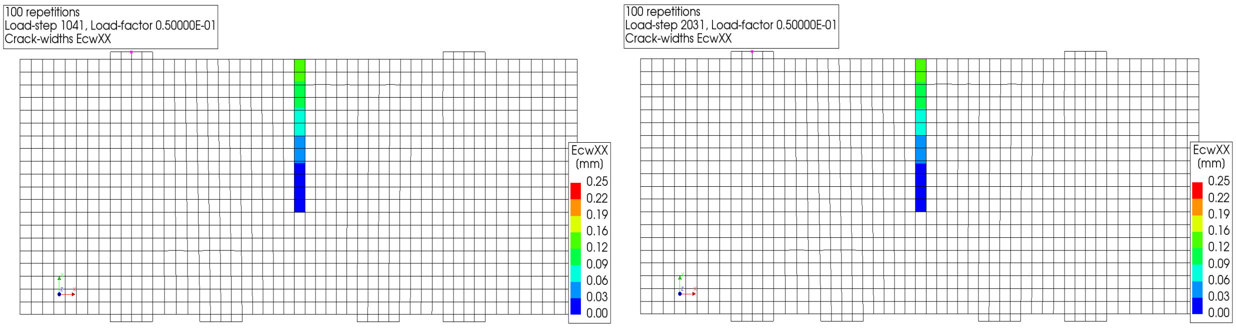

(c) EMM

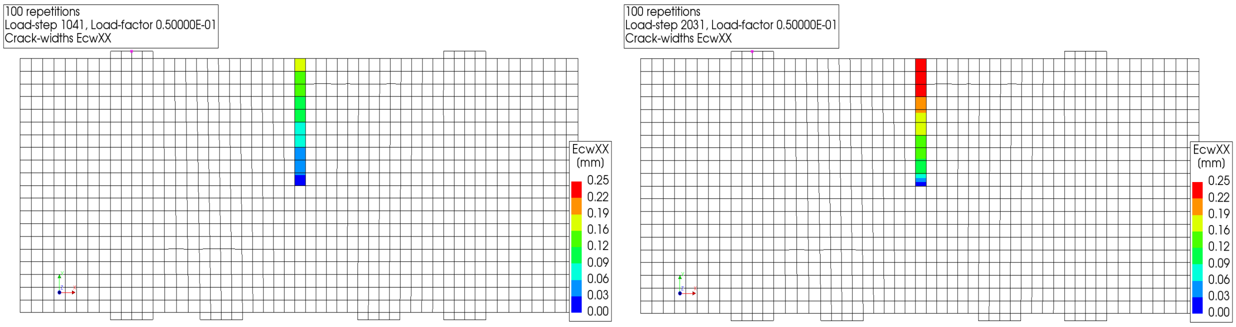

(d) EMM+degradation

Displacement set R2

Crack width plots showing start(left) and end(right) of a repetition set for 100 repetitions sample

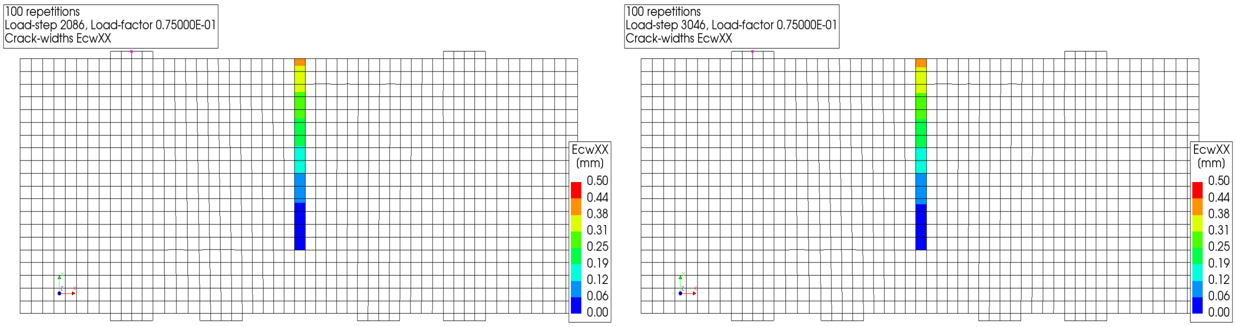

(e) EMM

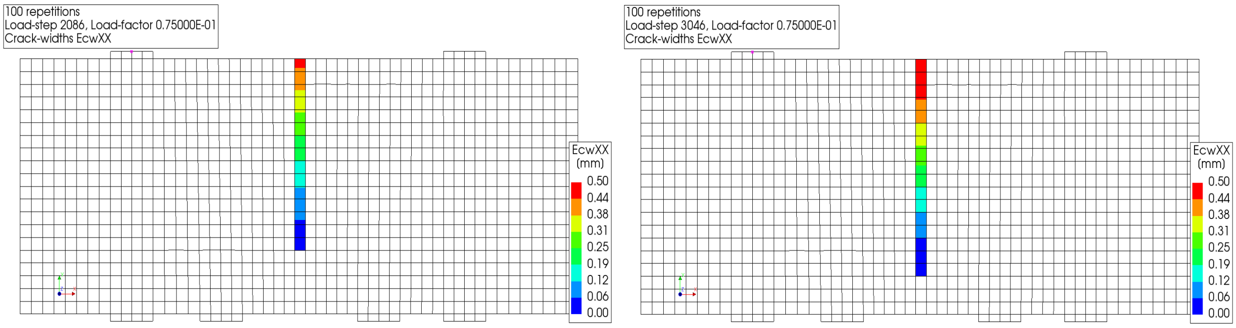

(f) EMM+degradation

Displacement set R3

Figure 5.20: Crack width plots showing start(left) and end(right) of a repetition set for 100 repetitions sample

5.3.2 Wall with an opening

The degradation model is tested for a wall with an opening and the results are presented in this section. The reader is directed towards the report “ Damage sensitivity of Groningen Masonry Structures - Experimental and computational studies ” [Korswagen et al., 2017] for all information regarding the material properties and modeling strategy considered for the wall. In this section only the results of the degradation model and its comparison with the EMM model is given.

The value of the calibration constant ξ_d was varied to 3.5 to exactly match the experimental results. The analysis is based on regular Newton-Raphson with displacement and force norm.

Refer Table 5.16 for convergence criteria details. Figure 5.21 shows the force vs displacement plots and the force reduction plots from EMM model(left) and EMM+degradation model(right). Here, it is noticeable that there is no plastic strain at the reloading point as the new model proposed assumes a secant slope for all unloading-reloading branches as explained in the last section. Also the force reduction for every displacement set shows no degradation for the EMM model and the EMM+degradation model follows a hyperbolic path as expected. Figure 5.22

shows a normalized force reduction graph for experiment and model generated results. It can be seen that, the amount and shape of the force reduction matches closely with that of the experimental results. Further calibration may be necessary to match the model results exactly with that of the experiment.

It is interesting to note that the EMM model took around 7 hours to run and the EMM+degradation model took around 22 hours on my system i.e. the EMM+degradation model took 3 times the EMM model in terms of computational time.

Table 5.16: Analysis details for wall sample

Number of repetitions	20
Element type	quadratic
Solution type	regular Netwon-Raphson
Convergence norm	displacement or force
Convergence tolerance	0.01
Simultaneously satisfy all norms	OFF

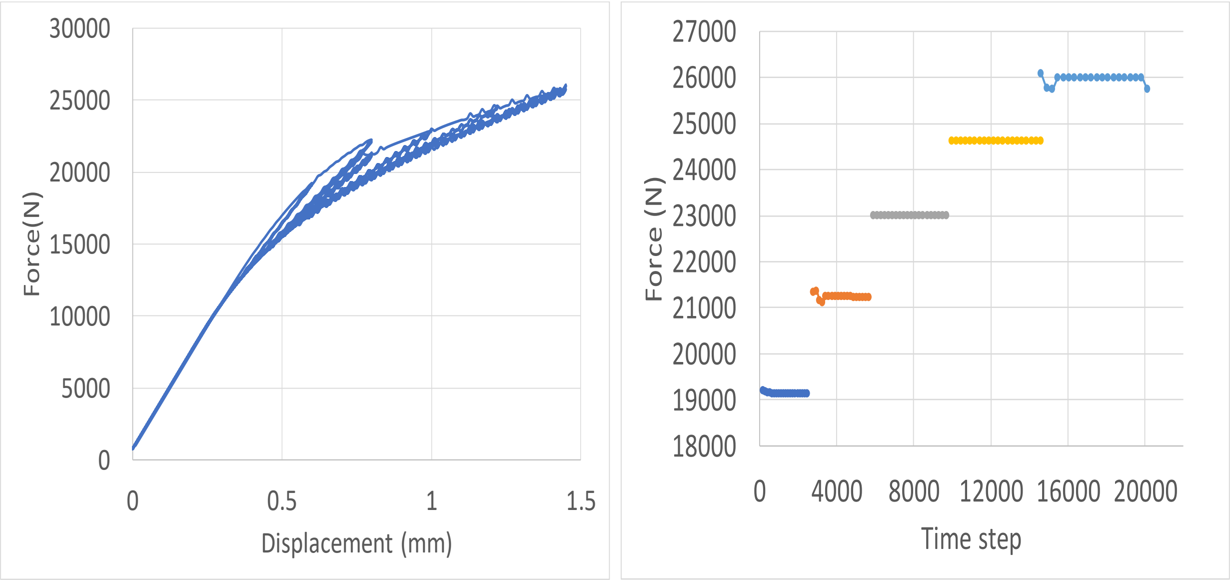

(a) EMM

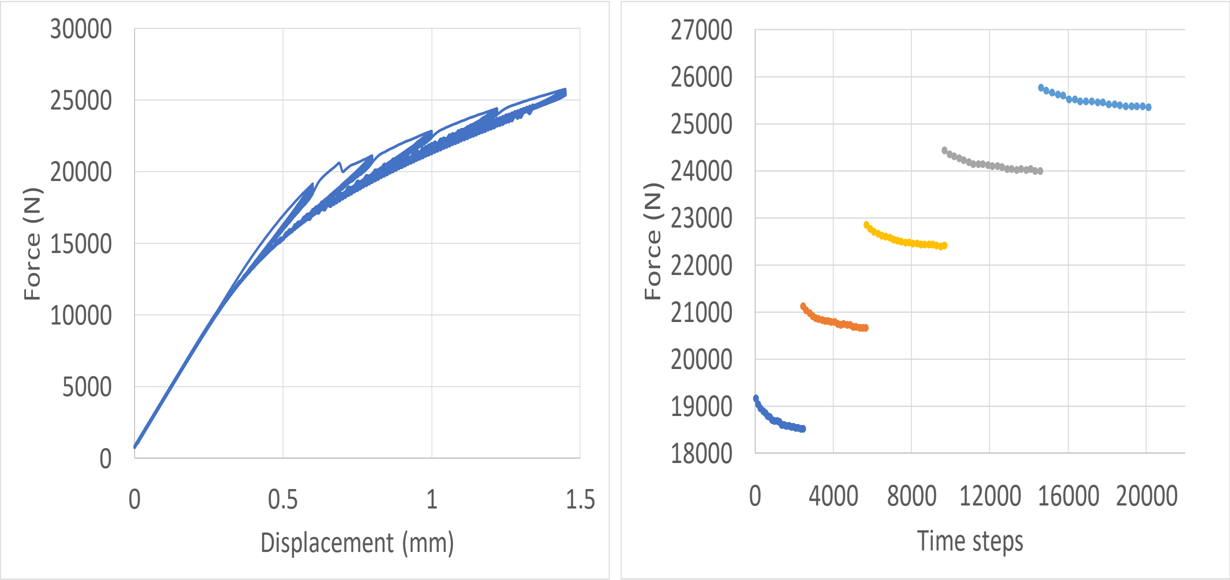

(b) EMM+degradation

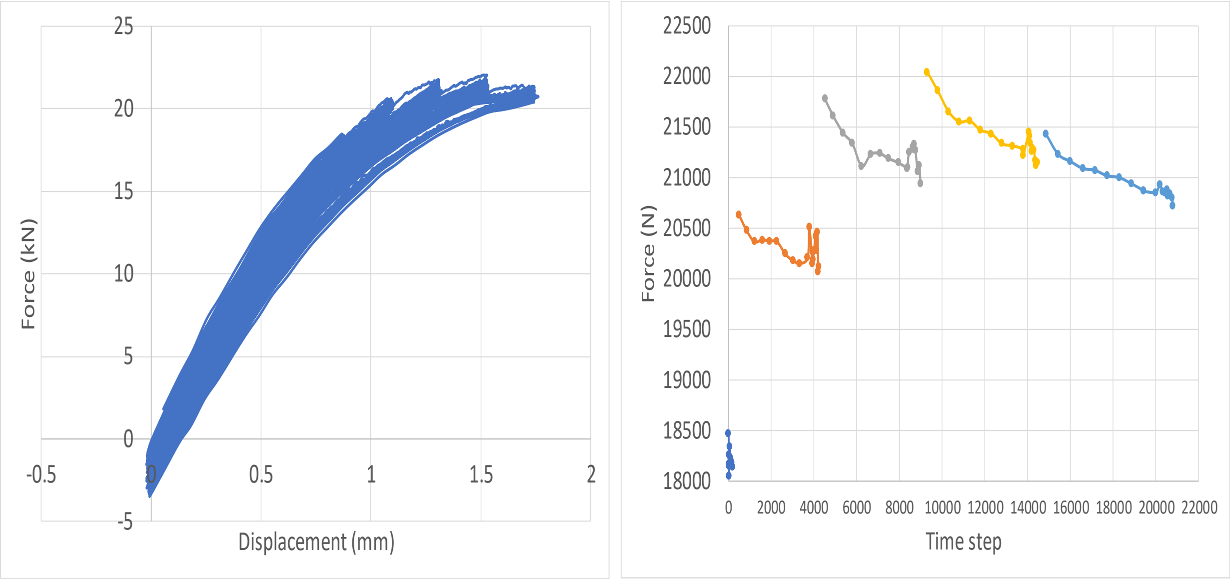

(c) Experiment

Figure 5.21: Force vs displacement(left) and force reduction vs timestep(right) for wall sample

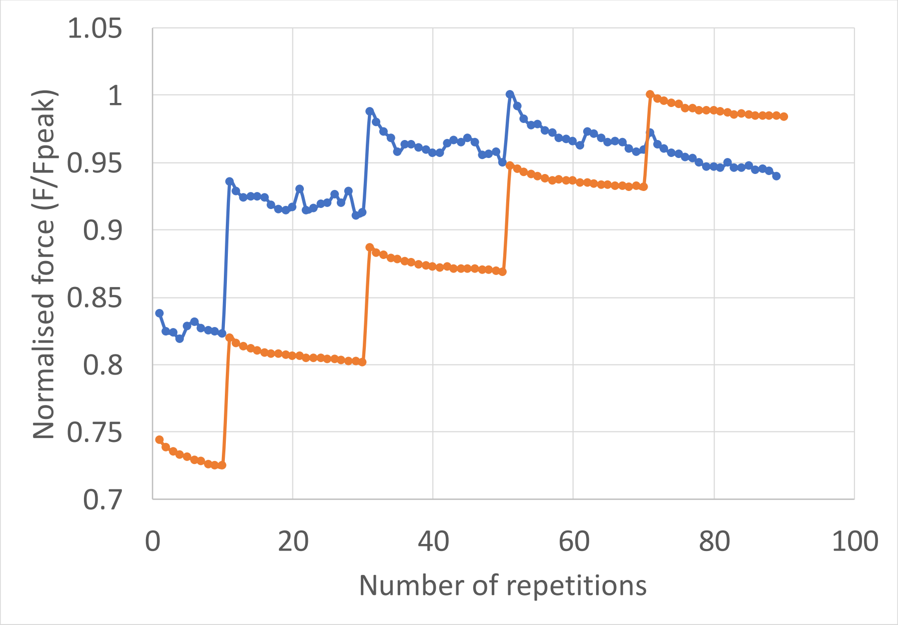

Figure 5.22: Normalised force vs number of repetitions comparing experiment and EMM+degradation model

Figure 5.23 shows the crack width plots of the wall sample at the end of each repetition displacement set. The contour plots have been calibrated based on the maximum values of crack width for the EMM+degradation model and as given in Table 5.17. It also gives the time step values in each repetition displacement set used for the pushover analysis of the wall.

Table 5.17: Time steps and corresponding crack width contour value

Repetition displacement set	Time step	Crack width contour value (mm)
1	2360	0.15
2	5540	0.44
3	9520	0.66
4	14378	0.90
5	20155	1.15

It is noticeable from the crack width plots that the new degradation model clearly shows the crack propagation, crack localization and crack width widening in each displacement set. At the end of the first displacement set two distinctive cracks at diagonally opposite corners of the window are visible. These cracks propagate further with successive displacement sets along the horizontal, towards the edges of the wall. Meanwhile, another crack at the bottom left edge appears after the second displacement set. This crack quickly becomes severe with a crack width of 1.15mm by the last displacement set. These crack width plots closely match with the DIC strain plots taken during the experiments. In the EMM model without degradation, the crack width remains the same for all the displacement sets which clearly deviates from that of the experimental results.

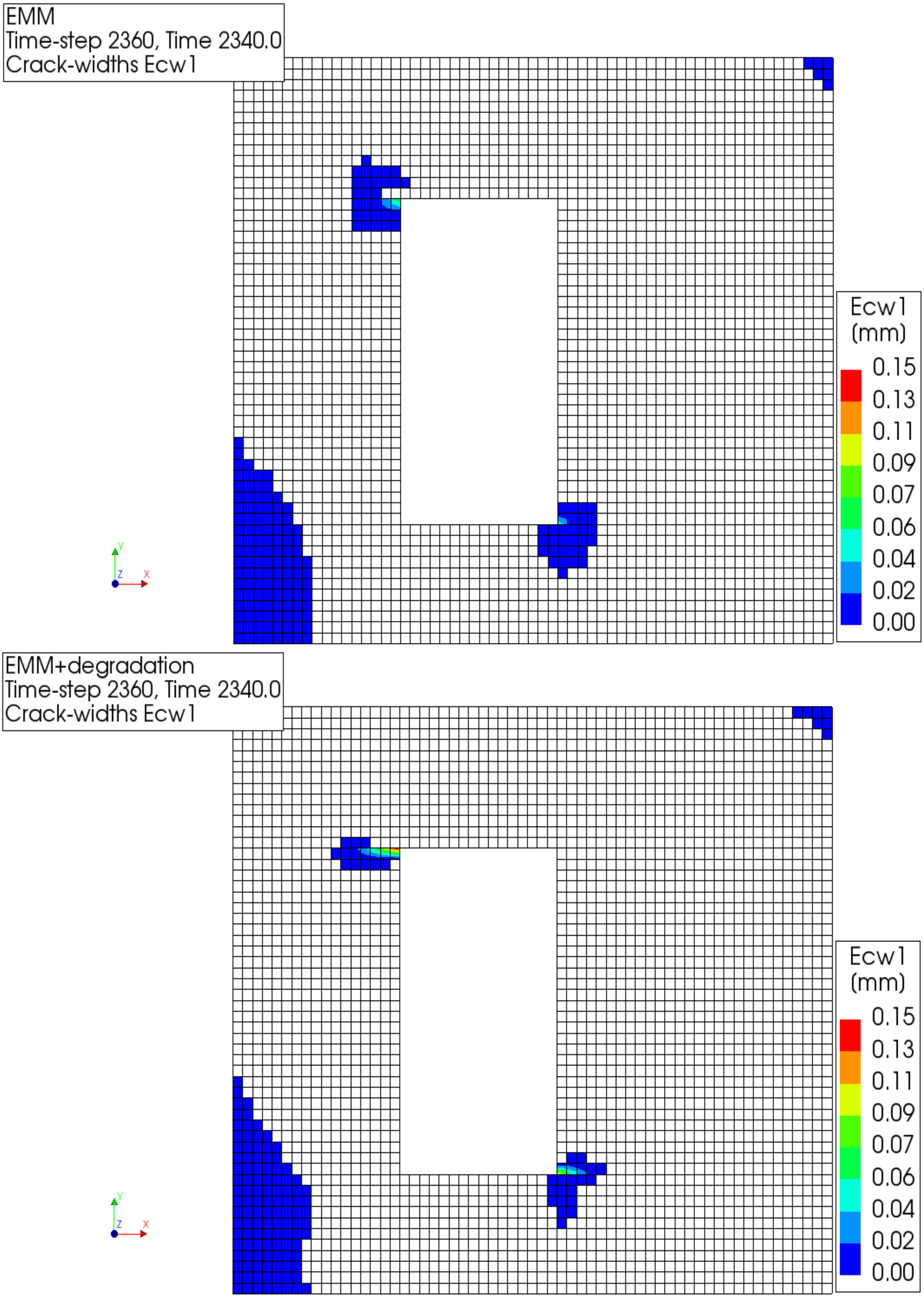

(a) Crack width plots showing EMM(top) and EMM+degradation(bottom) for displacement set 1

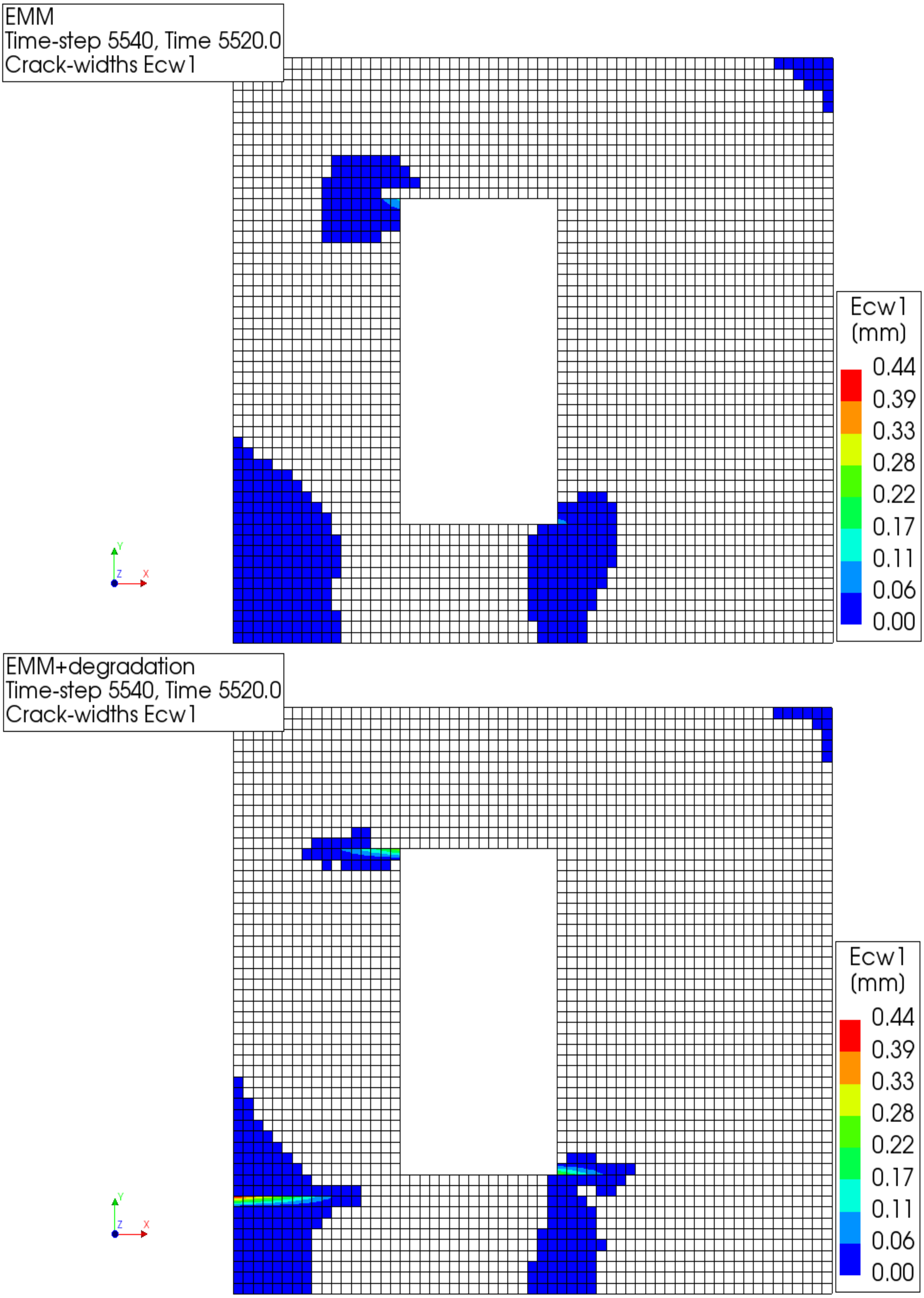

(b) Crack width plots showing EMM(top) and EMM+degradation(bottom) for displacement set 2

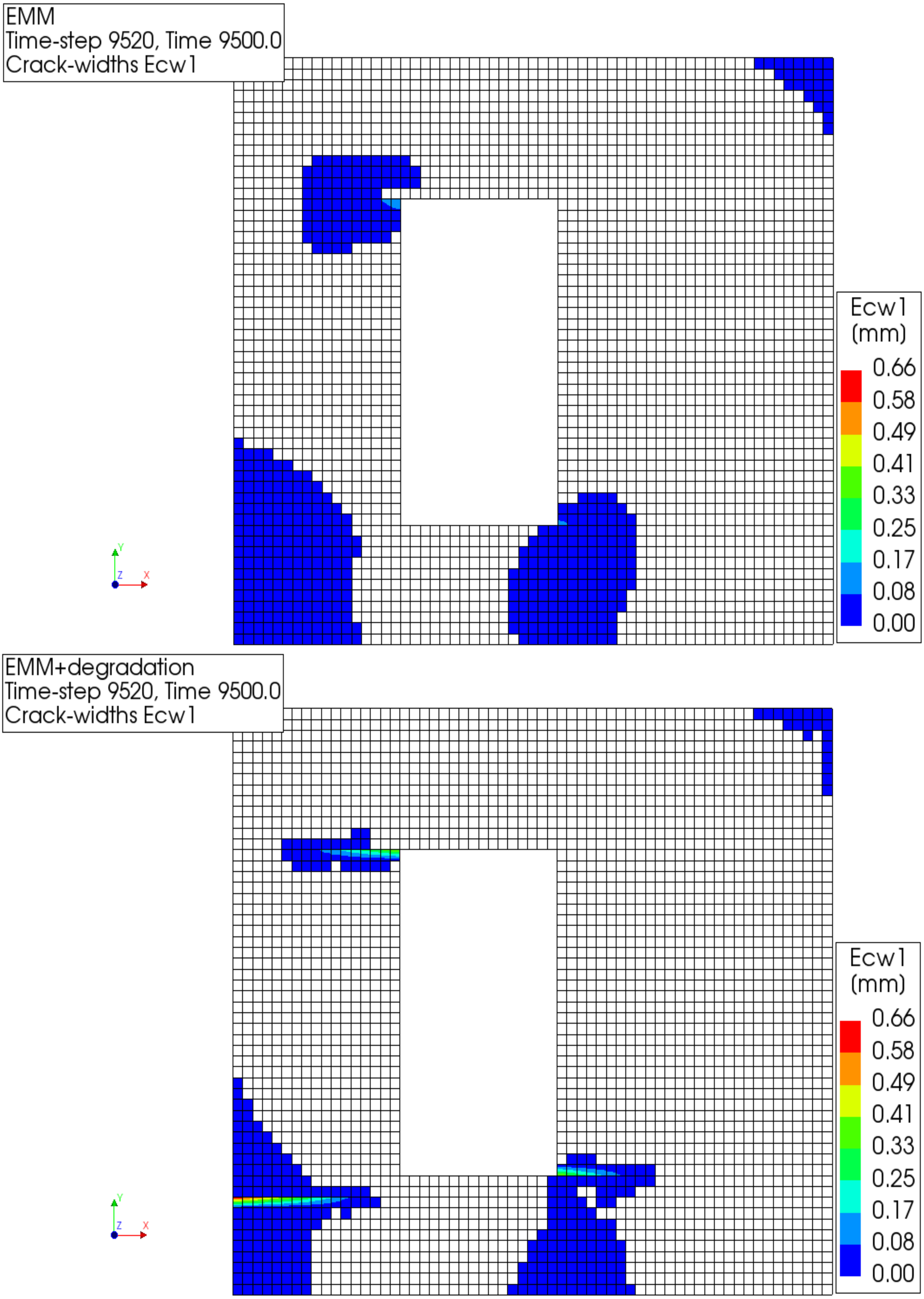

(c) Crack width plots showing EMM(top) and EMM+degradation(bottom) for displacement set 3

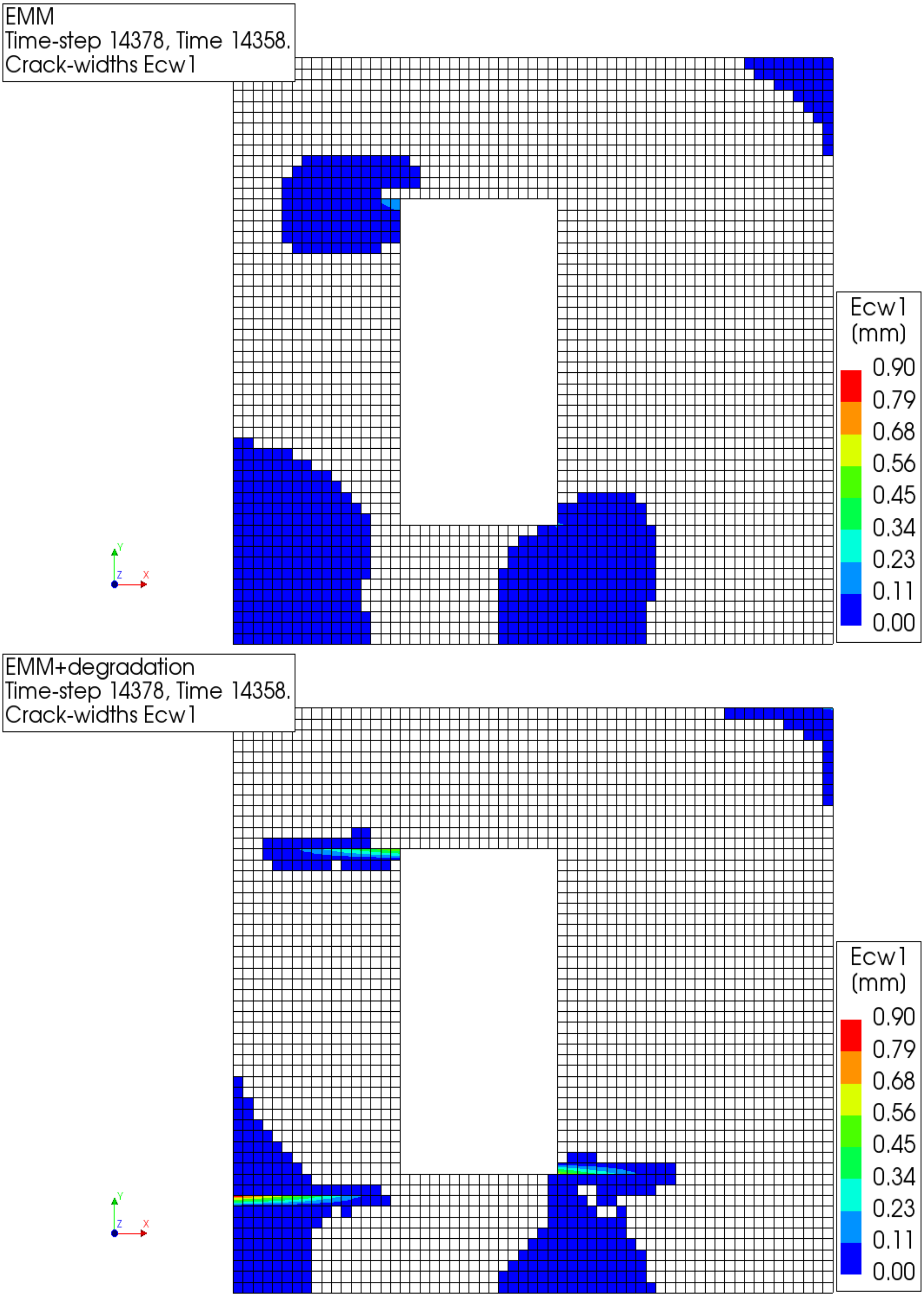

(d) Crack width plots showing EMM(top) and EMM+degradation(bottom)for displacement set 4

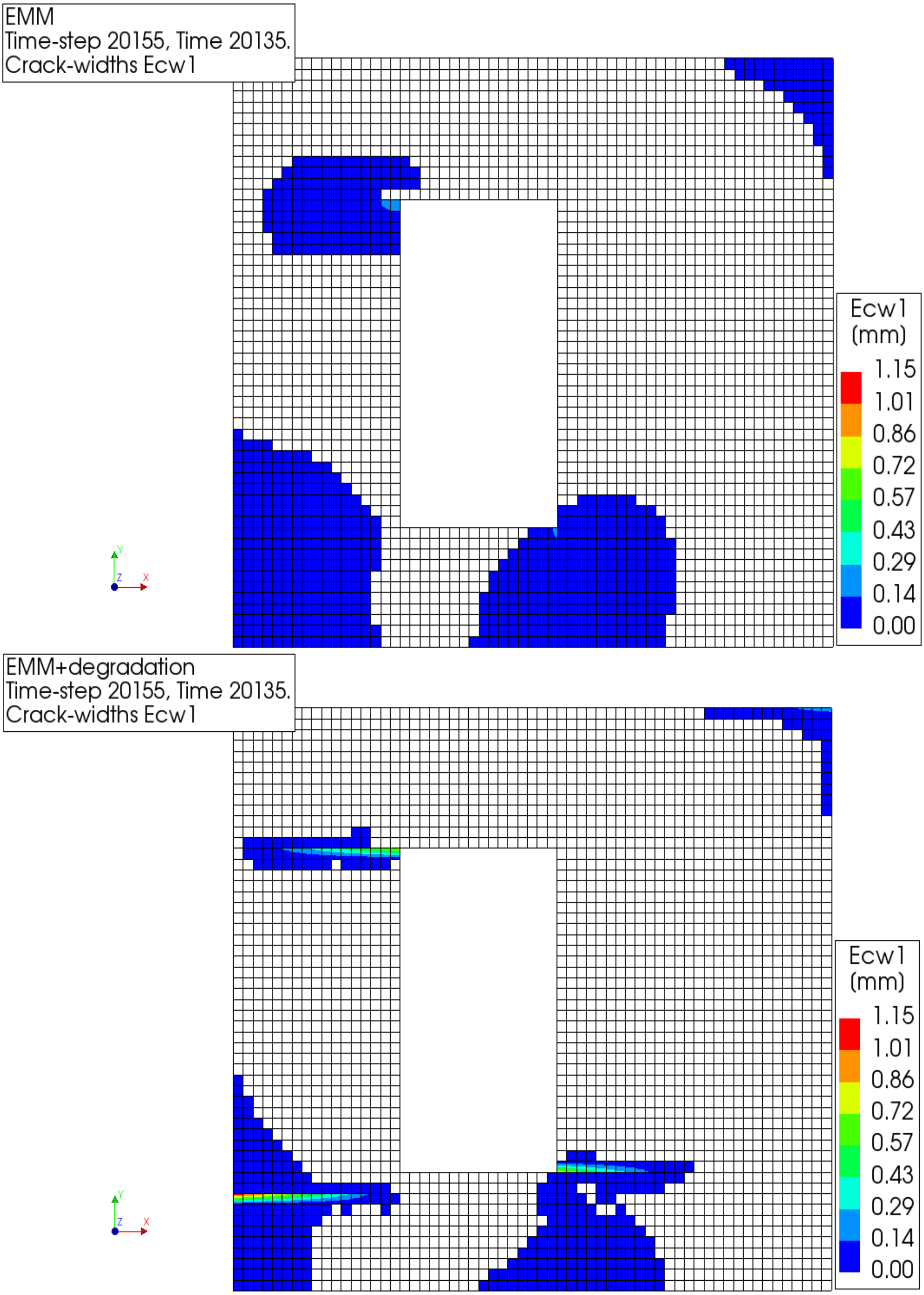

(e) Crack width plots showing EMM(top) and EMM+degradation(bottom)for displacement set 5

Figure 5.23: Crack width plots for a masonry wall with a window opening sample

5.4 Discussion and comparison between wall and window bank sample

The reduction in force during repetitions is different for the wall samples and the window bank samples. It is interesting to note that the degradation calibration constant ξ_d for the wall sample was close to twice that of the window bank sample. This gives a quantitative measure to verify the experimental observations, that the degradation for the window bank was at least twice as high as that of the wall tests. The lower the ξ_d value, the higher is the degradation. This may be due to the following 2 reasons:

- The tension strength of the masonry used for the wall analysis was based on the standard values as given in the report ”Damage sensitivity of Groningen earthquakes” [Korswagen et al., 2017]. These values reflect the strength of the bond between the bed joint and the brick unit as it is the weakest link. Whereas, for the window bank sample, since only the mid sheet is allotted the properties of EMM and the shape of the force vs displacement plots are matched with that of the experimental results, the tension strength values are calibrated. These values are no longer in the range of tension strength of bed joints (relatively lower), but rather in the range of tension strength of brick units (higher). Hence the calibration constant value for wall sample is close to twice the calibration value of window bank sample.

- The size of the structure and mode of failure together, also play an important role in the amount of degradation. The window bank sample is a small part of the wall. The mode of failure in window bank sample modeled as a four point bending specimen, is largely due to the tension crack that propagates along the vertical. Whereas, in the wall sample the failure may be due to a combined effect of tension cracking at first and then shearing between the bed-joint and the brick unit.

In order to ascertain the exact dependence of the calibration constant on these factors, a large number of experimental results need to be validated for different modes of failure.

From experiments it is seen that once the unloading starts the curve does not follow a secant branch, rather results in a slope that reaches a certain strain for zero stress, termed as plastic strain. This presence of plastic strain state plays a very important role in predicting the exact behaviour of masonry under repeated loading. Since the main focus of the hyperbolic model is to represent the degradation process, the plastic strain effect at the reloading end is neglected and hence, is considered as a limitation of the model. This limitation results in a different slope for the line joining the last repetition and the envelope, to be equal to the elastic branch. In order to eliminate the limitation, plastic strain is introduced at the reloading end as shown in appendix B which gives more accurate results compared to the experimental results. Further research needs to be carried out to perfect this aspect.

The window bank experiments are conducted in a Crack Mouth Opening Displacement (CMOD) control test, meaning the crack opening was controlled in every repetition and not the vertical displacement. Since while modeling of the window bank samples there is no option to control CMOD in DIANA, the model is based on vertical displacement control. The results from the sensors measuring the vertical displacement at the end of the specimen and at the mid point along the point of application of force are compared. This gives a fairly good estimate of the shape of the monotonic curve that can be used to justify the force vs displacement plot from the model.

The crack width plots show clearly the impact of stress reduction after every repetition. This reinforces the hypothesis that the stress reduction results in crack propagation and widening as observed in the experimental results. It can also be seen in both wall and window bank samples, that degradation does not cause additional cracks but only results in lengthening and widening of the existing crack.

The hyperbolic model is able to predict the shape of the force reduction quite accurately for 10, 30 and 100 repetitions. Although the degradation softened after 30 repetitions, it did not completely reach an asymptote. This aspect of accumulation of damage or ”the stabilizing point” is also captured by the hyperbolic model.

From the experimental results, it is observed that, the force reduction for the first repetition is larger than the force reduction at a later stage. The hyperbolic model can predict this behavior to some extent as seen in the 30 an 100 repetition samples.

The hyperbolic model works similarly for both the linear 4-node element and also the quadratic 8-node element. It is interesting to note that the energy norm gave accurate results with less computational effort, when compared to displacement and force norms. This may also be influenced by the type of failure and the analysis method being used.

Chapter 6

Conclusion and Recommendations

6.1 Conclusions

The objective of this thesis was to quantify the experimentally observed strength degradation in masonry structures through the development and implementation of a constitutive model. Existing models describing the masonry behaviour under cyclic loading by Naraine et al (1989) and models for concrete by Yankelevsky et al (1989), Hordijk (1991) were critically analysed and similarities between the two materials were identified. To further motivate the choices made in the development of the constitutive model, experimental results of two different samples, a window bank sample and a wall with an opening sample were studied. A mathematical model based on hyperbolic functions was formulated to capture the essence of degradation, leading to conceptualization of constitutive equations. Finally, computational analyses were performed using the new model in order to validate the implementation and to illustrate the potential of the hyperbolic model to capture degradation behaviour.

The two main goals of this research were:

- To understand the behavior of masonry under repeated loading by studying and comparing the experimental results of window bank tests and wall push over tests. Also, to understand the behaviour of concrete and other heterogeneous materials under cyclic loading.
- To formulate and build on the existing EMM constitutive model to effectively implement the aspect of degradation of masonry in tension mode-I type of fracture.

Regarding the first goal the following conclusions can be made:

- For studying the aesthetic damage of masonry due to light earthquakes, an experimental campaign was conducted by subjecting masonry window bank samples to repetitive loading. It was found that there was significant stress reduction after every repetition displacement set which was hypothesized as the result of crack propagation and widening during repetitions. Since repeated loading is very common during earthquakes, resulting in damage of masonry buildings, it was necessary to study the behavior of masonry under such a load.

- Similarly, concrete under cyclic loading also shows strength degradation due to accumulation of damage and crack propagation. There are a number of material models for concrete strength degradation for a single cycle but, very few consider repetitive loading effects.
- The strength degradation in masonry gradually stabilizes after 10 repetitions and is maximum in the first 10 repetitions.
- The tension constitutive model in the existing EMM in DIANA did not show degradation upon analysing the window bank tests. This was due to the secant unloading-reloading branch which only accounted for a stiffness degradation but not strength deterioration.

Regarding the second goal the following conclusions can be made.

- The hyperbolic model provided accurate results to understand the behaviour of masonry under repetitive loading. It was confirmed that the stress reduction was indeed due to the crack propagation and widening.
- The hyperbolic model was able to predict the stabilizing point accurately when compared to the experimental results. The gradual softening of the force reduction was effectively achieved by the use of a calibration factor. The lower the calibration factor, the higher is the degradation.
- The crack widths showed significant increase after each displacement set which was not the case with the existing EMM model.
- The percentage of force reduction from the experiments and the hyperbolic model were a close match with average force reduction within 5% of each other.

Conclusions based on sub questions from chapter 1 are given below:-

- The formula for degradation as given in equation 3.1 shows that, strength degradation depends on following input parameters:-

1. The strain at which the unloading starts, $(\epsilon_{uj}, \sigma_{uj})$.
2. The tension strength of the material, f_{ti}.
3. The strain upto which the specimen is unloaded, $(\epsilon_{rj}, \sigma_{rj})$.
4. Number of repetitions, n.

- Masonry fails due to progressive cracking wherein; micro cracks coalesce to form macro cracks and ultimately leads to failure. The formation of the micro cracks and their propagation is of particular interest for retrofitting and strengthening purposes. Since masonry is weak in tension, cracks appear when stresses exceed the tensile strength of masonry, as was seen in the window bank and wall samples. In testing of window bank samples, for light damage under repeated loading, it is seen that the degradation observed was due to the formation and propagation of cracks. By the formation of these cracks the energy absorbed and released by the specimen vary, i.e. there is an energy loss due to cracking. This process was clearly explained by the hyperbolic degradation model for the unloading-reloading branch of the tension constitutive behaviour. The mode II failure of masonry deals with shear cracks between brick and mortar interface. For in-plane cracking under plane stress conditions, the chances of shear cracking are very limited when compared to tension mode I fracture. Hence, the implementation of degradation in the tension mode I constitutive model is more important, than in shear or compression.

6.2 Recommendations

In this section, recommendations for further research based on the work in this thesis are discussed.

- In further research on this topic, it might be interesting to see the effects of introducing the plastic strain at the reloading end instead of a secant slope. It will be challenging to justify the choices for negative stress with positive strain as the Poisson's ratio for bricks is considered as 0. The calibration of the model may vary due to the change in slope but the accuracy of the results should remain the same.

- It is advisable to apply the model to a number of masonry structures of different sizes and shapes to eliminate the size effect that the calibration factor depends on. This will also help to verify the accuracy of the model and to narrow down the calibration factor to a certain range for different types of structures.

- Since the new model is based on cracking in tension mode-I fracture, it will be interesting to see the influence of shear i.e. mode-II and III type of failures and consequently to see the combined effect of all three modes of failure.

- Using the hyperbolic model for simple cases like bending tests, it is noted that the computational effort and time for analyzing such structures is high. It is of great importance to reduce the time required for an analysis and at the same time maintaining the accuracy. This can be achieved either by using better solution methods or by framing the USS in a more compact and efficient way.

Bibliography

D. P. Abrams, J. L. Noland, R. H. Atkinson, and P. Waugh. Response of clay-unit masonry to repeated compressive forces. In *Unknown Host Publication Title*, 1985.

Maurizio Angelillo, Paulo B. Lourenço, and Gabriele Milani. *Masonry behaviour and modelling*, pages 1–26. Springer Vienna, Vienna, 2014.

ARUP. Preliminary structural upgrading strategy for groningen. Report, ARUP, 2013.

Chiara Calderini and Sergio Lagomarsino. Continuum model for in-plane anisotropic inelastic behavior of masonry. *Journal of Structural Engineering*, 134(2):209–220, 2008. doi: 10.1061/(ASCE)0733-9445(2008)134:2(209).

Henrik Danielsson. *Perpendicular to grain fracture analysis of wooden structural elements - Models and applications.* PhD thesis, Lund University, 2013.

DIANA. Using user supplied subroutines, 2010. URL `https://dianafea.com/manuals/d943/Analys/node472.html`.

L Gambarotta and S Lagomarsino. Damage models for the seismic response of brick masonry shear walls. part i: the mortar joint model and its applications. *Earthquake engineering and structural dynamics*, 26(4):423–439, 1997.

CARLO Greco, GAETANO Manfredi, and MARISA Pecce. Cyclic degradation in reinforced concrete elements. In *Proc. XI World Conference on Earthquake Engineering, Acapulco*, 1996.

Dirk Arend Hordijk. Local approach to fatigue of concrete. *Doctoral Dissertation, Delft University of Technology*, 1991.

Paul Korswagen, Michele Longo, Edwin Meulman, and Carlijn van Hoogdalem. Damage sensitivity of groningen masonry structures - experimental and computational studies. Project report, Delft university of technology, 2017.

Kurzydowski Krzysztof, Magorzata Lewandowska, Wojciech wiszkowski, and Lewandowska-Szumie Magorzata. Degradation of engineering materials – implications to regenerative medicine. *Macromolecular Symposia*, 253. URL `https://onlinelibrary.wiley.com/doi/abs/10.1002/masy.200750701`.

Hamid R. Lotfi and P. Benson Shing. Interface model applied to fracture of masonry structures. *Journal of Structural Engineering*, 120(1):63–80, 1994.

Paulo Lourenco. Computational strategy for masonry structures. 01 1996.

Paulo Lourenco. Experimental and numerical issues in the modelling of the mechanical behaviour of masonry. 01 1998.

Paulo Lourenco, Jan G. Rots, and Johan Blaauwendraad. Continuum model for masonry: Parameter estimation and validation. 124, 06 1998.

Paulo Lourenco, Joaquim Barros, and José C. Almeida. Characterization of masonry under uniaxial tension. 01 2002.

Paulo B Lourenço and Jan G Rots. Multisurface interface model for analysis of masonry structures. *Journal of engineering mechanics*, 123(7):660–668, 1997.

Guido Magenes and A Della Fontana. Simplified non-linear seismic analysis of masonry buildings. 8:190–195, 01 1998.

Krishna Naraine and Sachchidanand Sinha. Behavior of brick masonry under cyclic compressive loading. *Journal of Structural Engineering*, 115(6):1432–1445, 1989.

Willem Leendert Nobel. A fibre flexure – lumped shear model for masonry structures. Master thesis, Delft university of technology, 2017.

Daniel V Oliveira. Experimental and numerical analysis of blocky masonry structures under cyclic loading. 2003.

OpenStax. Conic sections, 2018. URL `https://math.libretexts.org/TextMaps/Calculus/Book%3A_Calculus_(OpenStax)/11%3A_Parametric_Equations_and_Polar_Coordinates/11.5%3A_Conic_Sections`.

Duane E. Otter and Antoine E. Naaman. Model for response of concrete to random compressive loads. *Journal of Structural Engineering*, 115(11):2794–2809, 1989. doi: 10.1061/(ASCE)0733-9445(1989)115:11(2794).

Young J Park, Andrei M Reinhorn, and Sashi K Kunnath. Idarc: Inelastic damage analysis of reinforced concrete frame-shear-wall structures. 1987.

P. Pegon and A. Anthoine. Numerical strategies for solving continuum damage problems with softening: Application to the homogenization of masonry. *Computers and Structures*, 64(1): 623–642, 1997.

Luca Pelà, Elisa Canella, Alessandra Aprile, and Pere Roca. Compression test of masonry core samples extracted from existing brickwork. 119:230–240, 05 2016.

Andrea Penna, Sergio Lagomarsino, and Alessandro Galasco. A nonlinear macroelement model for the seismic analysis of masonry buildings. *Earthquake Engineering and Structural Dynamics*, 43(2):159–179, 2014.

J. G. Rots, F. Messali, R. Esposito, S. Jafari, and V. Mariani. *Computational modelling of masonry with a view to Groningen induced seismicity*, pages 227–238. CRC Press / Balkema - Taylor and Francis Group, 2016. ISBN 9781138029514.

JCM Schoenmakers. Fracture and failure mechanisms in timber loaded perpendicular to the grain by mechanical connections. 01 2010.

GMA Schreppers, A Garofano, F Messali, and JG Rots. Diana validation report for masonry modelling. Diana feareport2016-diana-r1601, Delft university of technology, 2016.

Siyavula. Hyperbolic functions, 2018. URL `https://www.siyavula.com/read/maths/grade-11/functions/05-functions-04`.

David Z Yankelevsky and Hans W Reinhardt. Uniaxial behavior of concrete in cyclic tension. *Journal of Structural Engineering*, 115(1):166–182, 1989.

A Zucchini and PB Lourenço. A micro-mechanical model for the homogenisation of masonry. *International Journal of Solids and Structures*, 39(12):3233–3255, 2002.

APPENDICES

A. User Supplied Sub-routine

```fortran
CDEC$ IF DEFINED(_WIN32)
CDEC$ ATTRIBUTES DLLEXPORT::USRMAT
CDEC$ END IF
      SUBROUTINE USRMAT( EPS0, DEPS, NS, AGE0, DTIME, TEMP0, DTEMP,
     $                   ELEMEN, INTPT, COORD, SE, ITER, USRMOD, USRVAL,
     $                   NUV, USRSTA, NUS, USRIND, NUI, SIGMA, STIFF )
C......................................................................
C$DDOC
C$DDOC   User-supplied subroutine for general nonlinear behaviour.
C$DDOC   Return updated stress and tangential stiffness matrix.
C$DDOC
C$DDOC ARGUMENTS:
C$DDOC   EPS0   D() In     - Strain vector at start of increment.
C$DDOC   DEPS   D() In     - Total strain increment.
C$DDOC   NS     I   In     - Number of stress components
C$DDOC   ITER   I   In     - Current iteration number.
C$DDOC   USRMOD C   In     - User model name.
C$DDOC   USRVAL D() In     - User parameters.
C$DDOC   NUV    I   In     - Number of user parameters.
C$DDOC   USRSTA D() InOut  - User state variables at start of increment.
C$DDOC                       Should be updated at output.
C$DDOC   NUS    I   In     - Number of user state variables.
C$DDOC   USRIND I() InOut  - User indicators at start of increment.
C$DDOC                       Should be updated at output.
C$DDOC   NUI    I   In     - Number of user state indicators.
C$DDOC   SIGMA  D() InOut  - Total stress at start of increment.
C$DDOC                       Current stress at output.
C$DDOC   STIFF  D() InOut  - Previous tangent stiffness.
C$DDOC                       Current tangent stiffness at output.
C........................................................................
C
      INTEGER          MSTR,   MOPCRK,   MCR
```

```
      PARAMETER      ( MSTR=6, MOPCRK=4, MCR=3 )
      DOUBLE PRECISION STFFAC,          SHRFAC,        SHRF
      PARAMETER      ( STFFAC=0.0001D0, SHRFAC=0.01D0, SHRF=1.2D0 )
C
      DOUBLE PRECISION DPMPAR
      LOGICAL          XSGTC
C
      INTEGER          NS, ITER, NUV, NUS, NUI,
     $                 USRIND(NUI)
      DOUBLE PRECISION EPS0(NS), DEPS(NS), USRVAL(NUV), USRSTA(NUS),
     $                 SIGMA(NS), STIFF(NS,NS)
      CHARACTER*6      USRMOD
C
      INTEGER          I, NCRACK, NOPCRK, NUMCR(3), CRACKS(2), IDIR(2),
     $                 ISCRK(6), ICRACK, NCR, FRCFAI, SHRCRK, FAIMEC
      DOUBLE PRECISION YOUN(3), SIG0(MSTR), GFT(2), GFC(2), HCRAC, FAC,
     $                 FT(2), FC(2), EPS(MSTR), ALPHA(2), UNLFAC,
     $                 TANPHI, EPSULT(2), EPSULC, SIGRF(2), COH0,
     $                 ELAXES(3,3), EPSCR(MCR*MOPCRK), COHESI, GFS,
     $                 SIGCR(MCR*MOPCRK), SHRMOD, TAUMAX, YOUN0(2),
     $                 CRAXES(MCR*MCR), SHRULT, SIGUR(2), SIGUE(2),
     $                 COH1, EPSP(MSTR), SHRMAX, SIGSHR, EPSSHR,
     $                 DEPSHR, SIOSHR, SHRM0, AA, AB, AC, LAMBDA(2),
     $                 FTALPH, LIMSTA, LIMST1, LIMST2, AS, YOUNGN(2),
     $                 SIGN1, SIGN2, SIGT1, SIGT2, TAUNT1, TAUNT2,AL(2),
     $                 AB1, AC1, AD1, AB2, AC2, AD2, AE1, AE2, EPSUR(2),
     $                 ANGLE0, ANGLE1, ANGLE2, LIMSS1, LIMSS2, COUNT,
     $                 FTALTP, EPSCP(2), EPSCFA(2), ESTAR, YSTAR,
     $                 EPSLR(2), SREP(2)

      CHARACTER*6      STRTYP
      LOGICAL          MEMBRA, SHELL, CRACKD, CRCKED, CRSHED, CRUSHD,
     $                 RECRACKD
```

```
    C... [Lines 66 to 115 are redacted]
116 C...  AT THE BEGINNING OF THE STEP THE PARAMETER FAIMEC
117 C... (RELATED TO THE FAILURE MECHANISM) IS SET TO ZERO
118       FAIMEC = 0
119 C...   THE STRAIN AT COMPRESSIVE PEAK IS EVALUATED{
    C... [Lines 119 to 154 are redacted]
155 C...  THE TENSILE BEHAVIOUR OF THE ELEMENT IS EVALUATED
156       DO 100, I = 1, 2
157 C...        ALPHA(1)=MAXIMUM TENSILE STRAIN EVER REACHED
158 C...        ALPHA(2)=MINIMUM COMPRESSIVE STRAIN EVER REACHED
159          ALPHA(1) = USRSTA(I)
160          ALPHA(2) = USRSTA(I+2)
161          SIGRF(1) = USRSTA(I+4)
162          SIGRF(2) = USRSTA(I+6)
163          SIGUR(I) = USRSTA(I+12)
164          SIGUE(I) = USRSTA(I+14)
165          LAMBDA(I) = USRSTA(I+16)
166          YOUNGN(I) = USRSTA(I+18)
167          EPSUR(I) = USRSTA(I+20)
168          EPSLR(I) = USRSTA(I+22)
169          AL(I) = USRSTA(I+24)
170          SREP(I) = USRSTA(I+26)
171          CRACKD   = USRIND(I)   .EQ. 1
172          RECRACKD = USRIND(I+5)
173          CRUSHD   = USRIND(I+2) .EQ. 1
174         IF ( EPS(I) .GE. 0.D0 ) THEN
175             IF ( EPS(I) .GT. FT(I)/YOUN0(I) ) THEN
176 C...          IF THE STRAIN IS LARGER THAN THE ELASTIC LIMIT
177 C...      IN TENSION THE PARAMETER FAIMEC IS INCREASED OF 1 OR 2
178 C...    (ACCORDING TO THE DIRECTION)
179               FAIMEC = FAIMEC + I
180             END IF
181             IF ( EPS(I) .GT. ALPHA(1) ) THEN
```

```
C...          NEW TENSILE EXTREME
               ALPHA(1) = EPS(I)
               IF (EPS(I) .GT. EPSULT(I) ) THEN
                  SIGMA(I) = EPS(I)*STFFAC
                  CRACKD = .TRUE.
               ELSE IF ( EPS(I) .GT. FT(I)/YOUNO(I)) THEN
                IF(LAMBDA(I).LE. 0.D0) THEN
                  SIGMA(I) = EPS(I)*STFFAC
                  CRACKD = .TRUE.
                ELSE IF (EPS(I) .LE. ((EPSULT(I)*FT(I)+(YOUNO(I)*AL(I)*
     $               (EPSULT(I)-FT(I)/YOUNO(I)))-(LAMBDA(I)*YOUNGN(I)*
     $               (EPSULT(I)-FT(I)/YOUNO(I))))/(YOUNO(I)*(EPSULT(I)-
     $                FT(I)/YOUNO(I))+FT(I))).AND.(RECRACKD))THEN
                    SIGMA(I) = (YOUNO(I)*(EPS(I)-AL(I))+(LAMBDA(I)*
     $                          YOUNGN(I)))
                  ELSE
                    SIGMA(I) = FT(I)*(1.D0 -(EPS(I)-FT(I)/YOUNO(I))/
     $                          (EPSULT(I)-FT(I)/YOUNO(I)))
                    CRACKD = .TRUE.
                    LAMBDA(I) = LAMBDA(I)/LAMBDA(I)
                  END IF
               ELSE
                  SIGMA(I) = EPS(I)*YOUNO(I)
               END IF
               SIGRF(1) = SIGMA(I)
               IF ( ITER .EQ. 0 ) THEN
                  YOUN(I) = YOUNO(I)
               ELSE
```

```
                  YOUN(I) = MAX( STFFAC*YOUN0(I), SIGRF(1)/ALPHA(1) )
               END IF
            ELSE IF ( ABS(ALPHA(1)) .GT. 1.D+6*DPMPAR(1) ) THEN
C...                   Tension unloading and reloading
                 IF (EPS(I) .GT. EPS0(I)) THEN
                   IF (SIGUE(I) .LE. SREP(I)) THEN
                     SIGMA(I)= LAMBDA(I)*EPS(I)*SIGRF(1)/ALPHA(1)
                   ELSE
                     LAMBDA(I) =(0.8D0)**(1.D0-(EPSLR(I)/ALPHA(1))-
     $                                ((FT(I)-SIGUE(I))/(3.D0*FT(I)+SIGUR(I)))
                     IF (LAMBDA(I) .LT. 0.D0) THEN
                     LAMBDA(I) = 0.D0
                     SIGMA(I)= EPS(I)*STFFAC
                     RECRACKD = .TRUE.
                     ELSE
                     SIGMA(I)= LAMBDA(I)*EPS(I)*SIGRF(1)/ALPHA(1)
                     YOUNGN(I) = SIGRF(1)
                     SREP(I) = SIGUR(I)
                     RECRACKD = .TRUE.
                     END IF
                   END IF
                  ELSE
                    SIGUE(I) = LAMBDA(I)*SIGRF(1)
                    SIGMA(I)= LAMBDA(I)*EPS(I)*SIGRF(1)/ALPHA(1)
                    SIGUR(I) = SIGMA(I)
                    IF((LAMBDA(I).EQ.1.D0)) THEN
                     EPSLR(I) = EPS(I)
                    END IF
                    EPSUR(I) = EPS(I)
                    IF (EPSUR(I) .NE. EPSLR(I)) THEN
```

```
                     EPSLR(I) = EPS(I)
                    END IF
                    AL(I) = ALPHA(1)
                  END IF
                IF ( ITER .EQ. 0 ) THEN
                    YOUN(I) = YOUN0(I)
                ELSE
                    YOUN(I) = MAX(STFFAC*YOUN0(I), SIGRF(1)/ALPHA(1))

                END IF
            ELSE
               SIGMA(I) = YOUN0(I) * EPS(I)
               YOUN(I) = YOUN0(I)
            END IF
         ELSE
            IF ( EPS(I) .LT. -FC(I)/YOUN0(I) ) THEN
C...          IF THE STRAIN IS LARGER THAN THE ELASTIC LIMIT
C...     IN COMPRESSION THE PARAMETER FAIMEC IS INCREASED OF
C...      4 OR 8 (ACCORDING TO THE DIRECTION){
C...     [Lines 254 to 332 are redacted]
         IF ( CRACKD ) THEN
            USRIND(I) = 1
            NCRACK = NCRACK + 1
            IDIR(NCRACK) = I
            NUMCR(NCRACK) = NCRACK
            IF ( EPS(I) .GT. 0.D0 ) THEN
               NOPCRK = NOPCRK + 1
               ISCRK(NCRACK) = 2
            ELSE
               ISCRK(NCRACK) = -2
            END IF
         END IF
         IF ( RECRACKD ) THEN
```

```
            USRIND(I+5) = 1
         END IF
         IF ( CRUSHD ) USRIND(I+2) = 1
         USRSTA(I)   = ALPHA(1)
         USRSTA(I+2) = ALPHA(2)
         USRSTA(I+4) = SIGRF(1)
         USRSTA(I+6) = SIGRF(2)
         USRSTA(I+12)  = SIGUR(I)
         USRSTA(I+14)  = SIGUE(I)
         USRSTA(I+16)  = LAMBDA(I)
         USRSTA(I+18) = YOUNGN(I)
         USRSTA(I+20) = EPSUR(I)
         USRSTA(I+22) = EPSLR(I)
         USRSTA(I+24) = AL(I)
         USRSTA(I+26) = SREP(I)
         CRCKED = CRCKED .OR. CRACKD
         CRSHED = CRSHED .OR. CRUSHD
  100 CONTINUE
C
      SHRMOD = SHRM0
C...  GIVEN THE GEOMETRY OF BRICKS AND MORTAR, THE STRESSES
C... NORMAL TO THE DIAGONALS ARE COMPUTED
C... [Lines 367 to the end of USS are redacted]
```

B. Improvements to the model

In this appendix, the existing model is extended, by including the plastic strain state. Figure 1 shows the changes to the degradation model to include plastic strain. The amount of plastic strain is based on experimental observations and comparison of various models as presented by [Oliveira, 2003] and is shown in Figure 2. From the literature an average value of 0.75 has been chosen to represent the point where the unloading branch crosses the strain axis (x axis) and further extended to intersect a point (0,-3$*\sigma_{uj}$) on the stress axis (y axis). The force vs displacement results of wall with a window opening from the EMM and the EMM+degradation+plastic strain model are shown in Figure 3. Figure 4 shows the comparison between the experimental results and the improved model. It is clear that by introducing the plastic strain, more accurate results can be obtained. Figure 5 the changes to the code made to simulate the effect of plastic strain state.

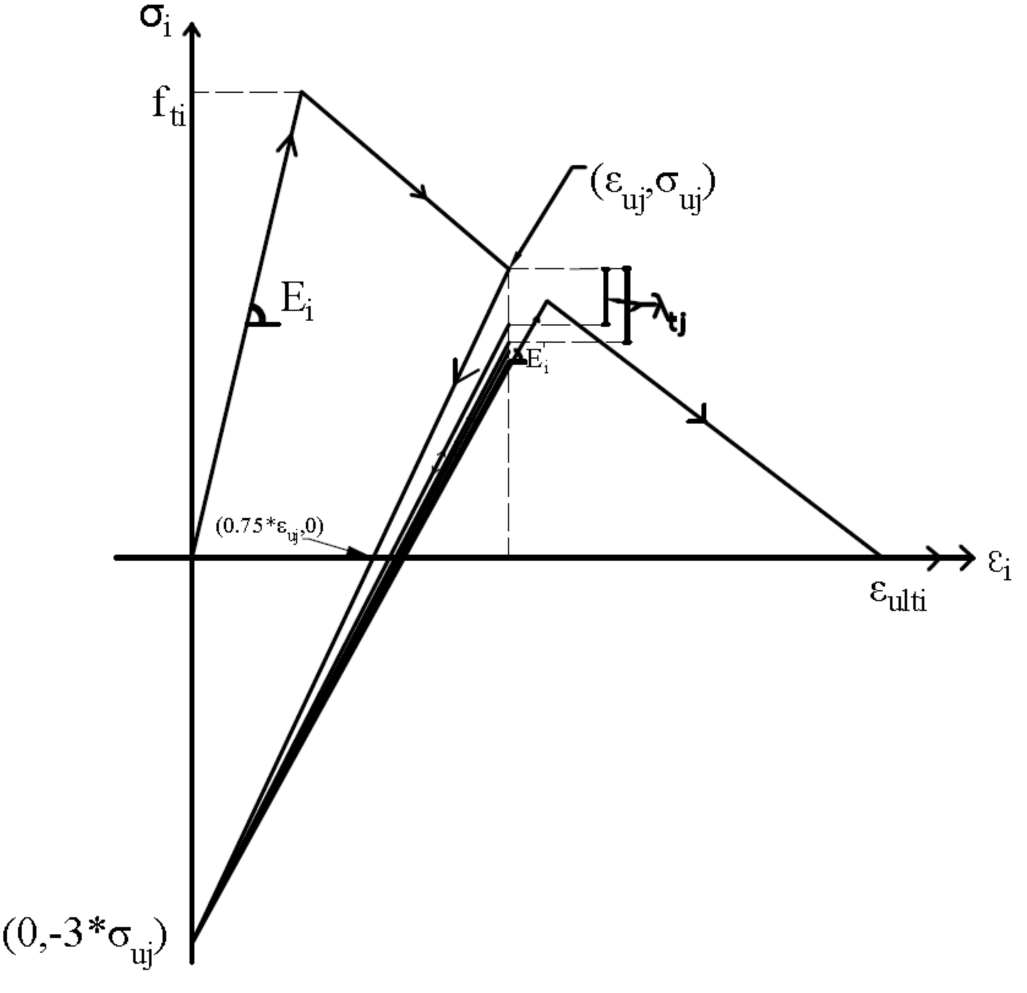

Figure 1: New updated degradation model including plastic strain

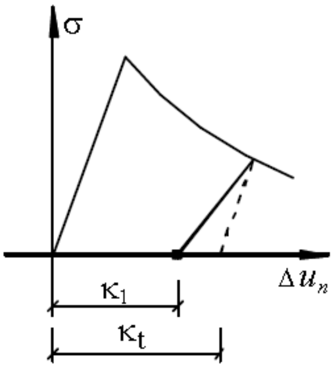

Numerical simulation	$\frac{\kappa_1}{\kappa_t}$	$\frac{\kappa_1}{\kappa_c}$	$\frac{\kappa_2}{\kappa_c}$	$\frac{\Delta\kappa_c}{\kappa_c}$
Gopalaratnam and Shah (1985)	0.76	—	—	—
Karsan and Jirsa (1969)	—	0.56	0.28	0.13
Reinhardt (1984)	0.73	—	—	—

Figure 2: The tension constitutive model as given in [Oliveira, 2003]

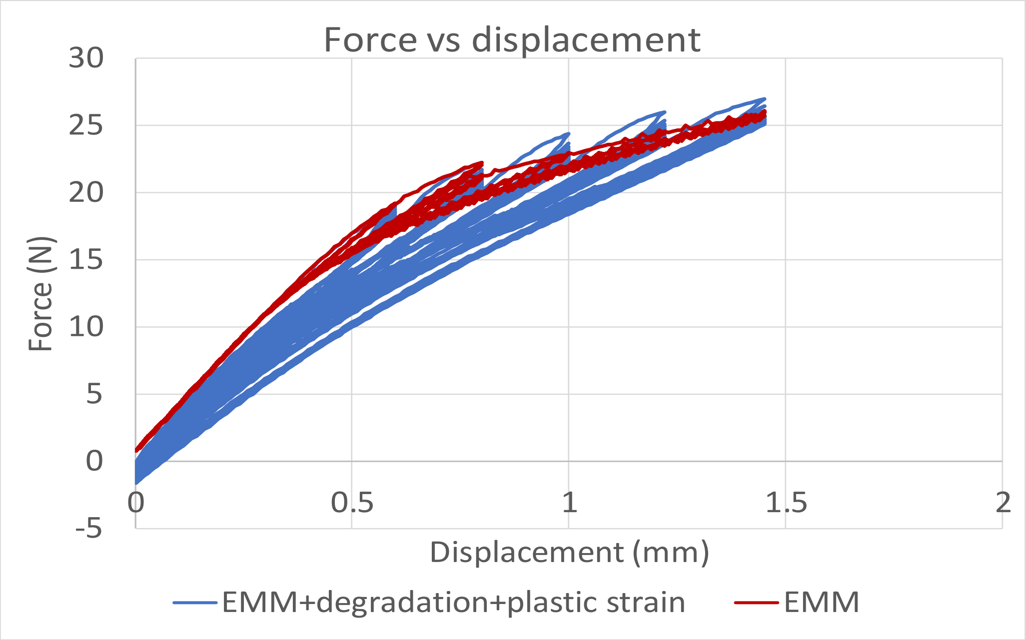

Figure 3: Force vs displacement graph for EMM and EMM+degradation+plastic strain

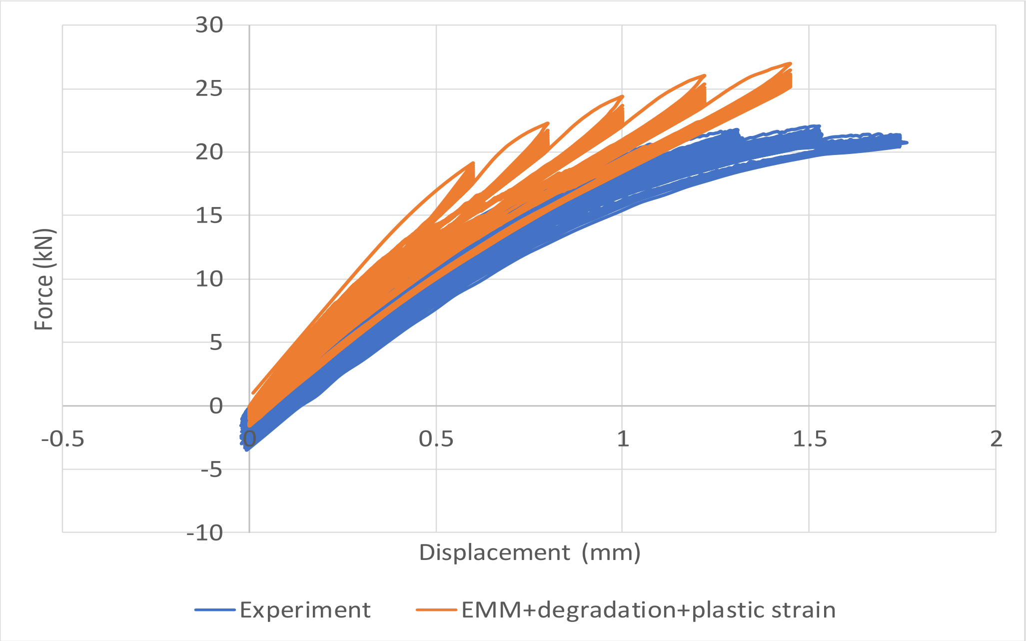

Figure 4: Force vs displacement graph for Experiment and EMM+degradation+plastic strain

```
C...               Tension unloading and reloading
                 IF (EPS(I) .GT. EPS0(I)) THEN
                   IF (SIGUE(I) .LE. SREP(I)) THEN
                     SIGMA(I)= LAMBDA(I)*EPS(I)*SIGRF(1)/ALPHA(1)
                   ELSE
                     LAMBDA(I)=(0.85D0)**(1.D0-(EPSLR(I)/ALPHA(1)))-
     $                           ((FT(I)-SIGUE(I))/(3.0D0*FT(I)+
     $                           ABS(SIGUR(I))))
                     IF (LAMBDA(I) .LT. 0.D0) THEN
                     LAMBDA(I) = 0.D0
                     SIGMA(I)= EPS(I)*STFFAC
                     RECRACKD = .TRUE.
                     ELSE
                    SIGMA(I)= ((EPS(I)-ALPHA(1))/ALPHA(1))*
     $                           (LAMBDA(I)*SIGRF(1)+3.D0*SIGRF(1))+
     $                            LAMBDA(I)*SIGRF(1)
                     YOUNGN(I) = SIGRF(1)
                     SREP(I) = SIGUR(I)
                     RECRACKD = .TRUE.
                     END IF
                   END IF
                  ELSE
                    SIGUE(I) = LAMBDA(I)*SIGRF(1)
                    SIGMA(I)= ((EPS(I)-ALPHA(1))/ALPHA(1))*
     $                           (LAMBDA(I)*SIGRF(1)+3.D0*SIGRF(1))+
     $                            LAMBDA(I)*SIGRF(1)
                    SIGUR(I) = SIGMA(I)
                    IF((LAMBDA(I).EQ.1.D0)) THEN
                     EPSLR(I) = EPS(I)
                    END IF
                    EPSUR(I) = EPS(I)
                    AL(I) = ALPHA(1)
                  END IF
```

Figure 5: USS code showing new model including plastic strain state